



Communications of  
**Science &  
Technology**

Volume 1  
Issue 1

# Editorial Team

---

ScopusEditor in Chief

**Meilana Dharma Putra**

Universitas Lambung Mangkurat, Indonesia

---

Associate Editor

**Noor Akhmad Setiawan**

Universitas Gadjah Mada, Indonesia

**Farid Fadhillah**

Al Imam Mohammad Ibn Saud Islamic University, Saudi Arabia

**Martha Arbayani Zaidan**

University of Helsinki, Finland

**Firdaus Prabowo**

WS Audiology, Singapore

---

## Editorial Board

### **Zubair Md. Fadlullah**

Lakehead University, Canada

### **Ahmed Abu-Siada**

Curtin University, Australia

### **Qiuwei Pan**

Erasmus Medical Center, Netherlands

### **Hanung Adi Nugroho**

Universitas Gadjah Mada, Indonesia

### **Andy Octavian Latief**

Institut Teknologi Bandung, Indonesia

### **Mohamad Saifudin Hakim**

Qassim University, Saudi Arabia

### **Taufiq Wirahman**

Badan Riset dan Inovasi Nasional, Indonesia

### **Firmansyah Nur Budiman**

Universitas Islam Indonesia, Indonesia

### **Rio Turnadi**

Pertamina University, Indonesia

### **Tri Agung Rohmat**

Universitas Gadjah Mada, Indonesia

### **Esa Prakasa**

Badan Riset dan Inovasi Nasional, Indonesia

### **Setyanto Tri Wahyudi**

Institut Pertanian Bogor, Indonesia

### **Ahmad Ridwan Tresna Nugraha**

Badan Riset dan Inovasi Nasional, Indonesia

### **Yudha Prawira Budiman**

Universitas Padjajaran, Indonesia

### **Adha Imam Cahyadi**

Universitas Gadjah Mada, Indonesia

### **Slamet**

Universitas Indonesia, Indonesia

### **M. Hadj Kali**

King Saud University, Saudi Arabia

### **Igi Ardiyanto**

Universitas Gadjah Mada, Indonesia

### **M. Hisyam Lee**

Universiti Teknologi Malaysia, Malaysia

### **Agus Kurniawan**

Universitas Gadjah Mada, Indonesia

### **Mohd. Ibrahim Shapiai**

Universiti Teknologi Malaysia, Malaysia

### **Muhamad Sahlan**

Universitas Indonesia, Indonesia



## COMMUNICATIONS IN SCIENCE AND TECHNOLOGY

📍 KOMUNITAS ILMUWAN DAN PROFESIONAL MUSLIM INDONESIA (KIPMI)

☀ P-ISSN : 25029258 <> E-ISSN : 25029266 📁 Subject Area : Engineering



**1.7375**  
Impact



**1173**  
Google Citations



**Sinta 1**  
Current Accreditation

🔍 [Google Scholar](#) 🦅 [Garuda](#) 🌐 [Website](#) 🌐 [Editor URL](#)

[History Accreditation](#)



**Submit**

# Rotating speed and magnetic pole dependency assisted on copper deposition onto aluminum alloy substrate for bacterial eradication application

Basori<sup>a,\*</sup>, Ruliyanta<sup>b</sup>, Maman Kartaman Ajiriyanto<sup>c</sup>, Rosika Kriswarini<sup>c</sup>, Heri Hardiyanti<sup>c</sup>, Cahaya Rosyidan<sup>d</sup>, Sigit Dwi Yudanto<sup>e</sup>, Evi Ulina Margaretha Situmorang<sup>f</sup>, Daniel Edbert<sup>g</sup>, Dwi Nanto<sup>h</sup>, Ferry Budhi Susetyo<sup>i</sup>

<sup>a</sup>Department of Mechanical Engineering, Universitas Nasional, Jakarta, 12520, Indonesia

<sup>b</sup>Department of Electrical Engineering, Universitas Nasional, Jakarta, 12520, Indonesia

<sup>c</sup>Research Center for Nuclear Material and Radioactive Waste Technology, National Research and Innovation Agency, Tangerang Selatan, 15314, Indonesia

<sup>d</sup>Department of Petroleum Engineering, Universitas Trisakti, Jakarta, 11440, Indonesia

<sup>e</sup>Research Center for Metallurgy, National Research and Innovation Agency, Tangerang Selatan, 15314, Indonesia

<sup>f</sup>Department of Physiology School of Medicine and Health Sciences, Atma Jaya Catholic University of Indonesia, Jakarta, 14440, Indonesia

<sup>g</sup>Department of Microbiology, Atma Jaya Catholic University of Indonesia, Jakarta, 14440, Indonesia

<sup>h</sup>Department of Physic Education, UIN Syarif Hidayatullah, Jakarta, 15412, Indonesia

<sup>i</sup>Department of Mechanical Engineering, Universitas Negeri Jakarta, Jakarta, 13220, Indonesia

## Article history:

Received: xx xxxx xxxx / Received in revised form: xx xxxx xxxx / Accepted: xx xxxx xxxx (to be inserted by publisher)

## Abstract

The present research conducted an electrodeposition of copper (Cu) over an aluminum (Al) alloy substrate, under influence various magnetic poles and rotating speeds. Several investigations in the present study were conducted, including deposition rate, current efficiency, surface morphology and phase, crystallographic orientation, antibacterial activity, and corrosion behavior. Increasing the rotation speed promoted to enhanced deposition rate and current efficiency for both magnetic poles. An increase in the deposition rate from 12.83 to 13.67  $\mu\text{m/h}$  leads to a change in surface morphology near the spheroidal, becoming a faceted structure. Presenting and rising in the rotation of a magnetic field rotation led to a reduced surface roughness and crystallite size of Cu film for both magnetic poles. The Cu film made without spinning magnetic has a characteristic highest bacterial inhibition zone around  $2.50 \pm 0.56 \text{ cm}^2$ . The CuRS50 sample has the lowest corrosion rate around 1.196 mpy.

**Keywords:** North and south pole; SEM; XRD; Antibacterial activity; Corrosion behavior.

## 1. Introduction

Due to its promising properties, copper (Cu) is widely used in many sectors, such as drinking water piping, heat exchangers, and medical equipment [1–3]. Cu coated onto aluminum (Al) alloy could enhance its properties, such as hardness and antimicrobial properties [4]. Cu electrodepositions attract many researchers to investigate formed Cu films. In their study, Brands *et al.* investigated the structure, surface morphology, electrical, optical, and magnetic properties of electrodeposited  $\text{Cu}_2\text{O}$  [5]. Augustin *et al.* investigated the effect of current density at Cu electrodeposition on the microstructure and hardness of Cu for

antimicrobial Al touch [4]. Antenucci *et al.* have improved (the mechanical and thermal properties) of open-cell Al foams through Cu electrodeposition [6].

Many factors, including the magnetic field, influenced the formed Cu films while electrodeposition was performed. The existing magnetic field at the electrodeposition process could appear to have several forces. The Lorentz force acts on a moving ion in the solution, resulting in convection flow [7]. The effects of the magnetic field may also relate to the electrokinetic-magnetohydrodynamic (MHD) effect which resulting the body force acting in the diffuse layer [8]. Another force due to the magnetic field is a paramagnetic gradient force [9]. The paramagnetic gradient force causes the movement of magnetic ions in the diffusion layer. Another possible force is a magnetic gradient force. This force acts on paramagnetic and diamagnetic ions [10].

\* Corresponding author.

Email: [basori@civitas.unas.ac.id](mailto:basori@civitas.unas.ac.id)

doi (to be inserted by publisher)



Due to the many forces exhibited by presenting a magnet, several researchers investigations were focused on unrotated magnetic field-induced Cu electrodeposition [7,11–15]. Miura *et al.* investigated the electrodeposition of Cu under 15 T of magnetic field and found extraordinary dendritic growth [12]. Murdoch *et al.* conducted an electrodeposition of Cu using influence 0.25 and 0.5 T placed on the working electrode's reverse, resulting in the lowest thickness when influencing 0.25 and 0.5 T with the south pole than the north pole [7]. Sudibyo *et al.* conducted electrodeposition of Cu using influence 300 and 900 G (neodymium magnet), resulting in higher grain when electrodeposition Cu using influence 900 G [15]. Yin *et al.* investigated anomalous Cu hydride phase during magnetic field-assisted electrodeposition of Cu. Presenting an anti-parallel magnetic field affecting the magnetohydrodynamic effect, could enhance the hydrogen evolution and result in poor film quality [11]. Kovalyov *et al.* have found that a weak magnetic field (0.5 and 0.7 mT) could affect the electrodeposition process, surface morphology, and texture [13]. Liu *et al.* have stated that magnetic field-assisted electrodeposition could change hydrogen bond structure, reduce the charge transfer resistance, and increase the electrolyte viscosity [14].

Electrodeposition assisted with a spinning magnetic field is considered to attract several researchers due to its ability to enhance the properties of films. Wang and Chen used 0.18 T of a magnetic field with various rotating speeds (1000–3000 rpm) when electrodeposition of nickel (Ni) and resulting presenting a magnetic field with various rotating speeds could decrease surface roughness [16]. Ji *et al.* fabricated Ni-SiC using an electrodeposition process and found that the exhibit rotating magnetic field makes SiC particle distribution more uniform [17]. Syamsuir *et al.* have stated presenting a rotating magnetic field (500 and 800 rpm) makes surface morphology more uniform [18]. Syamsuir *et al.* have found that an increase in the rotating speed of a magnetic field could decrease a corrosion rate due to more compact morphology [19].

According to the literature review mentioned above, there is no report of Cu electrodeposition under a spinning magnet (50 and 100 rpm); moreover, the influence of the spinning using different magnetic pole was also not conducted. In the present research, the electrodeposition of Cu over an Al alloy substrate is undertaken. The electrodeposition of Cu was influenced by various magnetic poles (north and south) and magnetic rotating speeds (0, 50, and 100 rpm). Several investigations were conducted using digital scales, scanning electron microscopy equipped with energy dispersive spectroscopy (SEM-EDS), X-ray diffraction, digital camera, optical microscope, and potentiostat apparatus.

## 2. Materials and Methods

### 2.1. Material

Al alloy (0.106 wt.% Si, 0.365 wt.% Fe, 0.055 wt.% Cu, 0.043 wt.% Mn, 0.030 wt.% Mg, 0.003 wt.% Zn, 0.002 wt.% Ni, 0.018 wt.% Ti, 0.003 wt.% Pb, and Al balance) used as cathode, while pure Cu was used as anode. Electrolyte solution was prepared by dissolving  $\text{CuSO}_4 \cdot 5\text{H}_2\text{O}$  (Merck) in

deionized water. 0.5 M  $\text{CuSO}_4 \cdot 5\text{H}_2\text{O}$  plus 20 mL of  $\text{H}_2\text{SO}_4$  fresh solution (250 ml) was used for electrodeposition of Cu.

### 2.2. Sample preparation

Firstly, Al alloy was cut  $2 \times 2$  cm for electrodeposition substrate using the shearing machine. Then, Cu film was made using a DC power supply (MDB PS-305DM) with 40 mA, 25 °C, and pH 5.5 for one h. Cu films were prepared under the influence of a clockwise rotating magnetic field, as seen in Fig. 1. The plating bath was placed on top of the rotation magnetic field equipment. Two pieces of neodymium magnet were stacked and arranged (6 parts) in the Teflon, as seen in Fig. 1. One piece of neodymium magnet has 0.08 T of intensity. The five variation samples were made; one sample was made without the influence of a rotating magnetic field as a baseline. The sample was made by influencing 50 rpm and 100 rpm. Moreover, different pole variations are also used in the present study. The complete sample name is seen in Table 1.

Table 1. Sample name and remark

Sample name	Remark
CuR0	without the influence of a rotating magnetic field
CuRN50	50 rpm, north pole near the substrate
CuRN100	100 rpm, north pole near the substrate
CuRS50	50 rpm, south pole near the substrate
CuRS100	100 rpm, south pole near the substrate

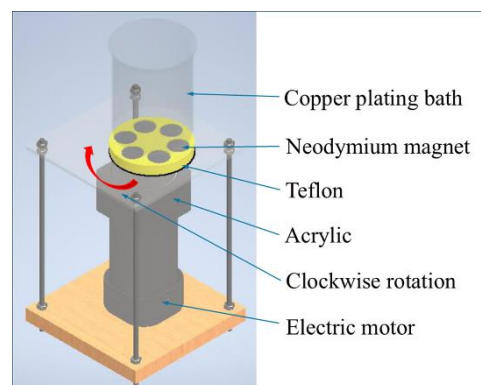


Fig. 1. Rotation magnetic field equipment

### 2.3. Characterizations

The deposition rate and current efficiency were measured similarly to previous studies [10]. Thermo Scientific SEM-EDS was used to investigate surface morphology and elements. According to SEM image, Image J software was used to measure the roughness of Cu film. X-ray diffraction was conducted using PANalytical (Cu K radiation) with step size  $0.02^\circ$  and then refined using GSAS software [20].

Antibacterial activity was investigated similarly according to previous studies [19]. Assessment of microbial reduction of various samples is adapted from ISO 22196 for non-porous material. *Staphylococcus aureus* (*S. aureus*) ATCC 25923 was used in this test. The inhibition zone was documented using a

digital camera and assessed using an unaided eye. The area of inhibition is measured by Image J software. Each measurement is performed five times to ensure the homogeneity of the data. The diffusible area is calculated by subtracting the area of inhibition from the size of the metal. One-way ANOVA analysis was conducted, to investigate whether there is significance between the polarities of the magnets. Moreover, the specimen was then removed from the plate using sterile forceps. The agar is re-incubated at  $35^{\circ}\text{C} \pm 2$  for 24 hours to observe the antimicrobial activity post-contact. The oxides of the metal that formed before and after the test were observed using Olympus CX23 microscope under  $180 \times$  magnification; any changes inside of the agar plate were documented.

Corrosion behavior was determined using potentiodynamic polarization method. The potentiodynamic polarization was conducted using Gamry potentiostat (Ref 600) in 0.9 % NaCl (room temperature) using 1 mV/s of scan rate. Cu films as working electrode, Ag/AgCl as reference electrode and Pt wire as counter electrode. Using the Tafel extrapolation method,  $I_{\text{corr}}$  and  $E_{\text{corr}}$  could be founded. Then Corrosion rate could be calculated using following equation [19].

$$\text{Corrosion rate (mpy)} = (C M I_{\text{corr}}) / (n \rho) \quad (1)$$

where C is constant (0.129 mpy), M is atomic weight (g/mol),  $I_{\text{corr}}$  is current density ( $\text{A}/\text{cm}^2$ ), n is the number electron involved, and  $\rho$  is Cu density ( $\text{g}/\text{cm}^3$ ).

### 3. Result and Discussion

#### 3.1. Deposition Rate and Current Efficiency

Fig. 2 shows the deposition rate and current efficiency of electrodeposition Cu over an Al alloy substrate. They have similar tendencies; an increase in magnet rotation speed leads to a rise in deposition rate and current efficiency.

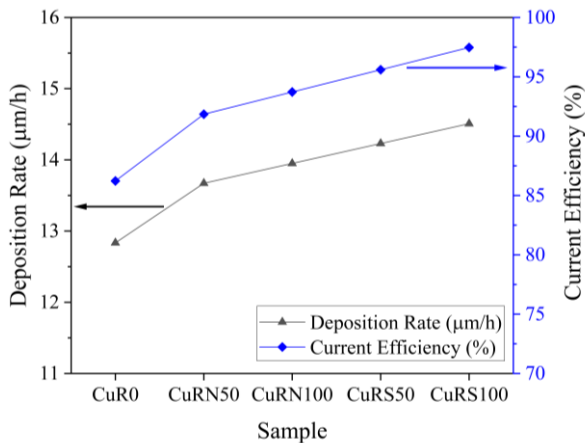


Fig. 2. Deposition rate and current efficiency of Cu electrodeposition

In the process of Cu electrodeposition, the oxidation process occurs at the anode, and a reduction process occurs at the cathode. An Al alloy (substrates) to be plated is placed at the cathode. When the current is applied, the Cu ions are depleted in the surroundings of the cathode, making a diffusion film upper around the cathode. Hydrogen evolution

is known to occur at the cathode during Cu electrodeposition from aqueous solutions [10]. Less hydrogen evolution would increase the deposition rate and current efficiency because hydrogen evolution can disturb the movement of the ions to the cathode. Presenting an anti-parallel magnetic field (north pole) affecting the MHD effect could enhance the hydrogen evolution, decrease current efficiency, and result in poor film quality [11]. According to Fig. 2, hydrogen evolution seems to influence the electrodeposition process when influenced by the north pole, therefore it has lesser current efficiency than the electrodeposition process when influenced by the south pole.

Cu films were made and influenced by the rotating south pole magnet, which has a higher deposition rate due to the magnetic field, which is parallel to the current direction and attracts more Cu ions onto the Al alloy surface [7]. Rotating the magnet below the electrolyte solution while the electrodeposition process was performed could induce Eddy electric field [19]. The Eddy electric field could act as an additional MHD flow convection effect [16]. Moreover, increasing the rotation speed could attract more Cu ions onto the Al alloy surface, consequently increasing the deposition rate and current efficiency.

#### 3.2. SEM-EDS and Roughness

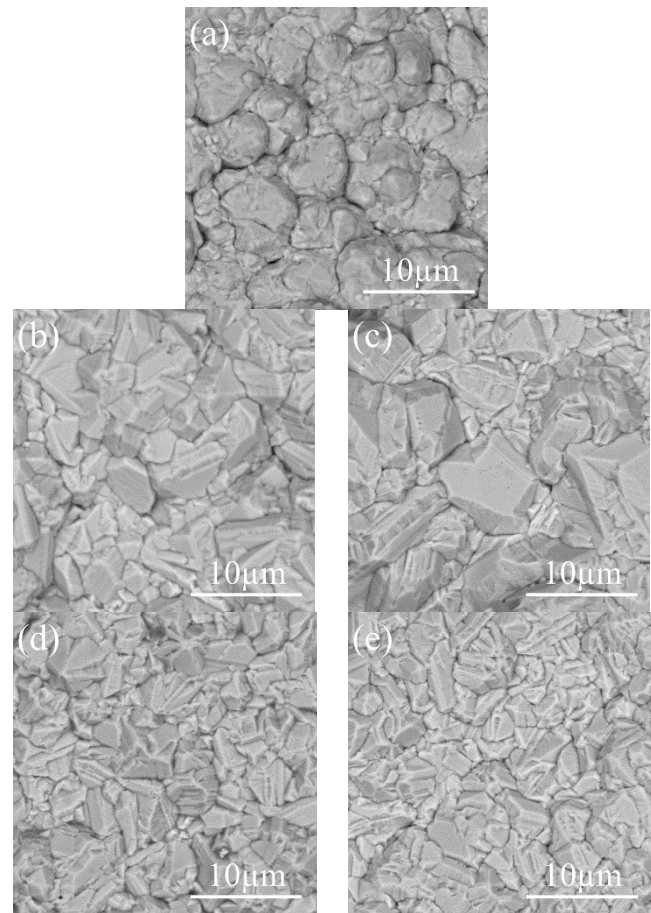


Fig. 3. SEM Cu layers: (a) CuR0; (b) CuRN50; (c) CuRN100; (d) CuRS50; and (e) CuRS100

Fig. 3 shows the SEM of various Cu film surfaces. Samples were made by influencing the north pole magnetic field,

which has a larger grain size than samples were created by affecting the south pole of a magnetic field.

According to Fig. 3, it can be seen that the Cu sample was made with no spinning magnetic influence, which led to the formation of morphology near the spheroidal. Cu samples were made with spinning magnetic assistance, leading to the forming of faceted structure morphology [10]. Moreover, a transformation from spheroidal to faceted structure is influenced by deposition rate. A higher deposition rate led to a nucleation rate; therefore, surface morphology varies. Samples made with influences from the north pole magnetic field have a low nucleation rate, hence having wider grain sizes than samples made by influencing the south pole magnetic field [7]. Moreover, an increase in the deposition rate from 12.83 to 13.67  $\mu\text{m/h}$  leads to a change in surface morphology near the spheroidal becoming faceted structure. The deposition rate between 13.67 and 14.51  $\mu\text{m/h}$  results in a faceted structure of surface morphology.

The south pole has an affecting magnetic field parallel to the current direction; therefore, Cu ions are more attracted to the Al alloy surface. On the contrary, the north pole has an affecting magnetic field that is anti-parallel to the current direction, reducing Cu ions' attraction onto the Al alloy surface. Moreover, Lorentz's forces rotate opposite each other on top of the surface specimen for different magnetic poles. This condition affected the sample film by influencing the South Pole to be smoother than the North Pole. Ji *et al.* stated that presenting a rotating magnetic field makes surface morphology more uniform [17]. In this case, the paramagnetic force has a similar tendency for different magnetic poles and, therefore, could be neglected, influencing surface morphology.

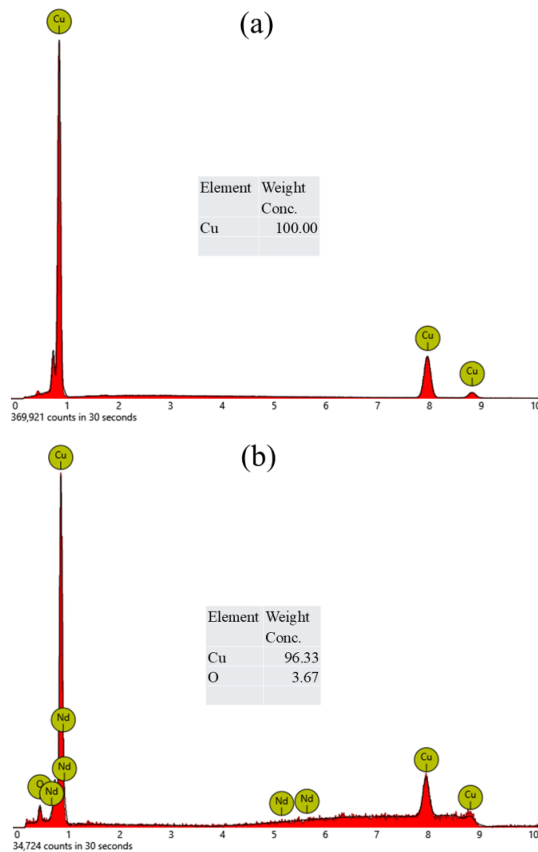
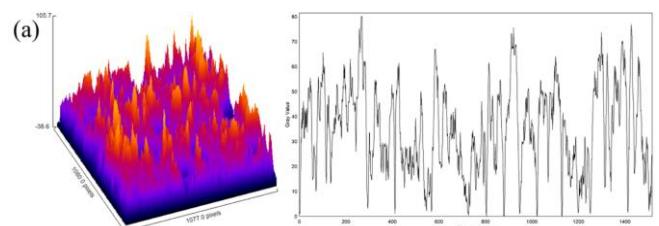


Fig. 4. EDS Cu layers: (a) CuR0; (b) CuRN50; (c) CuRN100; (d) CuRS50; and (e) CuRS100

According to Fig. 4, the spinning magnetic-assisted running at 50 rpm led to oxygen forming on the Cu surface. Moreover, enhanced magnetic rotation led to a decrease or disappearance of oxygen. Presenting oxygen on Cu film is one of the unique cases. Oxygen could form due to a secondary reaction on the anode. Moreover, oxygen could be formed due to sample storage and transport [19].





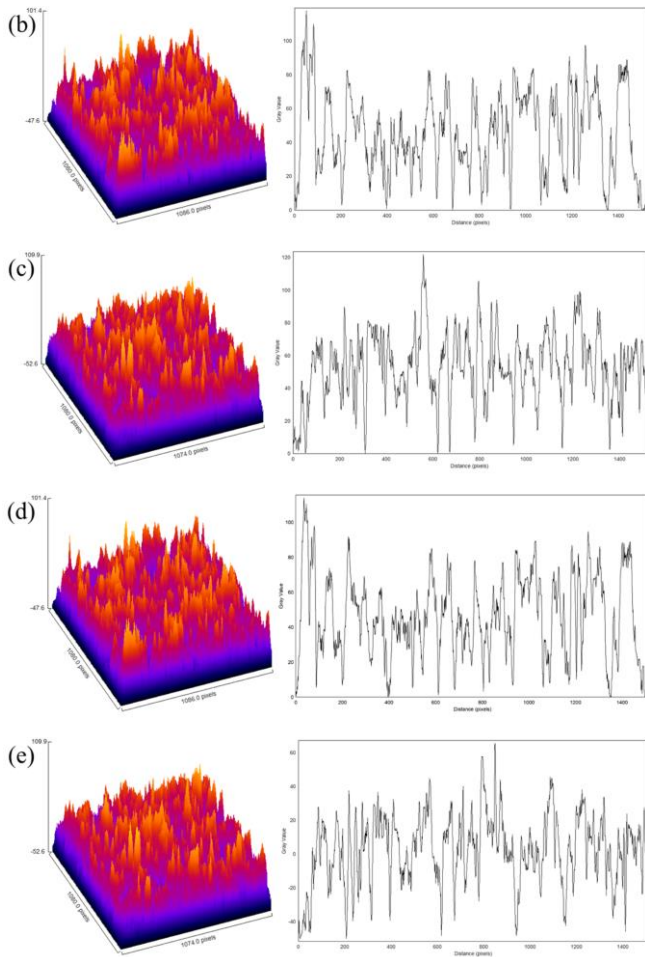


Fig. 5. Roughness Cu layers: (a) CuR0; (b) CuRN50; (c) CuRN100; (d) CuRS50; and (e) CuRS100

Fig. 5 presents the roughness analyzed result from the SEM image using ImageJ software. CuR0, CuRN50, CuRN100, CuRS50, and CuRS100 samples have a surface roughness of 34.62, 18.00, 17.38, 18.60, and 16.58  $\mu\text{m}$ , respectively. Presenting a magnetic field rotation led to a decrease in the surface roughness of Cu film. More rotation could also decrease surface roughness, which perfectly agrees with a previous study [19]. Wang and Chen have found presenting a magnetic field with various rotating speeds could decrease surface roughness [16]. This behavior is probably due to additional MHD flow, which could enhance the Cu ions' movement, and which is in line with the deposition rate result. A higher deposition rate would be resulting in a higher nucleation rate, consequently producing a smooth surface morphology. Moreover, the sample was made by north pole magnet influence has more roughness than sample was made by north pole magnet. This behavior probably due to MHD effect which could enhance the hydrogen evolution and resulting more roughness [11].

### 3.3. X-ray diffraction

The diffraction patterns of samples of Cu deposition on substrates composed of Al alloy plates are shown in Fig. 6. The five samples were identified to have Cu phase peaks at the indexed plane peaks (111), (200), (220), (311), and (222)

at angles  $2\theta = 43.31, 50.45, 74.13, 89.94,$  and  $95.15^\circ$ . The cubic crystal system is present in the Cu phase, and it has a space group of  $fm-3m$ . The cubic Cu phase peaks at these angles are consistent with findings from studies by Omar and Francisco Briones *et al.* [21,22]. This demonstrates that the procedure for depositing Cu on Al alloy plates has been successfully completed. At the indexed plane peaks (111), (200), (220), (311), and (400) of the five diffraction patterns, they were also found on the Al alloy plate substrate along with the copper phase. Xu *et al.* and Ayieko *et al.* presented a standard Al diffraction pattern that is identical to this peak of Al [23,24].

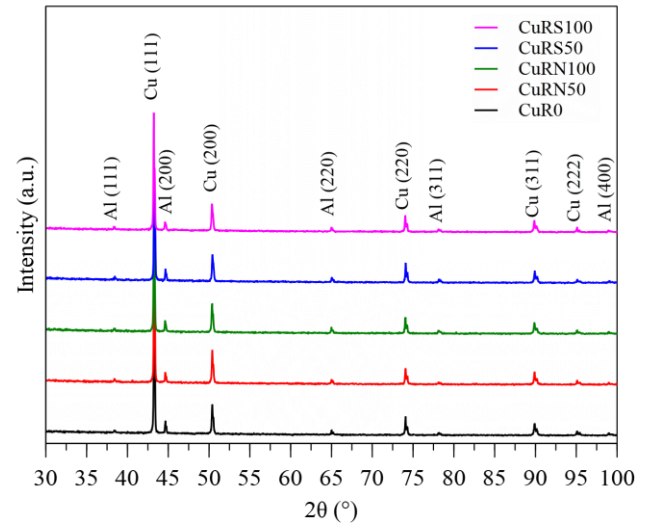


Fig. 6. X-ray diffraction pattern of various sample

Table 2. Crystallographic data calculated from various samples

Source	CuR0	CuRN50	CuRN100	CuRS50	CuRS100
Name: Copper (Cu)					
Space group: F m -3 m (225)					
Crystal system: cubic					
Lattice -a (nm)	0.3615	0.3615	0.3615	0.3615	0.3615
wRp (%)	10.10	10.37	10.24	9.86	10.30
GoF	1.067	1.106	1.087	1.045	1.056
Mean crystallite size (nm)	308	173	154	173	126
Micro-strain (%)	0.07	0.05	0.05	0.05	0.04

The mean crystallite size and lattice value of the five deposition samples are compared in order to further analyze the diffraction pattern. The Rietveld method was employed to determine the lattice of the five samples. The cubic Cu phase lattice of all five samples is measured at 0.3615 nm according to the calculation results. Changes in magnetic poles and rotating speed have no effect on the lattice value of the cubic Cu phase. The data from the crystallographic calculation can be found in Table 2. In order to determine the mean crystallite size, the Williamson-Hall plot method is utilised. In contrast

to the lattice value, the mean crystallite size is affected by the rotating speed and poles. The mean crystallite size becomes finer with the increase in magnet rotation speed which is in perfectly math with surface roughness analysis.

### 3.4. Antibacterial Activity

Antibacterial activity test after 24 hours of contact can be seen in Fig. 7. Material placement in the middle of Mueller Hinton agar inoculated with *S. aureus* ATCC 25923. Notice the inhibition zones around the material; the calculation is presented in Table 3. The metal ions diffuse into the agar to inhibit the growth of *S. aureus*.

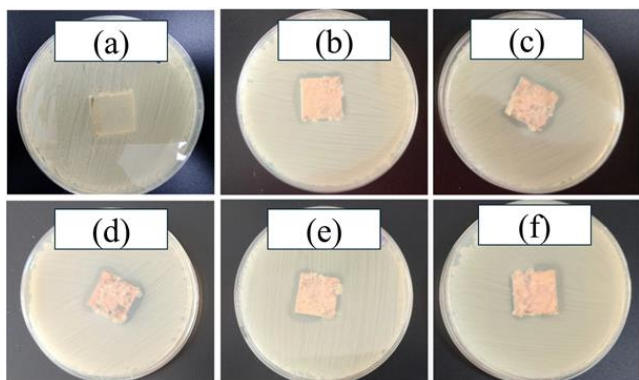


Fig. 7. Antibacterial activity test after 24-hour: (a) blank; (b) CuRN50; (c) CuRN100; (d) CuR0; (e) CuRS50; and (f) CuRS100

Cu, particularly in the form of metal-organic frameworks (MOFs) and nanoparticles, exhibits significant antibacterial activity against Gram-positive bacteria such as *S. aureus*. The peptidoglycan layer in Gram-positive bacteria plays a significant role in their susceptibility to Cu, although its direct interaction with Cu is not as straightforward as with other antimicrobial agents. Cu can induce modifications in the peptidoglycan layer, such as increased cross-linkage, which can affect the overall structure and function of the cell wall. These modifications can either enhance or reduce the susceptibility of Gram-positive bacteria to Cu, depending on the specific bacterial strain and environmental conditions [25,26]. In this research, the Cu induces contact killing. The antimicrobial activity of Cu is believed to involve contact-mediated killing, initiating membrane degradation. The susceptibility of Gram-positive strains to Cu is attributed to the thick peptidoglycan layer, which reduces cell wall permeability to other metal ions, including Zinc [27].

According to Fig. 7, the inoculum was totally annihilated by electroplated materials. The log reduction is not calculated due to the total killing of the bacteria. However, the total reduction of  $> 105$  CFU/mL might suggest a percentage reduction of  $> 99.999\%$  (see Table 3). Moreover, there is a zone of inhibition between the sample and bacterial lawn. Also visible inside the zone's white crystals and some bluish color change inside the agar. This suggests the Cu material diffused and interacted with the agar, resulting in a zone of bacterial growth inhibition.

As seen in Table 3, the widest diffusion zone is observed in CuR0 with the zone of diffusion and inhibition areas of 6.99

cm<sup>2</sup> and 2.5 cm<sup>2</sup>. This is statistically significant with  $p < 0.001$  (ANOVA; CI 95%). There is also significance in independent T-Test analyses between CuR0 and CuR50 group ( $p < 0.001$ ; CI 95%), R0 and R100 group ( $p < 0.001$ ; CI 95%), also between CuR50 and CuR100 Group ( $p < 0.001$ ; CI 95%). To investigate whether there is significance between the polarities of the magnets, independent T-test analyses were performed. There is no significance in the difference of outcome between the south pole group and north pole group ( $p=0.063$ ; CI 95%). The blank group did not show any inhibitions at all, the bacteria grew underneath the metal.

Table 3. The reduction of colony, and diffusible metal observation

Sample	Microbial reduction assessment		Diffusible metal observation	
	Initial load 0 h (CFU/mL)	Final load 24 h (CFU/mL)	Zone of diffusion (cm <sup>2</sup> )	Inhibition area (cm <sup>2</sup> )
Blank		0	4.01 $\pm$ 0.01	-0.48 $\pm$ 0.01
CuR0		0	6.99 $\pm$ 0.12	2.50 $\pm$ 0.56
CuRN50	$3.5 \times 10^5$	0	6.21 $\pm$ 0.01	1.61 $\pm$ 0.21
CuRN100		0	6.00 $\pm$ 0.02	1.89 $\pm$ 0.02
CuRS50		0	6.16 $\pm$ 0.41	1.73 $\pm$ 0.46
CuRS100		0	6.17 $\pm$ 0.01	2.14 $\pm$ 0.24

The use of magnetic rotation during material synthesis has a significant impact on the results. Materials synthesized without magnetic rotation (R0) show stronger antibacterial effects compared to those synthesized at 50 rpm or 100 rpm. However, increasing the magnet rotation notably enhances the size of the inhibition zone. As a result, the inhibition zone at 100 rpm is larger than that at 50 rpm. This condition is probably due to forming some oxygen on the Cu films surface as seen in EDS result which could disrupt transformation Cu to be Cu ions. Qu *et al.* has found that antibacterial behavior was influenced by Cu ions [28]. Release of Cu ions inside of the agar is lethal towards *S. aureus* [29].

Moreover, the generation of reactive oxygen species (ROS) and damage to cell membranes are the main ways in which metals' broad antibacterial potential has been extensively studied. Even so, metals can target particular cellular components and, when combined, are likely to improve pathogen clearance despite their non-specific activity. Conversely, Cu has the ability to change metabolic pathways in addition to causing damage to DNA and cell membranes through the generation of ROS. The combined mode of action has not yet been investigated, to the authors' knowledge, despite the fact that the modes of action of various metal ions have been well explored. The variability in antimicrobial efficaciousness between various combinations can be explained by the diverse chemical reactivity of metal ions with bacterial cells and their specific biological targets [30].

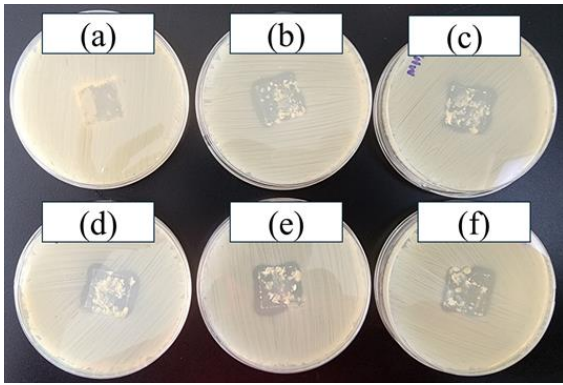


Fig. 8. After 24 hours of post contact test: (a) blank; (b) CuRN50; (c) CuRN100; (d) CuR0; (e) CuRS50; and (f) CuRS100

Fig. 8 shows the results after 24 hours of post-contact testing. The inhibitory zones appear after the removal of the material. Notice that there is some metal infiltrations inside of the agar on every plate. The infiltration causes the agar to crack. This suggests that there is a gas-forming or exothermic reaction inside of the agar, increasing the antimicrobial ability of the oligodynamic material. There are no anti-Staphylococcal effects on the blank material; therefore, there is a regrowth of microorganisms in the place where the metal was previously placed.

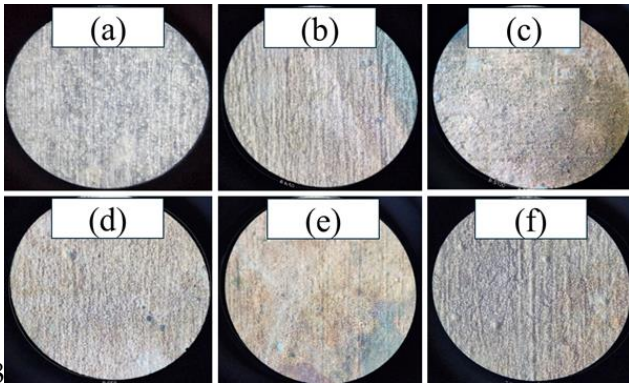


Fig. 9. Antibacterial activity pretest microscope observation: (a) blank; (b) CuRN50; (c) CuRN100; (d) CuR0; (e) CuRS50; and (f) CuRS100

Fig. 9 shows antibacterial activity pretest microscope observation, and Fig. 10 shows antibacterial activity post-test microscope observation. Microscopic observation of electroplated surfaces occurs under  $180 \times$  magnification optical microscope. There is a significant proportion in the formation of white crystals on the electroplated surface after tests. The crystals did not form on the surface of the blank. The Cu forms oxides, which change the color of the surface.

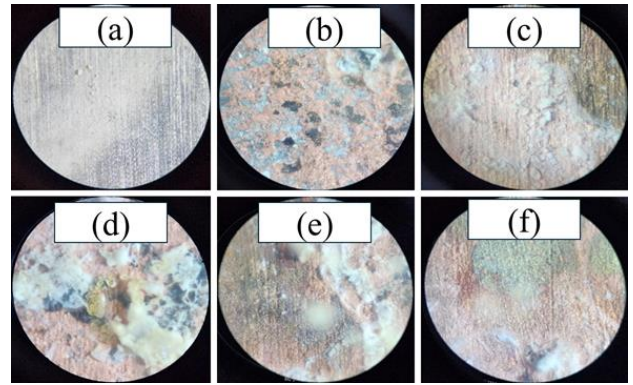


Fig. 10. Antibacterial activity post-test microscope observation: (a) blank; (b) CuRN50; (c) CuRN100; (d) CuR0; (e) CuRS50; and (f) CuRS100

### 3.5. Corrosion Test

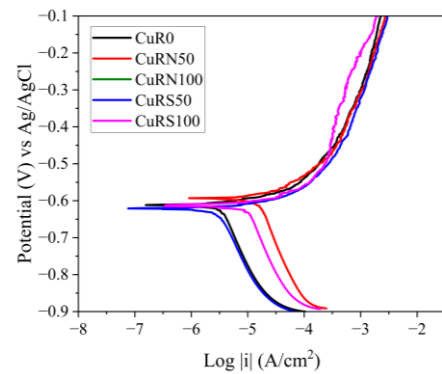


Fig. 10. Potentiodynamic polarization test curve

Fig. 10 represents potentiodynamic polarization test result in 0.9 % NaCl. Tafel extrapolation result could be seen in Table 4. Using Eq. (5) corrosion rate could be calculated and summarized in Table 4.

Table 4. Tafel extrapolation result and corrosion rate

Sample name	E <sub>corr</sub> (V) vs Ag/AgCl	I <sub>corr</sub> (A/cm <sup>2</sup> )	Corrosion rate (mpy)
CuR0	-0.612	$3.550 \times 10^{-6}$	1.624
CuRN50	-0.594	$2.010 \times 10^{-5}$	9.179
CuRN100	-0.599	$9.640 \times 10^{-6}$	4.408
CuRS50	-0.621	$2.620 \times 10^{-6}$	1.196
CuRS100	-0.614	$8.810 \times 10^{-6}$	4.026

Based on Table 4, it can be seen that when the electrodeposition process is influenced by a magnet that rotates with the north pole, it will increasingly shift the potential value to the positive direction. Meanwhile, when the electrodeposition process is influenced by a magnet that rotates with the south pole, it will increasingly shift the potential value towards the negative. The sample with the lowest corrosion rate is the CuRS50 sample probably due to higher oxygen on the Cu surface that could forming an oxide [31]. Therefore, that oxide could result in better protection from aggressive species in the 0.9 % NaCl medium.



#### 4. Conclusion

The Cu films were fabricated under a spinning magnetic field with various rotation speeds, and a magnetic pole was successfully conducted. Higher rotation speed is promoted to enhanced deposition rate and current efficiency for both magnetic poles. The Cu sample was fabricated with an un-present spinning magnetic influence, which led to the forming morphology near the spheroidal. Cu samples were made with spinning magnetic influence, which led to the forming morphology near the faceted structure. Magnetic-assisted spinning at 50 rpm led to oxygen forming on the Cu surface for both magnetic poles and enhanced rotation, which led to the decrease or disappearance of oxygen. Presenting and more of a magnetic field rotation led to decreased surface roughness and crystallite size of Cu film for both magnetic poles. The Cu sample was made without spinning magnetic and has the highest inhibition zone size, probably due to no oxygen on the Cu film surface. The sample with the lowest corrosion rate is the CuRS50 sample probably due to higher oxygen on the Cu surface that could form an oxide. Generally, Cu films successfully covered Al alloy and could transform it into oligodynamic material. Future recommendations in the present study are conducting electrodeposition of Cu with influencing rotation magnetic higher than 100 rpm.

#### Acknowledgements

This study has been supported by the Ministry of Education, Culture, Research, and Technology through grand funding Penelitian Fundamental-Reguler with contract number 087/LPPM-UNAS/VI/2024 and 815/LL3/AL.04/2024.

#### References

1. D. A. Lytle and C. P. White, *The effect of phosphate on the properties of copper drinking water pipes experiencing localized corrosion*, J. Fail. Anal. Prev. 14 (2014) 203–219.
2. M. M. Lachowicz, *A metallographic case study of formicary corrosion in heat exchanger copper tubes*, Eng. Fail. Anal. 111 (2020) 104502.
3. N. Thokala, C. Kealey, J. Kennedy, D. B. Brady and J. B. Farrell, *Characterisation of polyamide 11/copper antimicrobial composites for medical device applications*, Mater. Sci. Eng. C 78 (2017) 1179–1186.
4. A. Augustin, P. Huilgol, K. R. Udupa and U. B. K., *Effect of current density during electrodeposition on microstructure and hardness of textured Cu coating in the application of antimicrobial Al touch surface*, J. Mech. Behav. Biomed. Mater. 63 (2016) 352–360.
5. I. S. Brandt, M. A. Tumelero, S. Pelegrini, G. Zangari and A. A. Pasa, *Electrodeposition of Cu<sub>2</sub>O: growth, properties, and applications*, J. Solid State Electrochem. 21 (2017) 1999–2020.
6. A. Antenucci, S. Guarino, V. Tagliaferri and N. Ucciardello, *Improvement of the mechanical and thermal characteristics of open cell aluminum foams by the electrodeposition of Cu*, Mater. Des. 59 (2014) 124–129.
7. H. A. Murdoch, D. Yin, E. Hernández-Rivera and A. K. Giri, *Effect of applied magnetic field on microstructure of electrodeposited copper*, Electrochem. commun. 97 (2018) 11–15.
8. Q. Long, Y. Zhong and J. Wu, *Research progress of magnetic field techniques for electrodeposition of coating*, Int. J. Electrochem. Sci. 15 (2020) 8026–8040.
9. K. Kołodziejczyk, et al., *Influence of constant magnetic field on electrodeposition of metals, alloys, conductive polymers, and organic reactions*, J. Solid State Electrochem. 22 (2018) 1629–1674.
10. B. Soegijono, F. B. Susetyo, Yusmaniar and M. C. Fajrah, *Electrodeposition of paramagnetic copper film under magnetic field on paramagnetic aluminum alloy substrates*, e-Journal Surf. Sci. Nanotechnol. 18 (2020) 281–288.
11. D. Yin, H. A. Murdoch, B. Chad Hornbuckle, E. Hernández-Rivera and M. K. Dunstan, *Investigation of anomalous copper hydride phase during magnetic field-assisted electrodeposition of copper*, Electrochem. commun. 98 (2019) 96–100.
12. M. Miura, et al., *Magneto-Dendrite Effect: Copper Electrodeposition under High Magnetic Field*, Sci. Rep. 7 (2017) 1–8.
13. S. V. Kovalyov, O. B. Girin, C. Debiemme-Chouvy and V. I. Mishchenko, *Copper electrodeposition under a weak magnetic field: effect on the texturing and properties of the deposits*, J. Appl. Electrochem. 51 (2021) 235–243.
14. Y. Liu, et al., *Magnetic field intensified electrodeposition of low-concentration copper ions in aqueous solution*, Electrochim. Acta 432 (2022) 141201.
15. Sudibyo, M. B. How and N. Aziz, *Influences of magnetic field on the fractal morphology in copper electrodeposition*, in IOP Conference Series: Materials Science and Engineering, 285 (2018), pp. 012021.
16. T. Wang and W. Chen, *Effects of Rotating Magnetic Fields on Nickel Electro-Deposition*, ECS Electrochem. Lett. 4 (2015) D14–D17.
17. R. Ji, et al., *Preparation of Ni-SiC nano-composite coating by rotating magnetic field-assisted electrodeposition*, J. Manuf. Process. 57 (2020) 787–797.
18. S. Syamsuir, F. B. Susetyo, B. Soegijono, S. D. Yudanto, Basori and D. Nanto, *Nickel layers properties produced by electroplating were influenced by spinning permanent magnet*, in Journal of Physics: Conference Series, 2596 (2023), pp. 012008.
19. Syamsuir, et al., *Rotating-Magnetic-Field-Assisted Electrodeposition of Copper for Ambulance Medical Equipment*, Automot. Exp. 6 (2023) 290–302.
20. A. C. Larson and R. B. Von Dreele, *General Structure Analysis System (GSAS)*, Vol. 748, University of California, Los Alamos, 2004.
21. H. D. Omar, *Intensity Correction and Pole Figure Measurement of Copper Metallic by XRD*, J. Basic Appl. Sci. 12 (2016) 320–322.
22. F. Briones, V. Seriacopi, C. Martínez, J. L. Valin, D. Centeno and I. F. Machado, *The effects of pressure and pressure routes on the microstructural evolution and mechanical properties of sintered copper via SPS*, J. Mater. Res. Technol. 25 (2023) 2455–2470.
23. X. Xu, et al., *Effect of Mn content on microstructure and properties of 6000 series aluminum alloy*, Appl. Phys. A Mater. Sci. Process. 125 (2019) 1–9.
24. C. O. Ayieko, R. J. Musembi, A. A. Ogacho, B. O. Aduda, B. M. Muthoka and P. K. Jain, *Controlled Texturing of Aluminum Sheet for Solar Energy Applications*, Adv. Mater. Phys. Chem. 05 (2015) 458–466.

25. S. J. Kim, J. Chang and M. Singh, *Peptidoglycan architecture of Gram-positive bacteria by solid-state NMR*, Biochim. Biophys. Acta - Biomembr. 1848 (2015) 350–362.
26. X. Chen, et al., *Class A Penicillin-Binding Protein C Is Responsible for Stress Response by Regulation of Peptidoglycan Assembly in Clavibacter michiganensis*, Microbiol. Spectr. 10 (2022) .
27. S. Khafa, et al., *Copper and Zinc Metal–Organic Frameworks with Bipyrazole Linkers Display Strong Antibacterial Activity against Both Gram+ and Gram– Bacterial Strains*, Molecules 28 (2023) 6160.
28. X. Qu, H. Yang, B. Jia, Z. Yu, Y. Zheng and K. Dai, *Biodegradable Zn–Cu alloys show antibacterial activity against MRSA bone infection by inhibiting pathogen adhesion and biofilm formation*, Acta Biomater. 117 (2020) 400–417.
29. L. Huang, E. M. Fozo, T. Zhang, P. K. Liaw and W. He, *Antimicrobial behavior of Cu-bearing Zr-based bulk metallic glasses*, Mater. Sci. Eng. C 39 (2014) 325–329.
30. F. N. S. Raja, T. Worthington and R. A. Martin, *The antimicrobial efficacy of copper, cobalt, zinc and silver nanoparticles: alone and in combination*, Biomed. Mater. 18 (2023) 045003.
31. C. Zheng, J. Cao, Y. Zhang and H. Zhao, *Insight into the Oxidation Mechanism of a Cu-Based Oxygen Carrier ( $\text{Cu} \rightarrow \text{Cu}_2\text{O} \rightarrow \text{CuO}$ ) in Chemical Looping Combustion*, Energy and Fuels 34 (2020) 8718–8725.



Outlook

---

## [CST] Submission Acknowledgement

---

**From** Communications in Science and Technology (CST) <journal-noreply@kipmi.or.id>

**Date** Thu 9/26/2024 4:31 PM

**To** Ruliyanta <ruliyanto@civitas.unas.ac.id>; Maman Kartaman Ajiriyanto <mama014@brin.go.id>; Rosika Kriswarini <rosi004@brin.go.id>; Heri Hardiyanti <heri016@brin.go.id>; Cahaya Rosyidan <cahayarosyidan@trisakti.ac.id>; Sigit Dwi Yudanto <sigi012@brin.go.id>; Evi Ulina Margaretha Situmorang <evi.situmorang@atmajaya.ac.id>; Daniel Edbert <daniel.edbert@atmajaya.ac.id>; Dwi Nanto <dwi.nanto@uinjkt.ac.id>; fbudhi@unj.ac.id <fbudhi@unj.ac.id>

Hello,

Basori Basori has submitted the manuscript, "Rotating speed and magnetic pole dependency assisted on copper deposition onto aluminum alloy substrate for bacterial eradication application" to Communications in Science and Technology.

If you have any questions, please contact me. Thank you for considering this journal as a venue for your work.

Communications in Science and Technology

The following message is being delivered on behalf of Communications in Science and Technology.

---

**Komentar  
Reviewer atau  
Editor 1**



---

**[CST] Editor Decision**

---

**From** Meilana Dharma Putra (CST) <journal-noreply@kipmi.or.id>

**Date** Tue 11/5/2024 3:35 PM

**To** Basori Basori <basori@civitas.unas.ac.id>; Ruliyanta <ruliyanto@civitas.unas.ac.id>; Maman Kartaman Ajiriyanto <mama014@brin.go.id>; Rosika Kriswarini <rosi004@brin.go.id>; Heri Hardiyanti <heri016@brin.go.id>; Cahaya Rosyidan <cahayarosyidan@trisakti.ac.id>; Sigit Dwi Yudanto <sigi012@brin.go.id>; Evi Ulina Margaretha Situmorang <evi.situmorang@atmajaya.ac.id>; Daniel Edbert <daniel.edbert@atmajaya.ac.id>; Dwi Nanto <dwi.nanto@uinjkt.ac.id>; fbudhi@unj.ac.id <fbudhi@unj.ac.id>

Dear Authors,

Thank you for considering Communications in Science and Technology.

Please see the comments of the reviewers on the article entitled: "Rotating speed and magnetic pole dependency assisted on copper deposition onto aluminum alloy substrate for bacterial eradication application". I suggest you consider these comments, suggestions and questions and revise your article accordingly. The revised version of your submission is due by November 19, 2024.

For your guidance, reviewers' comments are appended below.

If you decide to revise the work, please submit a list of changes or a rebuttal against each point which is being raised and highlight the changes in manuscript when you submit the revised manuscript.

To submit a revision, please go to <https://cst.kipmi.or.id/> (login as an Author) within 14 days; after this time the manuscript will be considered as withdrawn.

For your information, submitting a revision to the journal does not guarantee acceptance of the manuscript, as it will undergo a second review.

Yours sincerely,

Meilana Dharma Putra  
Editor-in-Chief  
Communications in Science and Technology

#####

Editor:

1. Professional English editing by Publisher of CST should be assigned after the manuscript is accepted.
2. There are no citations of articles published in CST, suggesting limited relevance to the journal.

Reviewer #1:

1. The manuscript covers a potentially significant area of copper deposition on aluminum alloy substrates for antibacterial applications. However, the objectives of the study are presented ambiguously. The lack of clarity in the rationale for selecting specific rotation speeds and magnetic poles hampers the study's scientific impact. The authors should provide a clear justification for the choice of rotation speeds and pole conditions and specify how these align with the study's objectives. Additionally, more context on how these factors relate to the desired antibacterial

properties would strengthen the study's rationale.

2. While the study highlights that rotating magnetic fields and rotation speeds influence deposition morphology and corrosion rates, the link between these morphological changes and antibacterial efficacy remains underexplored. The authors should include a comprehensive analysis or discussion that explains how the surface morphology (spheroidal vs. faceted) and oxygen content impact bacterial inhibition. Furthermore, it would be helpful if the authors could quantitatively compare the antibacterial effectiveness of their Cu-coated samples with existing antibacterial coatings in the literature.

3. Several quantitative measurements, such as deposition rate and inhibition zone, are presented but lack accompanying statistical validation. Please conduct statistical analysis (e.g., ANOVA or t-tests) to confirm the significance of these findings. This analysis is essential to reinforce claims about optimal conditions, such as "CuRS50 having the lowest corrosion rate."

4. The manuscript requires substantial editing for clarity and readability, as several sections are confusing due to awkward phrasing and syntax. The authors should revise the manuscript to improve clarity and ensure that terms, such as "oligodynamic material," are defined precisely for accessibility.

Reviewer #2:

1. The study's novelty is limited, as the primary parameters (rotation speed and magnetic pole) have been previously explored in electrodeposition contexts. The authors should provide a stronger explanation of how their study advances current knowledge. Further, there is limited discussion on previous studies that used similar conditions, which would have helped place this work in the context of existing literature. Specifically, more references to recent studies on antibacterial coatings or similar deposition methods would enhance the study's relevance and highlight its contributions.

2. There appears to be inconsistency between the hypothesis and the methodology used. For instance, the rationale behind using only a two-pole magnetic setup is unclear, and the role of rotation speed as it relates to antibacterial activity is insufficiently explored. Without a clear hypothesis tying the observed results to antibacterial applications, the study lacks the focus needed for publication. To ensure future acceptance, the authors should design experiments that systematically explore how the magnetic field and rotation speed influence antibacterial properties and provide sufficient data to support each conclusion.

3. The results section lacks depth, as the authors mainly present raw data without thorough interpretation. For instance, the claim that "increased rotation speed increases deposition rate" is not discussed in relation to how this impacts overall coating quality or durability under bacterial exposure. Additionally, essential data such as comparative IC50 values for bacterial inhibition are missing. This information is critical for assessing the practical implications of this research.

4. The manuscript contains numerous grammatical errors and unclear sentences that hinder comprehension, such as the vague description of "oligodynamic materials" and "spherical versus faceted structures." I recommend significant revisions to the language and logical flow to improve scientific rigor.

The following message is being delivered on behalf of Communications in Science and Technology.

---

**Respon 1**

Title : Rotating speed and magnetic pole dependency assisted on copper deposition onto aluminum alloy substrate for bacterial eradication application

Authors : Basori, Ruliyanta, Maman Kartaman Ajiriyanto, Rosika Kriswarini, Heri Hardiyanti, Cahaya Rosyidan, Sigit Dwi Yudanto, Evi Ulina Margareta Situmorang, Daniel Edbert, Dwi Nanto, Ferry Budhi Susetyo

Corresponding author : Basori

#Editorial Office of Communications in Science and Technology

1. Professional English editing by Publisher of CST should be assigned after the manuscript is accepted.
2. There are no citations of articles published in CST, suggesting limited relevance to the journal.

**Response:**

1. We are grateful and agree with this policy. Thank you.
2. Three published papers in the Communications in Science and Technology journal have been cited (DOI: 10.21924/cst.5.1.2020.177, 10.21924/cst.8.2.2023.1280, and 10.21924/cst.9.1.2024.1442). Thank you.

**Reviewer #1:**

No.	Comment from Reviewer	Author Response
1	The manuscript covers a potentially significant area of copper deposition on aluminum alloy substrates for antibacterial applications. However, the objectives of the study are presented ambiguously. The lack of clarity in the rationale for selecting specific rotation speeds and magnetic poles hampers the study's scientific impact. The authors should provide a clear	<p>Thank you. We appreciated about this constructive comment.</p> <p>Reason for rotation and magnetic pole has mentioned in the introduction section as follow:</p> <p>“The use of a magnetic field during electrodeposition can influence the movement of ions towards the cathode surface. Adjusting magnetic field rotation during electrodeposition also influences the movement of ions. Furthermore, the different poles of the magnet selected also influence ion movement at</p>



	<p>justification for the choice of rotation speeds and pole conditions and specify how these align with the study's objectives. Additionally, more context on how these factors relate to the desired antibacterial properties would strengthen the study's rationale.</p>	<p>electrodeposition process. Generally, the ions' movement speed could affect the forming film's properties. According to the literature review above, higher rotation was used (<math>\geq 500</math> rpm) to influence the electrodeposition; therefore, the present study used 50 and 100 rpm. Syamsuir <i>et al.</i> used one piece of neodymium magnet arranged to spread five parts in the upside Teflon [25]. Therefore, the present research used more neodymium magnets to result in more influence of the magnetic field. Moreover, the influence of spinning using different magnetic poles was also not considered. Murdoch <i>et al.</i> found that different magnetic poles influenced the deposition process, resulting in different surface morphologies in Cu films [13]. Therefore, the present research comprehensively investigated the influence of the rotating speed and magnetic pole during Cu electrodeposition on the formation of the film for bacterial eradication applications.”</p> <p>More context about antibacterial properties has been added in the introduction section as follow:</p> <p>“Oxygen content on the Cu film surface could disrupt the transformation of Cu to Cu ions, reducing antibacterial performance [26]. The formation of surface morphology could have an impact on the antibacterial performance. Surface morphology, such as spheroidal and faceted structures, also contributed to the inhibition zone. A Cu film with spheroidal coating tends to create a higher inhibition zone [25].”</p> <p>And</p> <p>“The use of a magnetic field can influence the movement of ions towards the cathode surface. Adjusting magnetic field rotation also influences the movement of ions. Furthermore, the different poles of the magnet selected also influence ion movement. Generally, the ions' movement speed could affect the forming film's properties.”</p>
2	<p>While the study highlights that rotating magnetic fields and rotation speeds influence deposition morphology and corrosion rates, the link between these morphological changes and antibacterial efficacy remains underexplored. The authors should include a comprehensive</p>	<p>Thank you. We appreciated about this constructive comment.</p> <p>Several discussions have been added in the antibacterial Activity section as follows:</p> <p>“However, increasing magnet rotation significantly enhances the size of the inhibition zone. As a result, the inhibition zone at 100 rpm is larger than that at 50</p>

	<p>analysis or discussion that explains how the surface morphology (spheroidal vs. faceted) and oxygen content impact bacterial inhibition. Furthermore, it would be helpful if the authors could quantitatively compare the antibacterial effectiveness of their Cu-coated samples with existing antibacterial coatings in the literature.</p>	<p>rpm. This condition is probably due to forming some oxygen on the Cu films surface as seen in EDS result which could disrupt transformation Cu to be Cu ions. Qu <i>et al.</i> has found that antibacterial behavior was influenced by Cu ions [26]. Release of Cu ions inside of the agar is lethal towards <i>S. aureus</i> [40].”</p> <p>“As shown in Fig. 3, CuR0 surface morphology has formed near to spheroidal, while other samples have form faceted structure. Compared to Table 3, it can be seen that higher inhibition zone is seen in CuR0 sample. Therefore, it can be concluded that the spheroidal form results in the highest inhibition zone than the faceted structure, which is perfectly in agreement with previous study [25]. This condition probably occurs due to the spheroidal structure having a wider surface area than the faceted structure, which results in more Cu ions being released. Moreover, an increase in rotation leads to a decrease in roughness. Several researchers have found that roughness is independent of the inhibition zone which aligns with the present study [25,41].”</p> <p>“Cu as film has higher bacterial kill performance than bulk Cu [4].”</p>
3	<p>Several quantitative measurements, such as deposition rate and inhibition zone, are presented but lack accompanying statistical validation. Please conduct statistical analysis (e.g., ANOVA or t-tests) to confirm the significance of these findings. This analysis is essential to reinforce claims about optimal conditions, such as "CuRS50 having the lowest corrosion rate."</p>	<p>Thank you. We appreciated about this constructive comment.</p> <p>Commonly statistic validation for deposition rate is standard deviation. Therefore, we added error bar in Figure 2.</p> <p>Moreover, statistical analysis has been conducted in inhibition zone:</p> <p>“As seen in Table 3, the widest diffusion zone is observed in CuR0 with the zone of diffusion and inhibition areas of 6.99 cm<sup>2</sup> and 2.5 cm<sup>2</sup>. This is statistically significant with <math>p &lt; 0.001</math> (ANOVA; CI 95%). There is also significance in independent T-Test analyses between CuR0 and CuR50 group (<math>p &lt; 0.001</math>; CI 95%), R0 and R100 group (<math>p &lt; 0.001</math>; CI 95%), also between CuR50 and CuR100 Group (<math>p &lt; 0.001</math>; CI 95%). To investigate whether there is significance between the polarities of the magnets, independent T-test analyses were performed. There is no significant difference in the outcome between the south pole group and the north pole group (<math>p=0.063</math>; CI 95%). Moreover, there were no inhibitions in the blank group, and the bacteria grew underneath the metal.”</p>

		For corrosion behavior, it seems the data is not well tested. If the sample were retested, it will take a long time because of the queue to carry out the electrochemical test. The revision deadline given by the editor is 19 <sup>th</sup> November 2024. Moreover, focused on the present study is fabricated the Cu using electrodeposition process then characterize and tested in bacterial. For that reason, corrosion behavior was deleted.
4	The manuscript requires substantial editing for clarity and readability, as several sections are confusing due to awkward phrasing and syntax. The authors should revise the manuscript to improve clarity and ensure that terms, such as “oligodynamic material,” are defined precisely for accessibility.	Thank you. We appreciated about this constructive comment. Oligodynamic material has been revised. Moreover, if this manuscript accepted, professional English editing by Publisher of CST would be conducting.

## Reviewer #2:

No.	Comment from Reviewer	Author Response
1	The study's novelty is limited, as the primary parameters (rotation speed and magnetic pole) have been previously explored in electrodeposition contexts. The authors should provide a stronger explanation of how their study advances current knowledge. Further, there is limited discussion on previous studies that used similar conditions, which would have helped place this work in the context of existing literature. Specifically, more references to recent studies on antibacterial coatings or similar deposition methods would enhance the study's relevance and highlight its contributions.	<p>Thank you. We appreciated about this constructive comment.</p> <p>Novelty has been revised to:</p> <p>“The use of a magnetic field during electrodeposition can influence the movement of ions towards the cathode surface. Adjusting magnetic field rotation during electrodeposition also influences the movement of ions. Furthermore, the different poles of the magnet selected also influence ion movement at electrodeposition process. Generally, the ions' movement speed could affect the forming film's properties. According to the literature review above, higher rotation was used (<math>\geq 500</math> rpm) to influence the electrodeposition; therefore, the present study used 50 and 100 rpm. Syamsuir <i>et al.</i> used one piece of neodymium magnet arranged to spread five parts in the upside Teflon [25]. Therefore, the present research used more neodymium magnets to result in more influence of the magnetic field. Moreover, the influence of spinning using different magnetic poles was also not considered. Murdoch <i>et al.</i> found that different magnetic poles influenced the deposition process, resulting in different surface morphologies in Cu films [13]. Therefore, the present research</p>

		<p>comprehensively investigated the influence of the rotating speed and magnetic pole during Cu electrodeposition on the formation of the film for bacterial eradication applications.”</p> <p>Moreover, previous study that used similar condition have been added:</p> <p>“Augustin <i>et al.</i> investigated the effect of current density at Cu electrodeposition on the microstructure, hardness, and antibacterial activity of Cu for antimicrobial Al touch application [4]. Kuisor <i>et al.</i> fabricated CuO film using electrodeposition. Then, the film was tested for antibacterial activity using <i>Staphylococcus aureus</i> (<i>S. aureus</i>), which successfully reduced the bacterial colony during the experiment [11]. Isa <i>et al.</i> performed electrodeposition Cu over 304 stainless steels, and a coated sample was tested for antibacterial properties. At 10 minutes of exposure to the coated sample, a 100% reduction of <i>S. aureus</i> was successfully achieved [12].”</p> <p>And</p> <p>“Oxygen content on the Cu film surface could disrupt the transformation of Cu to Cu ions, reducing antibacterial performance [26]. The formation of surface morphology could have an impact on the antibacterial performance. Surface morphology, such as spheroidal and faceted structures, also contributed to the inhibition zone. A Cu film with spheroidal coating tends to create a higher inhibition zone [25].”</p>
2	<p>There appears to be inconsistency between the hypothesis and the methodology used. For instance, the rationale behind using only a two-pole magnetic setup is unclear, and the role of rotation speed as it relates to antibacterial activity is insufficiently explored. Without a clear hypothesis tying the observed results to antibacterial applications, the study lacks the focus needed for publication. To ensure future acceptance, the authors should design experiments that systematically explore how the magnetic field and rotation speed influence antibacterial properties</p>	<p>Thank you. We appreciated about this constructive comment. Our response as follows.</p> <p>Generally, the magnetic field is presented to influence the ion movement to the cathode surface. Adjusting the magnetic field rotation also influences ion movement. Furthermore, the different pole of the magnet selected also influences ion movement. The ions' movement speed could affect the forming film's properties. Moreover, oxygen content on the Cu film surface could disrupt the Cu transformation to Cu ions, reducing antibacterial performance. Another factor that could influence the antibacterial performance is the formation of surface morphology. Surface morphology formed, such as spheroidal and faceted structure, also contributed to the inhibition zone. A cu film with spheroidal tends to create a higher inhibition zone.</p>

	and provide sufficient data to support each conclusion.	
3	<p>The results section lacks depth, as the authors mainly present raw data without thorough interpretation. For instance, the claim that “increased rotation speed increases deposition rate” is not discussed in relation to how this impacts overall coating quality or durability under bacterial exposure. Additionally, essential data such as comparative IC50 values for bacterial inhibition are missing. This information is critical for assessing the practical implications of this research.</p>	<p>Thank you. We appreciated about this constructive comment.</p> <p>There is one factors were disrupting the deposition rate in the present study are magnetic field.</p> <p>“Cu films were made and influenced by the rotating south pole magnet, which has a higher deposition rate due to the magnetic field, which is parallel to the current direction and attracts more Cu ions onto the Al alloy surface [13]. Rotating the magnet under the electrolyte solution while the electrodeposition process was performed could induce an Eddy electric field [25]. The Eddy electric field could act as an additional MHD flow convection effect [22]. Moreover, increasing the rotation speed could attract more Cu ions onto the Al alloy surface, consequently increasing the deposition rate and current efficiency.”</p> <p>Moreover:</p> <p>“According to Fig. 3, it can be seen that the Cu sample was made with no spinning magnetic influence, which led to the formation of morphology near the spheroidal. Cu samples were made with spinning magnetic assistance, leading to the formation of faceted structure morphology [16]. Moreover, the transformation from spheroidal to faceted structure is influenced by the rate of deposition. A higher nucleation rate leads to a higher deposition rate, resulting in a variation in surface morphology [31]. Samples made with influences from the north pole magnetic field have a low nucleation rate, hence having wider grain sizes than samples made by influencing the south pole magnetic field [13]. Moreover, an increase in the deposition rate from 12.83 to 13.67 <math>\mu\text{m/h}</math> leads to a change in surface morphology near the spheroidal becoming faceted structure. The deposition rate between 13.67 and 14.51 <math>\mu\text{m/h}</math> results in a faceted structure of surface morphology.”</p> <p>Furthermore:</p> <p>“According to Fig. 4, the spinning magnetic-assisted running at 50 rpm led to oxygen forming on the Cu surface. Moreover, enhanced magnetic rotation led to a decrease or disappearance of oxygen. Presenting oxygen on Cu film is one of the unique cases. Oxygen could form due to a secondary reaction on the anode. Moreover, oxygen could be formed due to sample storage and transport [25].”</p>

		<p>Correlation between films with antibacterial as follows:</p> <p>“However, increasing magnet rotation significantly enhances the size of the inhibition zone. As a result, the inhibition zone at 100 rpm is larger than that at 50 rpm. This condition is probably due to forming some oxygen on the Cu films surface as seen in EDS result which could disrupt transformation Cu to be Cu ions. Qu <i>et al.</i> has found that antibacterial behavior was influenced by Cu ions [26]. Release of Cu ions inside of the agar is lethal towards <i>S. aureus</i> [40].</p> <p>As shown in Fig. 3, CuR0 surface morphology has formed near to spheroidal, while other samples have form faceted structure. Compared to Table 3, it can be seen that higher inhibition zone is seen in CuR0 sample. Therefore, it can be concluded that the spheroidal form results in the highest inhibition zone than the faceted structure, which is perfectly in agreement with previous study [25]. This condition probably occurs due to the spheroidal structure having a wider surface area than the faceted structure, which results in more Cu ions being released. Moreover, an increase in rotation leads to a decrease in roughness. Several researchers have found that roughness is independent of the inhibition zone which aligns with the present study [25,41].”</p>
4	<p>The manuscript contains numerous grammatical errors and unclear sentences that hinder comprehension, such as the vague description of “oligodynamic materials” and “spherical versus faceted structures.” I recommend significant revisions to the language and logical flow to improve scientific rigor.</p>	<p>Thank you. We appreciated about this constructive comment.</p> <p>If this manuscript accepted, professional English editing by Publisher of CST would be conducting.</p>

# Rotating speed and magnetic pole dependency assisted on copper deposition onto aluminum alloy substrate for bacterial eradication application

Basori<sup>a,\*</sup>, Ruliyanta<sup>b</sup>, Maman Kartaman Ajiriyanto<sup>c</sup>, Rosika Kriswarini<sup>c</sup>, Heri Hardiyanti<sup>c</sup>, Cahaya Rosyidan<sup>d</sup>, Sigit Dwi Yudanto<sup>e</sup>, Evi Ulina Margareta Situmorang<sup>f</sup>, Daniel Edbert<sup>g</sup>, Dwi Nanto<sup>h</sup>, Ferry Budhi Susetyo<sup>i</sup>

<sup>a</sup>Department of Mechanical Engineering, Universitas Nasional, Jakarta, 12520, Indonesia

<sup>b</sup>Department of Electrical Engineering, Universitas Nasional, Jakarta, 12520, Indonesia

<sup>c</sup>Research Center for Nuclear Material and Radioactive Waste Technology, National Research and Innovation Agency, Tangerang Selatan, 15314, Indonesia

<sup>d</sup>Department of Petroleum Engineering, Universitas Trisakti, Jakarta, 11440, Indonesia

<sup>e</sup>Research Center for Metallurgy, National Research and Innovation Agency, Tangerang Selatan, 15314, Indonesia

<sup>f</sup>Department of Physiology School of Medicine and Health Sciences, Atma Jaya Catholic University of Indonesia, Jakarta, 14440, Indonesia

<sup>g</sup>Department of Microbiology, Atma Jaya Catholic University of Indonesia, Jakarta, 14440, Indonesia

<sup>h</sup>Department of Physic Education, UIN Syarif Hidayatullah, Jakarta, 15412, Indonesia

<sup>i</sup>Department of Mechanical Engineering, Universitas Negeri Jakarta, Jakarta, 13220, Indonesia

## Article history:

Received: xx xxxx xxxx / Received in revised form: xx xxxx xxxx / Accepted: xx xxxx xxxx (to be inserted by publisher)

## Abstract

The present research conducted an electrodeposition of copper (Cu) over an aluminum (Al) alloy substrate, under influence various magnetic poles and rotating speeds. Several investigations in the present study were conducted, including deposition rate, current efficiency, surface morphology and phase, crystallographic orientation, and antibacterial activity. Increasing the rotation speed promoted to enhanced deposition rate and current efficiency for both magnetic poles influence. An increase in the deposition rate from 12.83 to 13.67  $\mu\text{m/h}$  leads to a change in surface morphology near the spheroidal, becoming a faceted structure. Presenting and rising in the rotation of a magnetic field rotation led to a reduced surface roughness and crystallite size of Cu film for both magnetic poles influence. The Cu film made without spinning magnetic has a characteristic highest bacterial inhibition zone around  $2.50 \pm 0.56 \text{ cm}^2$ .

**Keywords:** North and south pole; SEM; EDS; XRD; Antibacterial activity.

## 1. Introduction

Due to its promising properties, copper (Cu) is widely used in many sectors, such as drinking water piping, heat exchangers, and medical equipment [1–3]. Cu as film has higher bacterial kill performance than bulk Cu [4]. Moreover, Cu coated onto aluminum (Al) alloy could enhance its properties, such as antimicrobial properties [4]. Furthermore, coating synthesis can be conducted by means of electrochemical, spin coating, or spray methods [5–7]. Because of its simplicity and affordability, the electrodeposition method is a more suitable method for coating Cu onto Al alloy [8].

Cu electrodepositions attract many researchers to

investigate formed Cu films. In their study, Brands *et al.* investigated the structure, surface morphology, electrical, optical, and magnetic properties of electrodeposited  $\text{Cu}_2\text{O}$  [9]. Antenucci *et al.* have improved (the mechanical and thermal properties) of open-cell Al foams through Cu electrodeposition [10]. Augustin *et al.* investigated the effect of current density at Cu electrodeposition on the microstructure, hardness, and antibacterial activity of Cu for antimicrobial Al touch application [4]. Kuisor *et al.* fabricated CuO film using electrodeposition. Then, the film was tested for antibacterial activity using *Staphylococcus aureus* (*S. aureus*), which successfully reduced the bacterial colony during the experiment [11]. Isa *et al.* performed electrodeposition Cu over 304 stainless steels, and a coated sample was tested for antibacterial properties. At 10 minutes of exposure to the coated sample, a 100% reduction of *S. aureus* was successfully achieved [12].

\* Corresponding author.

Email: basori@civitas.unas.ac.id

doi (to be inserted by publisher)



Many factors, including the magnetic field, influenced the formed Cu films when electrodeposition was performed. The existing magnetic field at the electrodeposition process could appear to have several forces. The Lorentz force acts on a moving ion in the solution, resulting in convection flow [13]. The effects of the magnetic field may also relate to the electrokinetic-magnetohydrodynamic (MHD) effect which resulting the body force acting in the diffuse layer [14]. Another force due to the magnetic field is a paramagnetic gradient force [15]. The paramagnetic gradient force causes the movement of magnetic ions in the diffusion layer. Another possible force is a magnetic gradient force. This force acts on paramagnetic and diamagnetic ions [16]. Generally, introducing a magnetic field during the electrodeposition process leads to the arranging of moving ions towards the cathode.

Due to the many forces exhibited by presenting a magnet, several researchers investigations were focused on unrotated magnetic field-induced Cu electrodeposition [13,17–21]. Miura *et al.* investigated the electrodeposition of Cu under 15 T of magnetic field and found extraordinary dendritic growth [18]. Murdoch *et al.* conducted an electrodeposition of Cu using influence 0.25 and 0.5 T placed on the working electrode's reverse, resulting in the lowest thickness when influencing 0.25 and 0.5 T with the south pole than the north pole [13]. Sudibyo *et al.* conducted electrodeposition of Cu using influence 300 and 900 G (neodymium magnet), resulting in higher grain when electrodeposition Cu using influence 900 G [21]. Yin *et al.* investigated anomalous Cu hydride phase during magnetic field-assisted electrodeposition of Cu. Presenting an anti-parallel magnetic field affecting the magnetohydrodynamic effect, could enhance the hydrogen evolution and result in poor film quality [17]. Kovalyov *et al.* have found that a weak magnetic field (0.5 and 0.7 mT) could affect the electrodeposition process, surface morphology, and texture [19]. Liu *et al.* have stated that magnetic field-assisted electrodeposition could change hydrogen bond structure, reduce the charge transfer resistance, and increase the electrolyte viscosity [20].

Electrodeposition assisted with a spinning magnetic field is considered to attract several researchers due to its ability to enhance the properties of films. Wang and Chen used 0.18 T of a magnetic field with various rotating speeds (1000–3000 rpm) when electrodeposition of nickel (Ni) and results presenting a magnetic field with various rotating speeds could decrease surface roughness [22]. Ji *et al.* fabricated Ni-SiC using an electrodeposition process and found that the exhibit rotating magnetic field makes SiC particle distribution more uniform [23]. Syamsuir *et al.* have stated presenting a rotating magnetic field (500 and 800 rpm) at electrodeposition process makes surface morphology of the film more uniform [24]. Syamsuir *et al.* have found that increasing the rotating speed of a magnetic field (one piece of neodymium magnet arranged spread five parts in the upside Teflon) at electrodeposition process could transform surface morphology from spheroidal to faceted structure [25].

Oxygen content on the Cu film surface could disrupt the transformation of Cu to Cu ions, reducing antibacterial performance [26]. The formation of surface morphology could have an impact on the antibacterial performance. Surface

morphology, such as spheroidal and faceted structures, also contributed to the inhibition zone. A Cu film with spheroidal coating tends to create a higher inhibition zone [25].

The use of a magnetic field during electrodeposition can influence the movement of ions towards the cathode surface. Adjusting magnetic field rotation during electrodeposition also influences the movement of ions. Furthermore, the different poles of the magnet selected also influence ion movement at electrodeposition process. Generally, the ions' movement speed could affect the forming film's properties. According to the literature review above, higher rotation was used ( $\geq 500$  rpm) to influence the electrodeposition; therefore, the present study used 50 and 100 rpm. Syamsuir *et al.* used one piece of neodymium magnet arranged to spread five parts in the upside Teflon [25]. Therefore, the present research used more neodymium magnets to result in more influence of the magnetic field. Moreover, the influence of spinning using different magnetic poles was also not considered. Murdoch *et al.* found that different magnetic poles influenced the deposition process, resulting in different surface morphologies in Cu films [13]. Therefore, the present research comprehensively investigated the influence of the rotating speed and magnetic pole during Cu electrodeposition on the formation of the film for bacterial eradication applications. The electrodeposition of Cu was influenced by various magnetic poles (north and south) and magnetic rotating speeds (0, 50, and 100 rpm). Several investigations were conducted using digital scales, scanning electron microscopy equipped with energy dispersive spectroscopy (SEM-EDS), X-ray diffraction, digital camera, and optical microscope.

## 2. Materials and Methods

### 2.1. Material

Al alloy (0.106 wt.% Si, 0.365 wt.% Fe, 0.055 wt.% Cu, 0.043 wt.% Mn, 0.030 wt.% Mg, 0.003 wt.% Zn, 0.002 wt.% Ni, 0.018 wt.% Ti, 0.003 wt.% Pb, and Al balance) used as cathode, while pure Cu was used as anode. Electrolyte solution was prepared by dissolving  $\text{CuSO}_4 \cdot 5\text{H}_2\text{O}$  (Merck) in deionized water. 0.5 M  $\text{CuSO}_4 \cdot 5\text{H}_2\text{O}$  plus 20 mL of  $\text{H}_2\text{SO}_4$  fresh solution (250 ml) was used for electrodeposition of Cu.

### 2.2. Sample preparation

Firstly, Al alloy was cut  $2 \times 2$  cm for electrodeposition substrate using the shearing machine. Then, Cu film was made using a DC power supply (MDB PS-305DM) with 40 mA, 25 °C, and pH 5.5 for one h. Cu films were prepared under the influence of a clockwise rotating magnetic field, as seen in Fig. 1. The plating bath was placed on top of the rotation magnetic field equipment. Two pieces of neodymium magnet were stacked and arranged (six parts) in the upside Teflon, as seen in Fig. 1. One piece of neodymium magnet has 0.08 T of intensity. The five variation samples were made; one sample was made without the influence of a rotating magnetic field as a baseline. The sample was made by influencing 50 rpm and 100 rpm. Moreover, different pole variations are also used in the present study. The complete sample name is seen in Table 1.



Table 1. Sample name and remark

Sample name	Remark
CuR0	without the influence of a rotating magnetic field
CuRN50	50 rpm, north pole near the substrate
CuRN100	100 rpm, north pole near the substrate
CuRS50	50 rpm, south pole near the substrate
CuRS100	100 rpm, south pole near the substrate

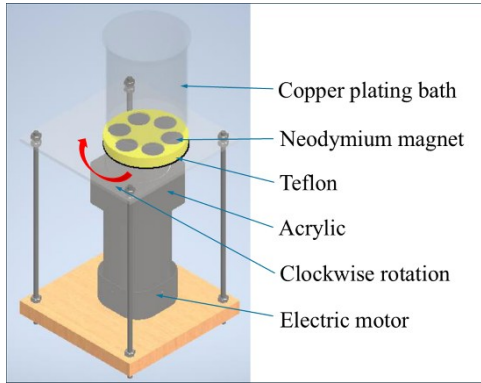


Fig. 1. Rotation magnetic field equipment

### 2.3. Characterizations

The deposition rate and current efficiency were measured similarly to previous studies [16]. Thermo Scientific SEM-EDS was used to investigate surface morphology and elements. According to SEM image, Image J software was used to measure the roughness of Cu film. X-ray diffraction was conducted using PANalytical (Cu K radiation) with step size  $0.02^\circ$  and then refined using GSAS software [27].

Antibacterial activity was investigated similarly according to previous studies [25]. Assessment of microbial reduction of various samples is adapted from ISO 22196 for non-porous material. *S. aureus* ATCC 25923 was used in this test. The inhibition zone was documented using a digital camera and assessed using an unaided eye. The area of inhibition is measured by Image J software. Each measurement is performed five times to ensure the homogeneity of the data. The diffusible area is calculated by subtracting the area of inhibition from the size of the metal. One-way ANOVA analysis was conducted, to investigate whether there is significance between the polarities of the magnets. Moreover, the specimen was then removed from the plate using sterile forceps. The agar is re-incubated at  $35^\circ\text{C} \pm 2$  for 24 hours to observe the antimicrobial activity post-contact. The oxides of the metal that formed before and after the test were observed using Olympus CX23 microscope under  $180 \times$  magnification; any changes inside of the agar plate were documented.

## 3. Result and Discussion

### 3.1. Deposition Rate and Current Efficiency

Fig. 2 shows the deposition rate and current efficiency of electrodeposition Cu over an Al alloy substrate. They have similar tendencies; an increase in magnet rotation speed leads

to a rise in deposition rate and current efficiency.

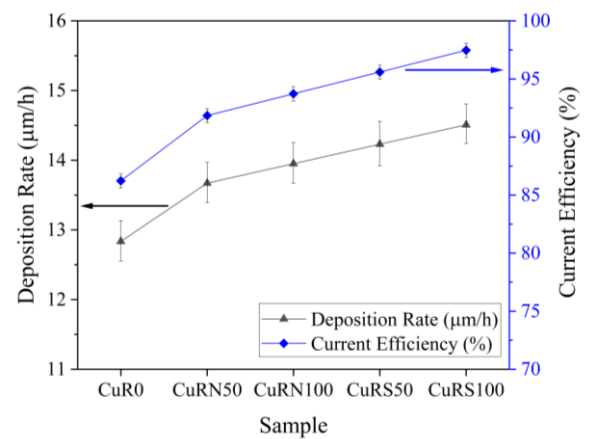


Fig. 2. Deposition rate and current efficiency of Cu electrodeposition

In the process of Cu electrodeposition, the oxidation process occurs at the anode, and a reduction process occurs at the cathode. An Al alloy (substrates) to be plated is placed at the cathode. When the current is applied, the Cu ions are depleted in the surroundings of the cathode, making a diffusion film upper around the cathode. Hydrogen evolution is known to occur at the cathode during Cu electrodeposition from aqueous solutions [16]. Less hydrogen evolution would increase the deposition rate and current efficiency because hydrogen evolution can disturb the movement of the ions to the cathode [28,29]. Presenting an anti-parallel magnetic field (north pole) that affects the MHD effect could enhance the hydrogen evolution, decrease current efficiency, and result in poor film quality [17]. According to Fig. 2, hydrogen evolution seems to influence the electrodeposition process when it is influenced by the north pole. Therefore, the electrodeposition process has a lesser current efficiency than the electrodeposition process when influenced by the south pole.

Cu films were made and influenced by the rotating south pole magnet, which has a higher deposition rate due to the magnetic field, which is parallel to the current direction and attracts more Cu ions onto the Al alloy surface [13]. Rotating the magnet under the electrolyte solution while the electrodeposition process was performed could induce an Eddy electric field [25]. The Eddy electric field could act as an additional MHD flow convection effect [22]. Moreover, increasing the rotation speed could attract more Cu ions onto the Al alloy surface, consequently increasing the deposition rate and current efficiency.

### 3.2. SEM-EDS and Roughness

Fig. 3 shows the SEM result of various Cu film surfaces. Samples were made by influencing the north pole magnetic field, which has a larger grain size than samples created by affecting the south pole of a magnetic field. Murdoch *et al.* have stated different pole were used to influencing deposition process would resulting different grain size[13]. Moreover, according to Lin *et al.* deposition time also contributing to the grain size were formed [30].

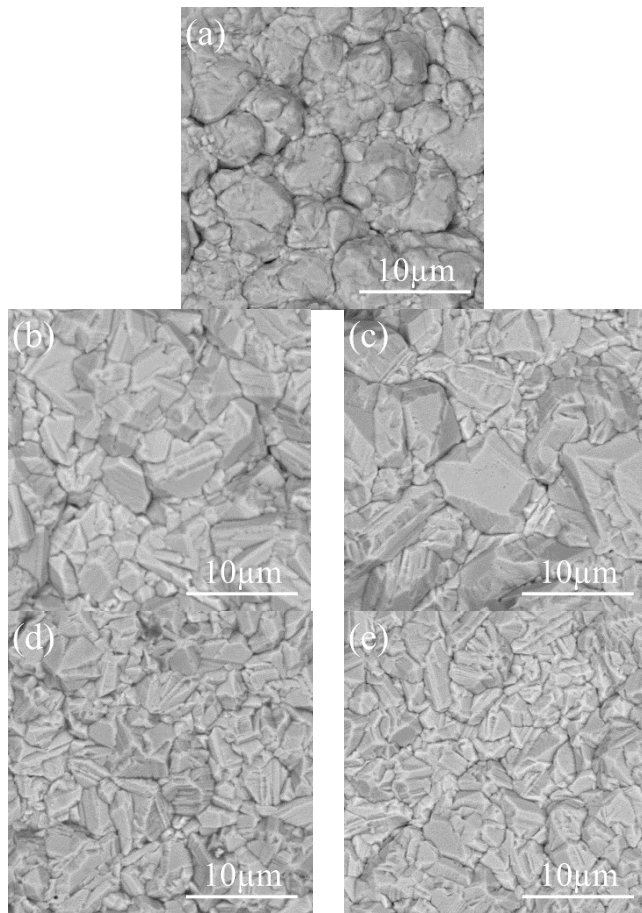
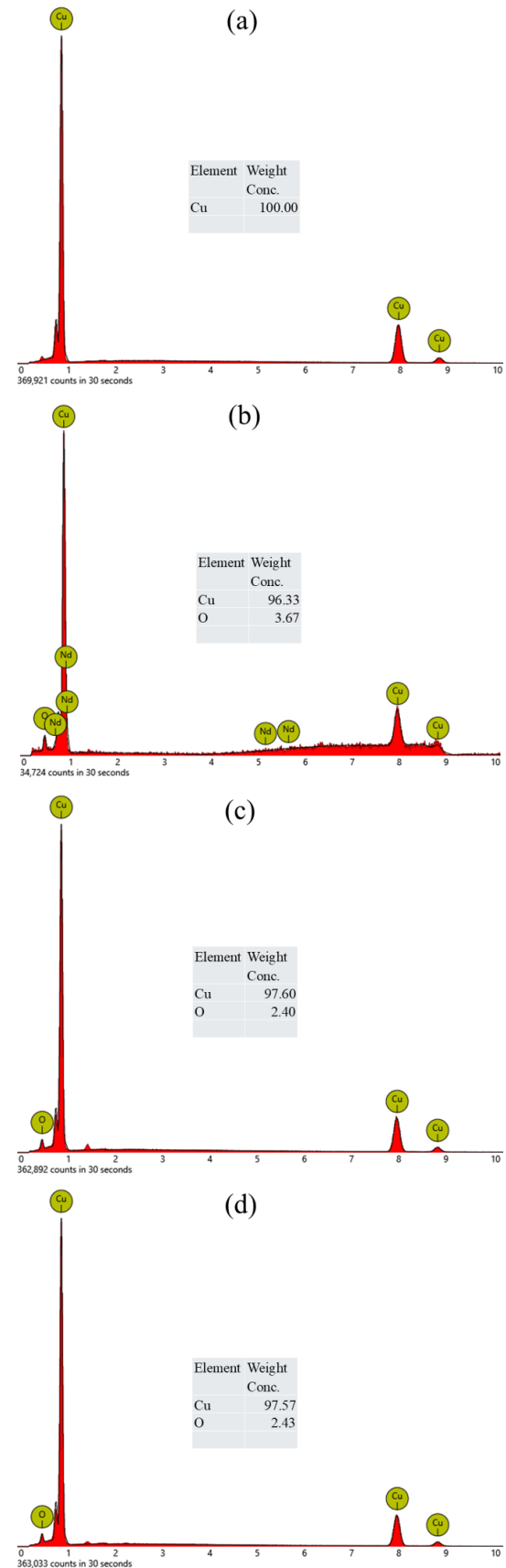


Fig. 3. SEM Cu layers: (a) CuR0; (b) CuRN50; (c) CuRN100; (d) CuRS50; and (e) CuRS100

According to Fig. 3, it can be seen that the Cu sample was made with no spinning magnetic influence, which led to the formation of morphology near the spheroidal. Cu samples were made with spinning magnetic assistance, leading to the formation of faceted structure morphology [16]. Moreover, the transformation from spheroidal to faceted structure is influenced by the rate of deposition. A higher nucleation rate leads to a higher deposition rate, resulting in a variation in surface morphology [31]. Samples made with influences from the north pole magnetic field have a low nucleation rate, hence having wider grain sizes than samples made by influencing the south pole magnetic field [13]. Moreover, an increase in the deposition rate from 12.83 to 13.67  $\mu\text{m}/\text{h}$  leads to a change in surface morphology near the spheroidal becoming faceted structure. The deposition rate between 13.67 and 14.51  $\mu\text{m}/\text{h}$  results in a faceted structure of surface morphology.

The south pole has an affecting magnetic field parallel to the current direction; therefore, Cu ions are more attracted to the Al alloy surface. On the contrary, the north pole has an affecting magnetic field that is anti-parallel to the current direction, reducing Cu ions' attraction onto the Al alloy surface. Moreover, Lorentz's forces rotate opposite each other on top of the surface specimen for different magnetic poles. This condition affected the sample film by influencing the South Pole to be smoother than the North Pole. Ji *et al.* stated that presenting a rotating magnetic field during

electrodeposition makes surface morphology more uniform [23]. In this case, the paramagnetic force has a similar tendency for different magnetic poles and, therefore, could be neglected, influencing surface morphology.



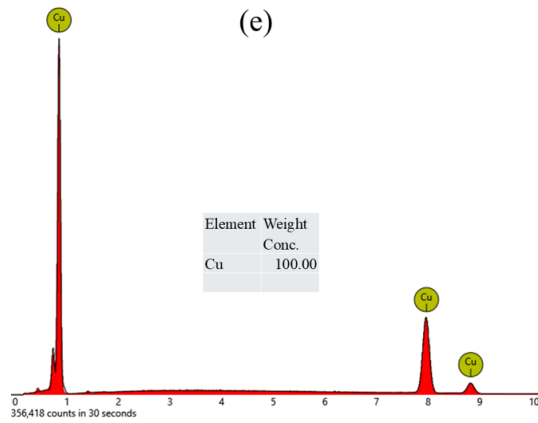


Fig. 4. EDS Cu layers: (a) CuR0; (b) CuRN50; (c) CuRN100; (d) CuRS50; and (e) CuRS100

According to Fig. 4, the spinning magnetic-assisted running at 50 rpm led to oxygen forming on the Cu surface. Moreover, enhanced magnetic rotation led to a decrease or disappearance of oxygen. Presenting oxygen on Cu film is one of the unique cases. Oxygen could form due to a secondary reaction on the anode. Moreover, oxygen could be formed due to sample storage and transport [25].

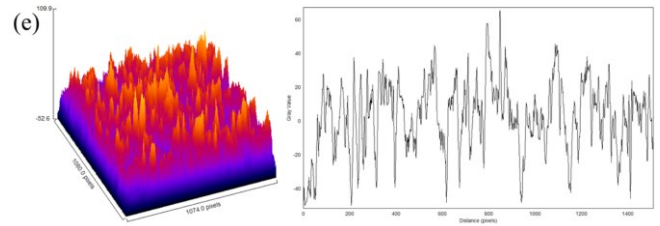
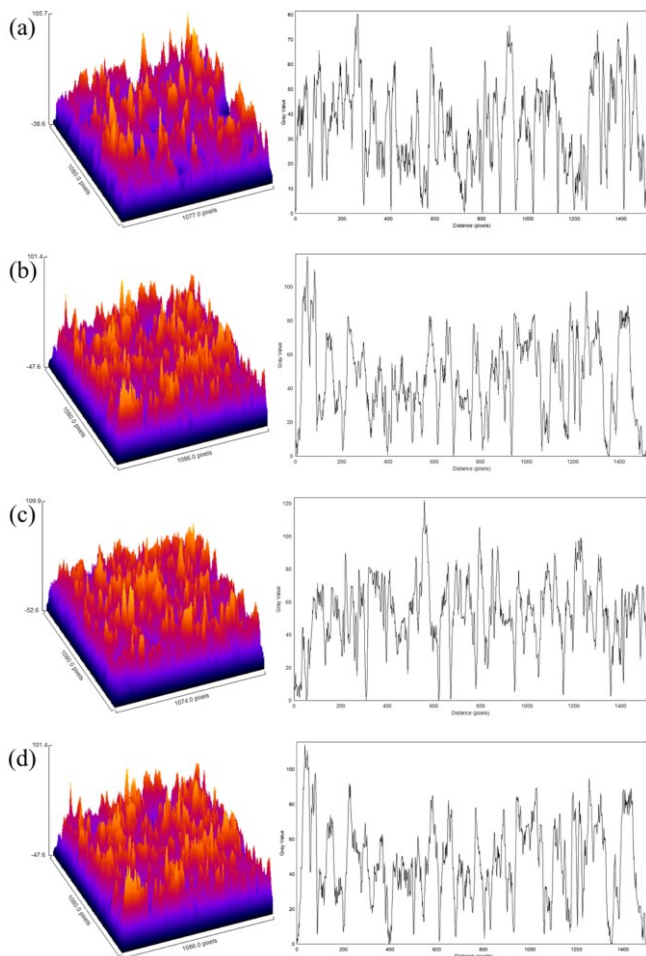


Fig. 5. Roughness Cu layers: (a) CuR0; (b) CuRN50; (c) CuRN100; (d) CuRS50; and (e) CuRS100

Fig. 5 presents the roughness analyzed result from the SEM image using ImageJ software. CuR0, CuRN50, CuRN100, CuRS50, and CuRS100 samples have a surface roughness of 34.62, 18.00, 17.38, 18.60, and 16.58  $\mu\text{m}$ , respectively. Presenting a magnetic field rotation during electrodeposition led to a decrease in the surface roughness of Cu film. More rotation could also decrease surface roughness, which perfectly agrees with a previous study [25]. Wang and Chen have found presenting a magnetic field during electrodeposition with various rotating speeds could decrease surface roughness [22]. This behavior is probably due to additional MHD flow, which could enhance the Cu ions' movement, and which is in line with the deposition rate result. A higher deposition rate would result in a higher nucleation rate, consequently producing a smooth surface morphology. Moreover, the sample made by north pole magnet influence has more roughness than sample made by north pole magnet. This behavior probably due to MHD effect which could enhance the hydrogen evolution and resulting more roughness [17].

### 3.3. X-ray diffraction

The diffraction patterns of samples of Cu deposition on substrates composed of Al alloy plates are shown in Fig. 6. The five samples were identified to have Cu phase peaks at the indexed plane peaks (111), (200), (220), (311), and (222) at angles  $2\theta = 43.31, 50.45, 74.13, 89.94, \text{ and } 95.15^\circ$ . The cubic crystal system is present in the Cu phase, and it has a space group of  $fm-3m$ . The cubic Cu phase peaks at these angles are consistent with findings from studies by Omar and Francisco Briones *et al.* [32,33]. This demonstrates that the procedure for depositing Cu on Al alloy plates has been successfully completed. At the indexed plane peaks (111), (200), (220), (311), and (400) of the five diffraction patterns, they were also found on the Al alloy plate substrate along with the copper phase. Xu *et al.* and Ayieko *et al.* presented a standard Al diffraction pattern that is identical to this peak of Al [34,35].



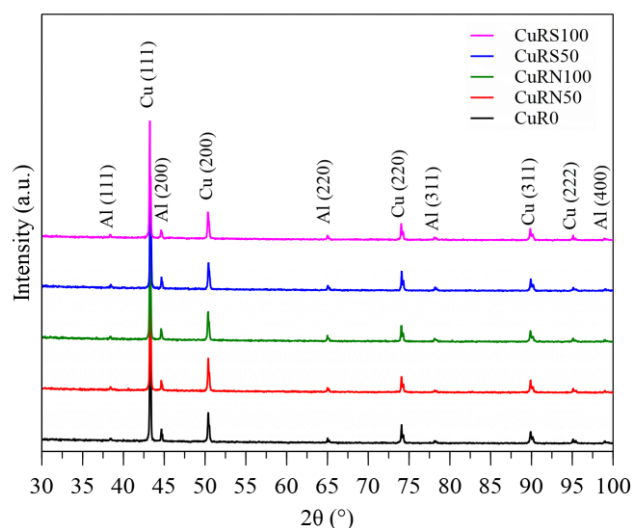


Fig. 6. X-ray diffraction pattern of various sample

Table 2. Crystallographic data calculated from various samples

Source	CuR0	CuRN50	CuRN100	CuRS50	CuRS100
Name: Copper (Cu)					
Space group: F m -3 m (225)					
Crystal system: cubic					
Lattice -a (nm)	0.3615	0.3615	0.3615	0.3615	0.3615
wRp (%)	10.10	10.37	10.24	9.86	10.30
GoF	1.067	1.106	1.087	1.045	1.056
Mean crystallite size (nm)	308	173	154	173	126
Micro-strain (%)	0.07	0.05	0.05	0.05	0.04

The mean crystallite size and lattice value of the five deposition samples are compared in order to further analyze the diffraction pattern. The Rietveld method was employed to determine the lattice of the five samples. The cubic Cu phase lattice of all five samples is measured at 0.3615 nm according to the calculation results. Changes in magnetic poles and rotating speed have no effect on the lattice value of the cubic Cu phase. The data from the crystallographic calculation can be found in Table 2. In order to determine the mean crystallite size, the Williamson-Hall plot method is utilised. In contrast to the lattice value, the mean crystallite size is affected by the rotating speed and poles. The mean crystallite size becomes finer with the increase in magnet rotation speed which is in perfectly math with surface roughness analysis.

### 3.4. Antibacterial Activity

Antibacterial activity test after 24 hours of contact can be seen on Fig. 7. Material placement in the middle of Mueller Hinton agar inoculated with *S. aureus* ATCC 25923. Notice the inhibition zones around the material; the calculation is presented in Table 3. The metal ions diffuse into the agar to inhibit the growth of *S. aureus*.

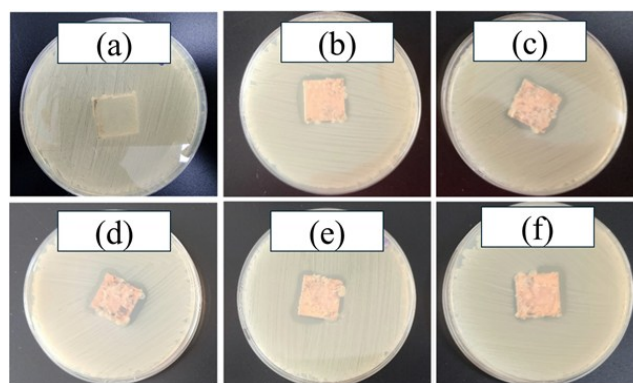


Fig. 7. Antibacterial activity test after 24 hours: (a) blank; (b) CuRN50; (c) CuRN100; (d) CuR0; (e) CuRS50; and (f) CuRS100

Cu, particularly in the form of metal-organic frameworks (MOFs) and nanoparticles, exhibits significant antibacterial activity against Gram-positive bacteria such as *S. aureus* [36]. The peptidoglycan layer in Gram-positive bacteria plays a significant role in their susceptibility to Cu, although its direct interaction with Cu is not as straightforward as with other antimicrobial agents. Cu can induce modifications in the peptidoglycan layer, such as increased cross-linkage, which can affect the overall structure and function of the cell wall. These modifications can either enhance or reduce the susceptibility of Gram-positive bacteria to Cu, depending on the specific bacterial strain and environmental conditions [37,38]. In this research, the Cu induces contact killing. The antimicrobial activity of Cu is believed to involve contact-mediated killing, initiating membrane degradation. The susceptibility of Gram-positive strains to Cu is attributed to the thick peptidoglycan layer, which reduces cell wall permeability to other metal ions, including Zinc [39].

According to Fig. 7, the inoculum was totally annihilated by electroplated materials. The log reduction is not calculated due to the total killing of the bacteria. However, the total reduction of  $> 105$  CFU/mL might suggest a percentage reduction of  $> 99.999\%$  (see Table 3). Moreover, there is a zone of inhibition between the sample and bacterial lawn. Also visible inside the zone's white crystals and some bluish color change inside the agar. This suggests the Cu material diffused and interacted with the agar, resulting in a zone of bacterial growth inhibition.

As seen in Table 3, the widest diffusion zone is observed in CuR0 with the zone of diffusion and inhibition areas of 6.99 cm<sup>2</sup> and 2.5 cm<sup>2</sup>. This is statistically significant with  $p < 0.001$  (ANOVA; CI 95%). There is also significance in independent T-Test analyses between CuR0 and CuR50 group ( $p < 0.001$ ; CI 95%), R0 and R100 group ( $p < 0.001$ ; CI 95%), also between CuR50 and CuR100 Group ( $p < 0.001$ ; CI 95%). To investigate whether there is significance between the polarities of the magnets, independent T-test analyses were performed. There is no significant difference in the outcome between the south pole group and the north pole group ( $p=0.063$ ; CI 95%). Moreover, there were no inhibitions in the blank group, and the bacteria grew underneath the metal.

Table 3. The reduction of colony, and diffusible metal observation

Sample	Microbial reduction assessment		Diffusible metal observation	
	Initial load 0 h (CFU/mL)	Final load 24 h (CFU/mL)	Zone of diffusion (cm <sup>2</sup> )	Inhibition area (cm <sup>2</sup> )
Blank		0	4.01 ±0.01	-0.48 ±0.01
CuR0		0	6.99 ±0.12	2.50 ±0.56
CuRN50	3.5 × 10 <sup>5</sup>	0	6.21 ±0.01	1.61 ±0.21
CuRN100		0	6.00 ±0.02	1.89 ±0.02
CuRS50		0	6.16 ±0.41	1.73 ±0.46
CuRS100		0	6.17 ±0.01	2.14 ±0.24

The use of magnetic rotation during material synthesis has a significant impact on the results. Materials synthesized without magnetic rotation (R0) show stronger antibacterial effects compared to those synthesized at 50 rpm or 100 rpm. However, increasing magnet rotation significantly enhances the size of the inhibition zone. As a result, the inhibition zone at 100 rpm is larger than that at 50 rpm. This condition is probably due to forming some oxygen on the Cu films surface as seen in EDS result which could disrupt transformation Cu to be Cu ions. Qu *et al.* has found that antibacterial behavior was influenced by Cu ions [26]. Release of Cu ions inside of the agar is lethal towards *S. aureus* [40].

As shown in Fig. 3, CuR0 surface morphology has formed near to spheroidal, while other samples have form faceted structure. Compared to Table 3, it can be seen that higher inhibition zone is seen in CuR0 sample. Therefore, it can be concluded that the spheroidal form results in the highest inhibition zone than the faceted structure, which is perfectly in agreement with previous study [25]. This condition probably occurs due to the spheroidal structure having a wider surface area than the faceted structure, which results in more Cu ions being released. Moreover, an increase in rotation leads to a decrease in roughness. Several researchers have found that roughness is independent of the inhibition zone which aligns with the present study [25,41].

Moreover, the generation of reactive oxygen species (ROS) and damage to cell membranes are the main ways in which metals' broad antibacterial potential has been extensively studied [42–44]. Even so, metals can target particular cellular components and, when combined, are likely to improve pathogen clearance despite their non-specific activity. Conversely, Cu has the ability to change metabolic pathways in addition to causing damage to DNA and cell membranes through the generation of ROS [45]. The combined mode of action has not yet been investigated, to the authors' knowledge, despite the fact that the modes of action of various metal ions have been well explored. The variability in antimicrobial efficaciousness between various combinations can be explained by the diverse chemical reactivity of metal ions with bacterial cells and their specific biological targets [46].

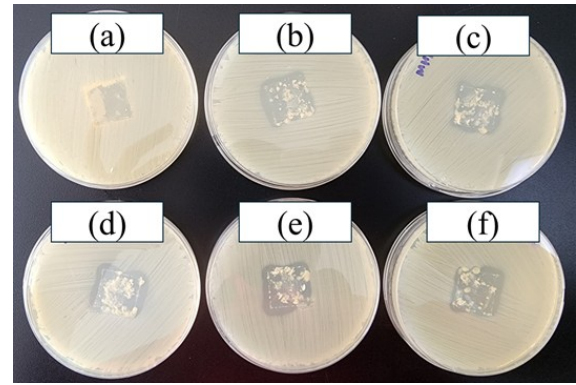


Fig. 8. After 24 hours of post contact test: (a) blank; (b) CuRN50; (c) CuRN100; (d) CuR0; (e) CuRS50; and (f) CuRS100

Fig. 8 shows the results after 24 hours of post-contact testing. The inhibitory zones appear after the removal of the material. Notice that there are some metal infiltrations inside of the agar on every plate. The infiltration causes the agar to crack. This suggests that there is a gas-forming or exothermic reaction inside of the agar, increasing the antimicrobial ability of the material [47]. There are no anti-Staphylococcal effects on the blank material; therefore, there is a regrowth of microorganisms in the place where the metal was previously placed.

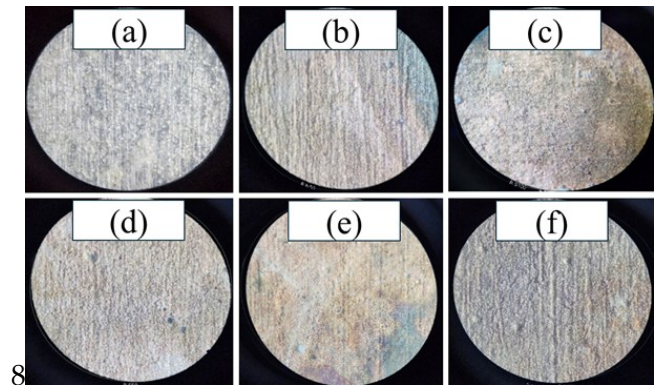


Fig. 9. Antibacterial activity pretest microscope observation: (a) blank; (b) CuRN50; (c) CuRN100; (d) CuR0; (e) CuRS50; and (f) CuRS100

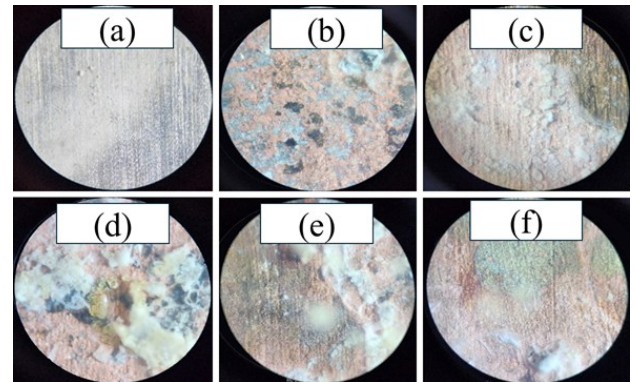


Fig. 10. Antibacterial activity post-test microscope observation: (a) blank; (b) CuRN50; (c) CuRN100; (d) CuR0; (e) CuRS50; and (f) CuRS100

Fig. 9 shows antibacterial activity pretest microscope observation, and Fig. 10 shows antibacterial activity post-test microscope observation. Microscopic observation of electroplated surfaces occurs under  $180\times$  magnification optical microscope. There is a significant proportion in the formation of white crystals on the electroplated surface after tests. The crystals did not form on the surface of the blank. The Cu forms oxides, which change the color of the surface. According to Marković et al., change color in the Cu due to adsorption or reduction Cu ions [48].

#### 4. Conclusion

The Cu films were fabricated under a spinning magnetic field with various rotation speeds, and a magnetic pole was successfully conducted. Higher rotation speed is promoted to enhanced deposition rate and current efficiency for both magnetic poles. The Cu sample was fabricated with an un-present spinning magnetic influence, which led to the forming morphology near the spheroidal. Cu samples were made with spinning magnetic influence, which led to the forming morphology near the faceted structure. Magnetic-assisted spinning at 50 rpm led to oxygen forming on the Cu surface for both magnetic poles and enhanced rotation, which led to the decrease or disappearance of oxygen. Presenting and more of a magnetic field rotation led to decreased surface roughness and crystallite size of Cu film for both magnetic poles. The Cu sample was made without spinning magnetic fields influence has the highest inhibition zone size, probably due to the absence of oxygen on the Cu film surface and the morphology near the spheroidal. Generally, Cu films successfully covered Al alloy and could transform it into antibacterial material. Future recommendations in the present study are conducting electrodeposition of Cu with influencing rotation magnetic higher than 100 rpm.

#### Acknowledgements

This study has been supported by the Ministry of Education, Culture, Research, and Technology through grand funding Penelitian Fundamental-Reguler with contract number 087/LPPM-UNAS/VI/2024 and 815/LL3/AL.04/2024.

#### References

1. D. A. Lytle and C. P. White, *The effect of phosphate on the properties of copper drinking water pipes experiencing localized corrosion*, J. Fail. Anal. Prev. 14 (2014) 203–219.
2. M. M. Lachowicz, *A metallographic case study of formicary corrosion in heat exchanger copper tubes*, Eng. Fail. Anal. 111 (2020) 104502.
3. N. Thokala, C. Kealey, J. Kennedy, D. B. Brady and J. B. Farrell, *Characterisation of polyamide 11/copper antimicrobial composites for medical device applications*, Mater. Sci. Eng. C 78 (2017) 1179–1186.
4. A. Augustin, P. Huilgol, K. R. Udupa and U. B. K., *Effect of current density during electrodeposition on microstructure and hardness of textured Cu coating in the application of antimicrobial Al touch surface*, J. Mech. Behav. Biomed. Mater. 63 (2016) 352–360.
5. A. M. Alghamdi and F. Fadhillah, *Thin film composite polyelectrolyte multilayer nanofiltration membrane fabricated using spin assisted layer by layer assembly: Application of solution diffusion film model*, Commun. Sci. Technol. 5 (2020) 10–15.
6. C. Santoso, Ratnawati and Slamet, *Utilization of glycerol solution for hydrogen production by a combination of photocatalysis and electrolysis processes with Fe-TiO<sub>2</sub> nanotubes*, Commun. Sci. Technol. 8 (2023) 208–215.
7. W. Trisunaryanti, K. Wijaya and A. M. Tazkia, *Preparation of Ni/ZSM-5 and Mo/ZSM-5 catalysts for hydrotreating palm oil into biojet fuel*, Commun. Sci. Technol. 9 (2024) 161–169.
8. A. Lelevic and F. C. Walsh, *Electrodeposition of Ni-P alloy coatings: A review*, Surf. Coatings Technol. 369 (2019) 198–220.
9. I. S. Brandt, M. A. Tumelero, S. Pelegrini, G. Zangari and A. A. Pasa, *Electrodeposition of Cu<sub>2</sub>O: growth, properties, and applications*, J. Solid State Electrochem. 21 (2017) 1999–2020.
10. A. Antenucci, S. Guarino, V. Tagliaferri and N. Ucciardello, *Improvement of the mechanical and thermal characteristics of open cell aluminum foams by the electrodeposition of Cu*, Mater. Des. 59 (2014) 124–129.
11. A. Kusior, J. Mazurkow, P. Jelen, M. Bik, S. Raza, M. Wdowiak et al., *Copper Oxide Electrochemical Deposition to Create Antiviral and Antibacterial Nanocoatings*, Langmuir 40 (2024) 14838–14846.
12. N. N. C. Isa, Y. Mohd, M. H. M. Zaki and S. A. S. Mohamad, *Electrodeposition of copper coating on 304 stainless steel substrate: Physicochemical properties and antibacterial activity*, in ADVANCED MATERIALS FOR SUSTAINABILITY AND GROWTH: Proceedings of the 3rd Advanced Materials Conference 2016 (3rd AMC 2016), 1901 (2017), pp. 020009.
13. H. A. Murdoch, D. Yin, E. Hernández-Rivera and A. K. Giri, *Effect of applied magnetic field on microstructure of electrodeposited copper*, Electrochem. commun. 97 (2018) 11–15.
14. Q. Long, Y. Zhong and J. Wu, *Research progress of magnetic field techniques for electrodeposition of coating*, Int. J. Electrochem. Sci. 15 (2020) 8026–8040.
15. K. Kołodziejczyk, E. Miękoś, M. Zieliński, M. Jaksender, D. Szczukocki, K. Czarny et al., *Influence of constant magnetic field on electrodeposition of metals, alloys, conductive polymers, and organic reactions*, J. Solid State Electrochem. 22 (2018) 1629–1674.
16. B. Soegijono, F. B. Susetyo, Yusmaniar and M. C. Fajrah, *Electrodeposition of paramagnetic copper film under magnetic field on paramagnetic aluminum alloy substrates*, e-Journal Surf. Sci. Nanotechnol. 18 (2020) 281–288.
17. D. Yin, H. A. Murdoch, B. Chad Hornbuckle, E. Hernández-Rivera and M. K. Dunstan, *Investigation of anomalous copper hydride phase during magnetic field-assisted electrodeposition of copper*, Electrochem. commun. 98 (2019) 96–100.
18. M. Miura, Y. Oshikiri, A. Sugiyama, R. Morimoto, I. Mogi, M. Miura et al., *Magneto-Dendrite Effect: Copper Electrodeposition under High Magnetic Field*, Sci. Rep. 7 (2017) 1–8.
19. S. V. Kovalyov, O. B. Girin, C. Debiemme-Chouvy and V. I. Mishchenko, *Copper electrodeposition under a weak magnetic field: effect on the texturing and properties of the deposits*, J. Appl. Electrochem. 51 (2021) 235–243.
20. Y. Liu, B. Zheng, T. Zhang, Y. Chen, J. Liu, Z. Wang et al., *Magnetic field intensified electrodeposition of low-concentration*



- copper ions in aqueous solution, *Electrochim. Acta* 432 (2022) 141201.
21. Sudibyo, M. B. How and N. Aziz, Influences of magnetic field on the fractal morphology in copper electrodeposition, in *IOP Conference Series: Materials Science and Engineering*, 285 (2018), pp. 012021.
22. T. Wang and W. Chen, *Effects of Rotating Magnetic Fields on Nickel Electro-Deposition*, *ECS Electrochem. Lett.* 4 (2015) D14–D17.
23. R. Ji, K. Han, H. Jin, X. Li, Y. Liu, S. Liu et al., *Preparation of Ni-SiC nano-composite coating by rotating magnetic field-assisted electrodeposition*, *J. Manuf. Process.* 57 (2020) 787–797.
24. S. Syamsuir, F. B. Susetyo, B. Soegijono, S. D. Yudanto, Basori and D. Nanto, Nickel layers properties produced by electroplating were influenced by spinning permanent magnet, in *Journal of Physics: Conference Series*, 2596 (2023), pp. 012008.
25. Syamsuir, F. B. Susetyo, B. Soegijono, S. D. Yudanto, Basori, M. K. Ajiriyanto et al., *Rotating-Magnetic-Field-Assisted Electrodeposition of Copper for Ambulance Medical Equipment*, *Automot. Exp.* 6 (2023) 290–302.
26. X. Qu, H. Yang, B. Jia, Z. Yu, Y. Zheng and K. Dai, *Biodegradable Zn–Cu alloys show antibacterial activity against MRSA bone infection by inhibiting pathogen adhesion and biofilm formation*, *Acta Biomater.* 117 (2020) 400–417.
27. A. C. Larson and R. B. Von Dreele, *General Structure Analysis System (GSAS)*, Vol. 748, University of California, Los Alamos, 2004.
28. X. Qiao, H. Li, W. Zhao and D. Li, *Effects of deposition temperature on electrodeposition of zinc-nickel alloy coatings*, *Electrochim. Acta* 89 (2013) 771–777.
29. M. A. Lopez-Heredia, P. Weiss and P. Layrolle, *An electrodeposition method of calcium phosphate coatings on titanium alloy*, *J. Mater. Sci. Mater. Med.* 18 (2007) 381–390.
30. Y. Lin, J. Pan, H. F. Zhou, H. J. Gao and Y. Li, *Mechanical properties and optimal grain size distribution profile of gradient grained nickel*, *Acta Mater.* 153 (2018) 279–289.
31. D. Grujicic and B. Pesic, *Reaction and nucleation mechanisms of copper electrodeposition from ammoniacal solutions on vitreous carbon*, *Electrochim. Acta* 50 (2005) 4426–4443.
32. Halo Dalshad Omar, *Intensity Correction and Pole Figure Measurement of Copper Metallic by XRD*, *J. Basic Appl. Sci.* 12 (2016) 320–322.
33. F. Briones, V. Seriacopi, C. Martínez, J. L. Valin, D. Centeno and I. F. Machado, *The effects of pressure and pressure routes on the microstructural evolution and mechanical properties of sintered copper via SPS*, *J. Mater. Res. Technol.* 25 (2023) 2455–2470.
34. X. Xu, Z. Liu, B. Zhang, H. Chen, J. Zhang, T. Wang et al., *Effect of Mn content on microstructure and properties of 6000 series aluminum alloy*, *Appl. Phys. A Mater. Sci. Process.* 125 (2019) 1–9.
35. C. O. Ayieko, R. J. Musembi, A. A. Ogacho, B. O. Aduda, B. M. Muthoka and P. K. Jain, *Controlled Texturing of Aluminum Sheet for Solar Energy Applications*, *Adv. Mater. Phys. Chem.* 05 (2015) 458–466.
36. M. Hubab and M. A. Al-Ghouti, *Recent advances and potential applications for metal-organic framework (MOFs) and MOFs-derived materials: Characterizations and antimicrobial activities*, *Biotechnol. Reports* 42 (2024) e00837.
37. S. J. Kim, J. Chang and M. Singh, *Peptidoglycan architecture of Gram-positive bacteria by solid-state NMR*, *Biochim. Biophys. Acta - Biomembr.* 1848 (2015) 350–362.
38. X. Chen, Y. Li, K. Bai, M. Gu, X. Xu, N. Jiang et al., *Class A Penicillin-Binding Protein C Is Responsible for Stress Response by Regulation of Peptidoglycan Assembly in Clavibacter michiganensis*, *Microbiol. Spectr.* 10 (2022).
39. S. Khafa, L. Olivieri, C. Di Nicola, R. Pettinari, C. Pettinari, A. Tombesi et al., *Copper and Zinc Metal–Organic Frameworks with Bipyrazole Linkers Display Strong Antibacterial Activity against Both Gram+ and Gram– Bacterial Strains*, *Molecules* 28 (2023) 6160.
40. L. Huang, E. M. Fozo, T. Zhang, P. K. Liaw and W. He, *Antimicrobial behavior of Cu-bearing Zr-based bulk metallic glasses*, *Mater. Sci. Eng. C* 39 (2014) 325–329.
41. M. A. Hajduga, S. Węgrzynkiewicz, J. Waś-Solipiwo, M. Hajduga and M. B. Hajduga, *Innovative solutions from the field of the material science and medicine in the interior of modern ambulances*, *Mater. Sci. Forum* 844 (2016) 50–54.
42. P. L. Lam, R. S. M. Wong, K. H. Lam, L. K. Hung, M. M. Wong, L. H. Yung et al., *The role of reactive oxygen species in the biological activity of antimicrobial agents: An updated mini review*, *Chem. Biol. Interact.* 320 (2020) 109023.
43. S. Alfei, G. C. Schito, A. M. Schito and G. Zuccari, *Reactive Oxygen Species (ROS)-Mediated Antibacterial Oxidative Therapies: Available Methods to Generate ROS and a Novel Option Proposal*, *Int. J. Mol. Sci.* 25 (2024).
44. A. A. Dayem, M. K. Hossain, S. Bin Lee, K. Kim, S. K. Saha, G. M. Yang et al., *The role of reactive oxygen species (ROS) in the biological activities of metallic nanoparticles*, *Int. J. Mol. Sci.* 18 (2017) 1–21.
45. A. R. Mir, J. Pichtel and S. Hayat, *Copper: uptake, toxicity and tolerance in plants and management of Cu-contaminated soil*, *BioMetals* 34 (2021) 737–759.
46. F. N. S. Raja, T. Worthington and R. A. Martin, *The antimicrobial efficacy of copper, cobalt, zinc and silver nanoparticles: alone and in combination*, *Biomed. Mater.* 18 (2023) 045003.
47. S. Y. Tsai, Y. M. Liu, Z. W. Lin and C. P. Lin, *Antimicrobial activity effects of electrolytically generated hypochlorous acid-treated pathogenic microorganisms by isothermal kinetic simulation*, *J. Therm. Anal. Calorim.* 148 (2023) 1613–1627.
48. D. Marković, C. Deeks, T. Nunney, Ž. Radovanović, M. Radoičić, Z. Šaponjić et al., *Antibacterial activity of Cu-based nanoparticles synthesized on the cotton fabrics modified with polycarboxylic acids*, *Carbohydr. Polym.* 200 (2018) 173–182.

**Komentar  
Reviewer atau  
Editor 2**





---

**[CST] Editor Decision**

---

**From** Meilana Dharma Putra (CST) <journal-noreply@kipmi.or.id>

**Date** Wed 1/8/2025 11:09 AM

**To** Basori Basori <basori@civitas.unas.ac.id>; Ruliyanta <ruliyanto@civitas.unas.ac.id>; Maman Kartaman Ajiriyanto <mama014@brin.go.id>; Rosika Kriswarini <rosi004@brin.go.id>; Heri Hardiyanti <heri016@brin.go.id>; Cahaya Rosyidan <cahayarosyidan@trisakti.ac.id>; Sigit Dwi Yudanto <sigi012@brin.go.id>; Evi Ulina Margaretha Situmorang <evi.situmorang@atmajaya.ac.id>; Daniel Edbert <daniel.edbert@atmajaya.ac.id>; Dwi Nanto <dwi.nanto@uinjkt.ac.id>; fbudhi@unj.ac.id <fbudhi@unj.ac.id>

Dear Authors,

Thank you for considering Communications in Science and Technology.

Please see the comments of the reviewers on the article entitled: "Rotating speed and magnetic pole dependency assisted on copper deposition onto aluminum alloy substrate for bacterial eradication application". I suggest you consider these comments, suggestions and questions and revise your article accordingly. The revised version of your submission is due by January 28, 2025. For your guidance, reviewers' comments are appended below.

If you decide to revise the work, please submit a list of changes or a rebuttal against each point which is being raised and highlight the changes in manuscript when you submit the revised manuscript.

To submit a revision, please go to <https://cst.kipmi.or.id/> (login as an Author) within 21 days; after this time the manuscript will be considered as withdrawn.

For your information, submitting a revision to the journal does not guarantee acceptance of the manuscript, as it will undergo a third review (if required).

Yours sincerely,

Meilana Dharma Putra  
Editor-in-Chief  
Communications in Science and Technology

---

Reviewer #1:

1. Provide quantitative justification for the specific selection of 50 and 100 rpm rather than higher or lower values.

Include experimental validation of magnetic field strength (e.g., Gauss measurements) to support claims about increased magnetic influence.

2. Provide quantitative Cu ion release data (e.g., ICP-MS analysis) to confirm how different surface morphologies affect ion dissolution. Conduct additional antibacterial tests, such as time-dependent bacterial killing assays, to provide deeper mechanistic insight. Expand the discussion by comparing the inhibition zones observed with those reported in similar copper-based coatings in previous studies.

Reviewer #2:

1. Provide correlation analysis ( $R^2$  values) between deposition rate, surface morphology, and

inhibition zone size. If corrosion behavior cannot be retested, include alternative durability tests (e.g., accelerated aging tests, adhesion tests) to demonstrate coating stability.

2. Discuss how increased deposition rate impacts long-term coating durability.

Provide SEM/AFM analysis of coating thickness and uniformity to correlate surface morphology with performance.

3. Conduct a full professional language review (beyond the journal's standard editing). Improve logical flow between sections to make the study easier to understand.

The following message is being delivered on behalf of Communications in Science and Technology.

---

# **Respon 2**

**Title** : Rotating speed and magnetic pole dependency assisted on copper deposition onto aluminum alloy substrate for bacterial eradication application

**Authors** : Basori, Ruliyanta, Maman Kartaman Ajiriyanto, Rosika Kriswarini, Heri Hardiyanti, Cahaya Rosyidan, Sigit Dwi Yudanto, Evi Ulina Margareta Situmorang, Daniel Edbert, Dwi Nanto, Ferry Budhi Susetyo

**Corresponding author** : Basori

**Reviewer #1:**

No.	Comment from Reviewer	Author Response	Page
1	<ul style="list-style-type: none"> <li>Provide quantitative justification for the specific selection of 50 and 100 rpm rather than higher or lower values.</li> </ul>	<ul style="list-style-type: none"> <li>Justification for the specific selection of 50 and 100 rpm rather than higher or lower values has been added in the last paragraph of the introduction. Thank you.</li> </ul>	<ul style="list-style-type: none"> <li>2</li> </ul>
	<ul style="list-style-type: none"> <li>Include experimental validation of magnetic field strength (e.g., Gauss measurements) to support claims about increased magnetic influence.</li> </ul>	<ul style="list-style-type: none"> <li>Validation of the magnetic field strength has been added in the experimental method section. Thank you.</li> </ul>	<ul style="list-style-type: none"> <li>3</li> </ul>
2	<ul style="list-style-type: none"> <li>Provide quantitative Cu ion release data (e.g., ICP-MS analysis) to confirm how different surface morphologies affect ion dissolution.</li> </ul>	<ul style="list-style-type: none"> <li>We are pleased about that suggestion. However, we cannot conduct a deep investigation into this because the electrodeposition process was performed using a DC power supply (dissolved anode method). If the electrodeposition process were to be undertaken using potentiostat (undissolved anode method), we would probably test it. Furthermore, the reason we used a DC power supply for electrodeposition is that it is cheaper than using potentiostat. To the best of our knowledge, industrial manufacturing has always used this method. We apologize for this. Thank you.</li> </ul>	<ul style="list-style-type: none"> <li></li> </ul>
	<ul style="list-style-type: none"> <li>Conduct additional antibacterial tests, such as time-dependent bacterial killing assays, to provide deeper mechanistic insight.</li> </ul>	<ul style="list-style-type: none"> <li>Additional antibacterial tests (killing assays/ microbial reduction) have been added for 1, 2, 4, 6, and 12 h. Thank you.</li> </ul>	<ul style="list-style-type: none"> <li>9</li> </ul>
	<ul style="list-style-type: none"> <li>Expand the discussion by comparing the inhibition zones observed with those reported in similar copper-based coatings in previous studies.</li> </ul>	<ul style="list-style-type: none"> <li>The discussion of comparing inhibition zones has been added to the result and discussion. Thank you.</li> </ul>	<ul style="list-style-type: none"> <li>8</li> </ul>

**Reviewer #2:**

No.	Comment from Reviewer	Author Response	Page
1	<ul style="list-style-type: none"> <li>Provide correlation analysis (<math>R^2</math> values) between deposition rate, surface morphology, and inhibition zone size.</li> <li>If corrosion behavior cannot be retested, include alternative durability tests (e.g., accelerated aging tests, adhesion tests) to demonstrate coating stability.</li> </ul>	<ul style="list-style-type: none"> <li>We are pleased about that suggestion. But, we cannot conduct this. Based on our experience writing a paper, we never conducted an <math>R^2</math> value analysis. We always connect the characterization result to mechanical properties or electrochemical behavior where conducting. Several of our papers are as follows:   <a href="https://doi.org/10.31603/ae.9067">https://doi.org/10.31603/ae.9067</a>  <a href="http://dx.doi.org/10.5599/jese.161510.5829/IJE.2023.36.06C.18">http://dx.doi.org/10.5599/jese.161510.5829/IJE.2023.36.06C.18</a>  <a href="https://doi.org/10.1380/ejsnt.2024-00310.1088/1742-6596/2377/1/012002">https://doi.org/10.1380/ejsnt.2024-00310.1088/1742-6596/2377/1/012002</a>  <a href="https://doi.org/10.1088/1742-6596/2596/1/012014">10.1088/1742-6596/2596/1/012014</a>  <a href="https://doi.org/10.1088/1742-6596/2596/1/012008">10.1088/1742-6596/2596/1/012008</a>  <a href="http://jase.tku.edu.tw/articles/jase-202504-28-04-0016">http://jase.tku.edu.tw/articles/jase-202504-28-04-0016</a>  <a href="https://doi.org/10.17675/2305-6894-2023-12-1-15">10.17675/2305-6894-2023-12-1-15</a> </li> <li>However, in the other paper, we conducted statistical analysis for grain distribution (<a href="https://doi.org/10.26554/sti.2024.9.3.529-538">10.26554/sti.2024.9.3.529-538</a>); therefore, according to the SEM result, we conducted statistical analysis to find grain distribution. We apologize for this. Thank you.</li> <li>Several tests have been added, such as electrochemical measurement (OCP and potentiodynamic polarization test) and hardness test, to determine the electrochemical behavior and hardness value of the Cu films. Each test describes the quality of Cu films. Thank you.</li> </ul>	<ul style="list-style-type: none"> <li>4-5</li> <li>9-10</li> </ul>
2	<ul style="list-style-type: none"> <li>Discuss how increased deposition rate impacts long-term coating durability.</li> <li>Provide SEM/AFM analysis of coating thickness and uniformity to correlate surface morphology with performance.</li> </ul>	<ul style="list-style-type: none"> <li>We are pleased about that suggestion. But, we connect the deposition rate to the long-term coating durability. Deposition rate greatly affects the speed of Cu ions towards the cathode. This condition will have an impact on the layer thickness. We apologize for this. Thank you.</li> <li>The SEM cross-section was conducted to see the thickness of the Cu layers (average thickness section). Moreover, we cannot correlate the surface morphology to the electrochemical behavior because we don't see porosity on the surface morphology. However, in our other paper, we found a porous surface morphology</li> </ul>	<ul style="list-style-type: none"> <li>4</li> <li>4</li> </ul>

		that can be related to the corrosion rate ( <a href="https://doi.org/10.1380/ejssnt.2024-003">https://doi.org/10.1380/ejssnt.2024-003</a> ). We apologize for this. Thank you.	
3	Conduct a full professional language review (beyond the journal's standard editing). Improve logical flow between sections to make the study easier to understand.	The editor has also commented similarly to the reviewer. Therefore, professional English editing by the Publisher of CST would be assigned after the manuscript is accepted. Thank you	

# Rotating Speed and Magnetic Pole Dependency Assisted on Copper Deposition onto Aluminum Alloy Substrate for Bacterial Eradication Application

Basori<sup>a,\*</sup>, Ruliyanta<sup>b</sup>, Maman Kartaman Ajiriyanto<sup>c</sup>, Rosika Kriswarini<sup>c</sup>, Heri Hardiyanti<sup>c</sup>, Cahaya Rosyidan<sup>d</sup>, Sigit Dwi Yudanto<sup>e</sup>, Evi Ulina Margareta Situmorang<sup>f</sup>, Daniel Edbert<sup>g</sup>, Dwi Nanto<sup>h</sup>, Ferry Budhi Susetyo<sup>i</sup>

<sup>a</sup>Department of Mechanical Engineering, Universitas Nasional, Jakarta, 12520, Indonesia

<sup>b</sup>Department of Electrical Engineering, Universitas Nasional, Jakarta, 12520, Indonesia

<sup>c</sup>Research Center for Nuclear Material and Radioactive Waste Technology, National Research and Innovation Agency, Tangerang Selatan, 15314, Indonesia

<sup>d</sup>Department of Petroleum Engineering, Universitas Trisakti, Jakarta, 11440, Indonesia

<sup>e</sup>Research Center for Metallurgy, National Research and Innovation Agency, Tangerang Selatan, 15314, Indonesia

<sup>f</sup>Department of Physiology School of Medicine and Health Sciences, Atma Jaya Catholic University of Indonesia, Jakarta, 14440, Indonesia

<sup>g</sup>Department of Microbiology, Atma Jaya Catholic University of Indonesia, Jakarta, 14440, Indonesia

<sup>h</sup>Department of Physic Education, UIN Syarif Hidayatullah, Jakarta, 15412, Indonesia

<sup>i</sup>Department of Mechanical Engineering, Universitas Negeri Jakarta, Jakarta, 13220, Indonesia

## Article history:

Received: xx xxxx xxxx / Received in revised form: xx xxxx xxxx / Accepted: xx xxxx xxxx (to be inserted by publisher)

## Abstract

Copper (Cu) coated onto aluminum (Al) alloy could enhance its properties, such as antimicrobial properties, corrosion resistance and hardness value. The present research conducted an electrodeposition of Cu over an Al alloy substrate under influence various magnetic poles and rotating speeds. Several investigations in the present study were conducted, including deposition rate, current efficiency, coating thickness, surface morphology and phase, crystallographic orientation, antibacterial activity, electrochemical behavior, and hardness test. Increasing the rotation speed promoted to enhanced deposition rate and current efficiency for both magnetic poles influence. An increase in the deposition rate from 12.83 to 13.67  $\mu\text{m/h}$  leads to increase thickness, a change in surface morphology near the spheroidal, becoming a faceted structure. Presenting and rising in the rotation of a magnetic field rotation led to a reduced surface roughness and crystallite size of Cu film for both magnetic poles influence. The Cu film made without spinning magnetic has a characteristic of highest bacterial inhibition zone around  $2.50 \pm 0.56 \text{ cm}^2$ . The CuRN50 sample has the lowest corrosion rate, around 0.055 mmpy. The CuRS100 sample has the highest hardness value around 80.72 HV due to has lowest crystallite size.

**Keywords:** North and south pole; SEM-EDS; XRD; Electrochemical behavior; Hardness.

## 1. Introduction

Due to its promising properties, copper (Cu) is widely used in many sectors, such as drinking water piping, heat exchangers, and medical equipment [1–3]. Cu as film has higher bacterial kill performance than bulk Cu [4]. Moreover, Cu coated onto aluminum (Al) alloy could enhance its properties, such as antimicrobial properties, corrosion resistance and hardness value [4,5]. Furthermore, coating synthesis can be conducted by means of electrochemical, spin coating, or spray methods [6–8]. Because of its simplicity and

affordability, the electrodeposition method is a more suitable method for coating Cu onto Al alloy [9].

Cu electrodepositions attract many researchers to investigate formed Cu films. In their study, Brands *et al.* investigated the structure, surface morphology, electrical, optical, and magnetic properties of electrodeposited  $\text{Cu}_2\text{O}$  [10]. Antenucci *et al.* have improved (the mechanical and thermal properties) of open-cell Al foams through Cu electrodeposition [11]. Augustin *et al.* investigated the effect of current density at Cu electrodeposition on the microstructure, hardness, and antibacterial activity of Cu for antimicrobial Al touch application [4]. Kuisor *et al.* fabricated CuO film using electrodeposition. Then, the film was tested for antibacterial activity using *Staphylococcus aureus* (S.

\* Corresponding author.

Email: [basori@civitas.unas.ac.id](mailto:basori@civitas.unas.ac.id)

doi (to be inserted by publisher)





*aureus*), which successfully reduced the bacterial colony during the experiment [12]. Isa *et al.* performed electrodeposition Cu over 304 stainless steels, and a coated sample was tested for antibacterial properties. At 10 minutes of exposure to the coated sample, a 100 % reduction of *S. aureus* was successfully achieved [13].

Many factors, including the magnetic field, influenced the formed Cu films when electrodeposition was performed. The existing magnetic field at the electrodeposition process could appear to have several forces. The Lorentz force acts on a moving ion in the solution, resulting in convection flow [14]. The effects of the magnetic field may also relate to the electrokinetic-magnetohydrodynamic (MHD) effect which resulting the body force acting in the diffuse layer [15]. Another force due to the magnetic field is a paramagnetic gradient force [16]. The paramagnetic gradient force causes the movement of magnetic ions in the diffusion layer. Another possible force is a magnetic gradient force. This force acts on paramagnetic and diamagnetic ions [17]. Generally, introducing a magnetic field during the electrodeposition process leads to the arranging of moving ions towards the cathode.

Due to the many forces exhibited by presenting a magnet, several researchers investigations were focused on unrotated magnetic field-induced Cu electrodeposition [14,18–22]. Miura *et al.* investigated the electrodeposition of Cu under 15 T of magnetic field and found extraordinary dendritic growth [19]. Murdoch *et al.* conducted an electrodeposition of Cu using influence 0.25 and 0.5 T placed on the working electrode's reverse, resulting in the lowest thickness when influencing 0.25 and 0.5 T with the south pole than the north pole [14]. Sudibyo *et al.* conducted electrodeposition of Cu using influence 300 and 900 G (neodymium magnet), resulting in higher grain when electrodeposition Cu using influence 900 G [22]. Yin *et al.* investigated anomalous Cu hydride phase during magnetic field-assisted electrodeposition of Cu. Presenting an anti-parallel magnetic field affecting the magnetohydrodynamic effect, could enhance the hydrogen evolution and result in poor film quality [18]. Kovalyov *et al.* have found that a weak magnetic field (0.5 and 0.7 mT) could affect the electrodeposition process, surface morphology, and texture [20]. Liu *et al.* have stated that magnetic field-assisted electrodeposition could change hydrogen bond structure, reduce the charge transfer resistance, and increase the electrolyte viscosity [21].

Electrodeposition assisted with a spinning magnetic field is considered to attract several researchers due to its ability to enhance the properties of films. Wang and Chen used 0.18 T of a magnetic field with various rotating speeds (1000–3000 rpm) when electrodeposition of nickel (Ni) and results presenting a magnetic field with various rotating speeds could decrease surface roughness [23]. Ji *et al.* fabricated Ni-SiC using an electrodeposition process and found that the exhibit rotating magnetic field makes SiC particle distribution more uniform [24]. Syamsuir *et al.* have stated presenting a rotating magnetic field (500 and 800 rpm) at electrodeposition process makes surface morphology of the film more uniform [25]. Syamsuir *et al.* have found that increasing the rotating speed of a magnetic field (one piece of neodymium magnet arranged spread five parts in the upside Teflon) at electrodeposition

process could transform surface morphology from spheroidal to faceted structure [5].

Oxygen content on the Cu film surface could disrupt the transformation of Cu to Cu ions, reducing antibacterial performance [26]. The formation of surface morphology could have an impact on the antibacterial performance. Surface morphology, such as spheroidal and faceted structures, also contributed to the inhibition zone. A Cu film with spheroidal coating tends to create a higher inhibition zone [5].

The use of a magnetic field during electrodeposition can influence the movement of ions towards the cathode surface. Adjusting magnetic field rotation during electrodeposition also influences the movement of ions. Furthermore, the different poles of the magnet selected also influence ion movement at electrodeposition process. Generally, the ions' movement speed could affect the forming film's properties. According to the literature review above, higher rotation was used ( $\geq 500$  rpm) to influence the electrodeposition; therefore, the present study used 50 and 100 rpm. 50, and 100 rpm speed rotation were chosen according to previous study where conducting Cu electrodeposition using barreling apparatus [27]. Syamsuir *et al.* used one piece of neodymium magnet arranged to spread five parts in the upside Teflon [5]. Therefore, the present research used more neodymium magnets to result in more influence of the magnetic field. Moreover, the influence of spinning using different magnetic poles was also not considered. Murdoch *et al.* found that different magnetic poles influenced the deposition process, resulting in different surface morphologies in Cu films [14]. Therefore, the present research comprehensively investigated the influence of the rotating speed and magnetic pole during Cu electrodeposition on the formation of the film for bacterial eradication applications. The electrodeposition of Cu was influenced by various magnetic poles (north and south) and magnetic rotating speeds (0, 50, and 100 rpm). Several investigations were conducted using digital scales, scanning electron microscopy equipped with energy dispersive spectroscopy (SEM-EDS), X-ray diffraction, digital camera, optical microscope, potentiostat dan Vickers hardness.

## 2. Materials and Methods

### 2.1. Material

Al alloy (0.106 wt.% Si, 0.365 wt.% Fe, 0.055 wt.% Cu, 0.043 wt.% Mn, 0.030 wt.% Mg, 0.003 wt.% Zn, 0.002 wt.% Ni, 0.018 wt.% Ti, 0.003 wt.% Pb, and Al balance) used as cathode, while pure Cu was used as anode. Electrolyte solution was prepared by dissolving  $\text{CuSO}_4 \cdot 5\text{H}_2\text{O}$  (Merck) in deionized water. Electrolyte solution (250 ml of volume) was used for electrodeposition and has a composition 0.5 M  $\text{CuSO}_4 \cdot 5\text{H}_2\text{O}$  plus 20 ml of  $\text{H}_2\text{SO}_4$ .

### 2.2. Sample preparation

Firstly, Al alloy was cut  $2 \times 2$  cm for electrodeposition substrate using the shearing machine. Then, Cu film was made using a DC power supply (MDB PS-305DM) with 40 mA, 25 °C, and pH 5.5 for one h. Cu films were prepared under the influence of a clockwise rotating magnetic field, as seen in

Fig. 1. The plating bath was placed on top of the rotation magnetic field equipment. Two pieces of neodymium magnet were stacked and arranged (six parts) in the upside Teflon, as seen in Fig. 1. One piece of neodymium magnet has 0.08 T of intensity (measured using gauss meter TD-8620). The five variation samples were made; one sample was made without the influence of a rotating magnetic field as a baseline. The sample was made by influencing 50 rpm and 100 rpm. Moreover, different pole variations are also used in the present study. The complete sample name is seen in Table 1.

Table 1. Sample name and remark

Sample name	Remark
CuR0	without the influence of a rotating magnetic field
CuRN50	50 rpm, north pole near the substrate
CuRN100	100 rpm, north pole near the substrate
CuRS50	50 rpm, south pole near the substrate
CuRS100	100 rpm, south pole near the substrate

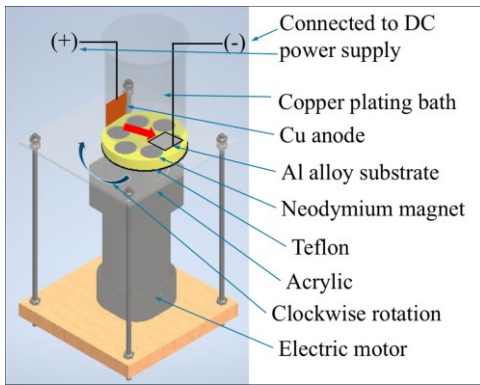


Fig. 1. Rotation magnetic field equipment

### 2.3. Characterizations

The deposition rate and current efficiency were measured similarly to previous studies [17]. Thermo Scientific SEM-EDS was used to investigate surface morphology and elements. The cross section also investigated using SEM apparatus to measure Cu layer thickness. According to SEM image, Image J software was used to measure grain distribution and the roughness of Cu film. X-ray diffraction was conducted using PANalytical (Cu K radiation) with step size  $0.02^\circ$  and then refined using GSAS software [28].

Antibacterial activity was investigated similarly according to previous studies [5]. Assessment of microbial reduction of various samples is adapted from ISO 22196 for non-porous material. *S. aureus* ATCC 25923 was used in this test. The inhibition zone was documented using a digital camera and assessed using an unaided eye. The area of inhibition is measured by Image J software. Each measurement is performed five times to ensure the homogeneity of the data. The diffusible area is calculated by subtracting the area of inhibition from the size of the metal. One-way ANOVA analysis was conducted, to investigate whether there is significance between the polarities of the magnets. Moreover, the specimen was then removed from the plate using sterile

forceps. The agar is re-incubated at  $35^\circ\text{C} \pm 2$  for 24 hours to observe the antimicrobial activity post-contact. The oxides of the metal that formed before and after the test were observed using Olympus CX23 microscope under  $180\times$  magnification; any changes inside of the agar plate were documented. In addition, microbial reduction test observations also conducted (1, 2, 4, 6 and 12 h).

The electrochemical test was conducted using Ossila potentiostat in 0.9 % NaCl (room temperature). Prior to the electrochemical test, Cu films were mounted and left open area for  $1 \times 1 \text{ cm}^2$ . Cu films as working electrode, Ag/AgCl as reference electrode and Pt wire as counter electrode. There are two kinds tested in electrochemical behavior measurement, such as open circuit potential (OCP) and potentiodynamic polarization. OCP was performed until 1200 seconds, while potentiodynamic polarization was performed from -1 to -0.1 V using 5 mV/s of scan rate. The potentiodynamic polarization data was analyzed using the Tafel extrapolation method to find  $I_{\text{corr}}$  and  $E_{\text{corr}}$ . Afterward, corrosion rate could be calculated using following equation [29].

$$\text{Corrosion rate (mmpy)} = K ((a I_{\text{corr}})/(n D)) \quad (1)$$

where K is constant (0.00327 mmpy), a is atomic weight,  $I_{\text{corr}}$  is corrosion current density ( $\mu\text{A}/\text{cm}^2$ ), n is the number electron involved, and D is Cu density ( $\text{g}/\text{cm}^3$ ).

The hardness test was performed using Future-Tech (FV-300e) Vickers hardness tester. Five repeatable measurements were conducted over Cu layer by using 1 kg of load.

## 3. Results and Discussion

### 3.1. Deposition Rate and Current Efficiency

Fig. 2 shows the deposition rate and current efficiency of electrodeposition Cu over an Al alloy substrate. They have similar tendencies; an increase in magnet rotation speed leads to a rise in deposition rate and current efficiency.

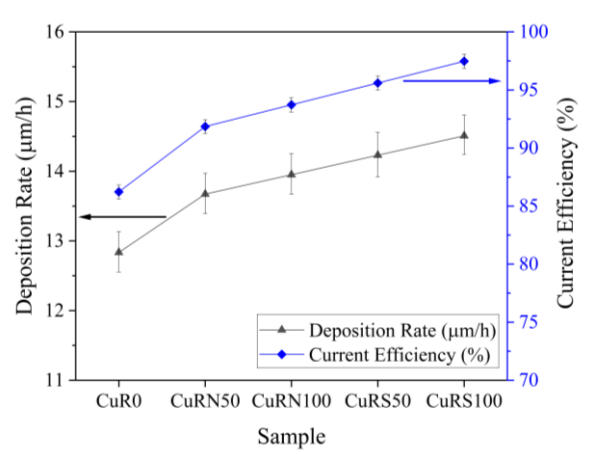


Fig. 2. Deposition rate and current efficiency of Cu electrodeposition

In the process of Cu electrodeposition, the oxidation process occurs at the anode and a reduction process occurs at the cathode. An Al alloy (substrates) to be plated is placed at the cathode. When the current is applied, the Cu ions are depleted in the surroundings of the cathode, making a

diffusion film upper around the cathode. Hydrogen evolution is known to occur at the cathode during Cu electrodeposition from aqueous solutions [17]. Less hydrogen evolution would increase the deposition rate and current efficiency because hydrogen evolution can disturb the movement of the ions to the cathode [30,31]. Presenting an anti-parallel magnetic field (north pole) that affects the MHD effect could enhance the hydrogen evolution, decrease current efficiency, and result in poor film quality [18]. According to Fig. 2, hydrogen evolution seems to influence the electrodeposition process when it is influenced by the north pole. Therefore, the electrodeposition process has a lesser current efficiency than the electrodeposition process when influenced by the south pole.

Cu films made and influenced by the rotating south pole magnet has a higher deposition rate due to the magnetic field, which is parallel to the current direction and attracts more Cu ions onto the Al alloy surface [14]. Rotating the magnet under the electrolyte solution while the electrodeposition process was performed could induce an Eddy electric field [5]. The Eddy electric field could act as an additional MHD flow convection effect [23]. Moreover, increasing the rotation speed could attract more Cu ions onto the Al alloy surface, consequently increasing the deposition rate and current efficiency.

### 3.2. Average Thickness

Figs 3 and 4 shows thickness of various Cu layers and average thickness of Cu layers. Compared to the average thickness to the deposition rate (Fig. 2), there is a correlation between them. Increasing the deposition rate leads to an increase in the average of Cu layers thickness, which is similar to the Syamsuir *et al.* study [27]. Furthermore, it seems that average coating thickness is higher than thickness found by calculating from deposition rate. In example, ideally average coating thickness of CuR0 sample is 12.83  $\mu\text{m}$  due to deposition sample for one hour. Unfortunately, average coating thickness of CuR0 sample is 27.17  $\mu\text{m}$ . This behavior is probably due to the SEM cross section being conducted on an area near to the anode (red arrow Fig. 1). According to Yang *et al.*, end area of the cathode resulting higher thickness than middle area [32]. Therefore, average thickness is higher than deposition rate value.

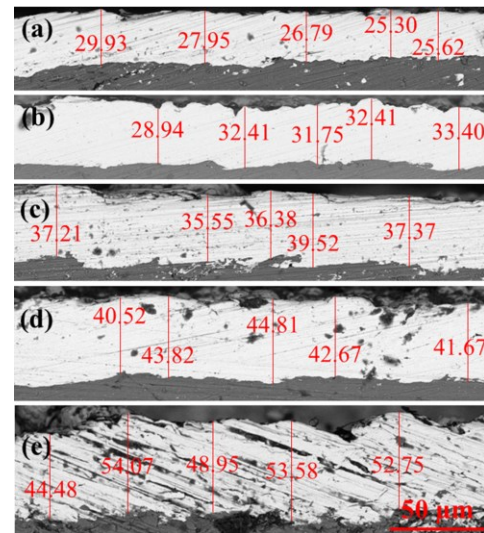


Fig. 3. Thickness of various Cu layers: (a) CuR0; (b) CuRN50; (c) CuRN100; (d) CuRS50; and (e) CuRS100

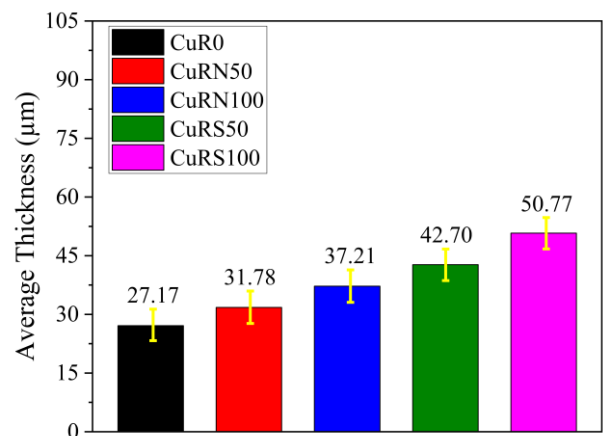


Fig. 4. Cu layers average thickness

### 3.3. SEM-EDS and Roughness

Fig. 5 shows the SEM result and grain distribution of various Cu film surfaces. Samples were made by influencing the north pole magnetic field, which has a larger grain size than samples created by affecting the south pole of a magnetic field. Generally, presenting the south pole magnetic field influence leads to decrease grain size. Meanwhile presenting south pole magnetic field influence leads to increase grain size which is in line with previous study [33]. Murdoch *et al.* have stated different poles used to influence deposition process that would result different grain size [14]. Moreover, according to Lin *et al.* deposition time also contribute to the formed grain size [34].



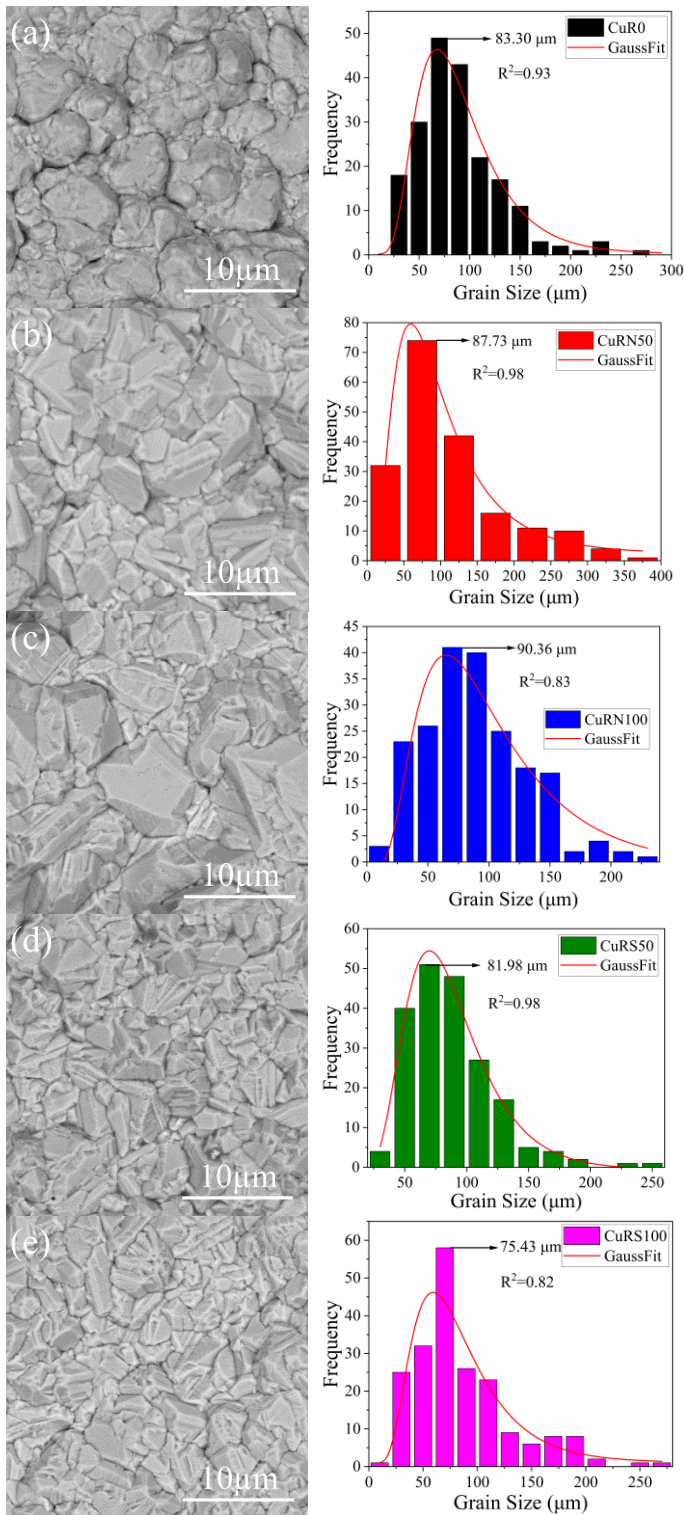
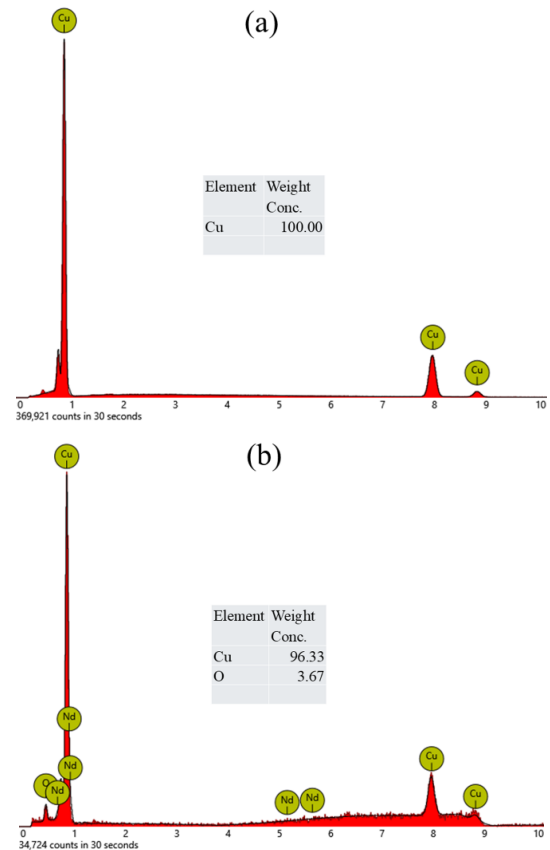


Fig. 5. SEM and grain distribution of Cu layers: (a) CuR0; (b) CuRN50; (c) CuRN100; (d) CuRS50; and (e) CuRS100

According to Fig. 5, the Cu sample was made with no spinning magnetic influence, which led to the formation of morphology near the spheroidal. Cu samples were made with spinning magnetic assistance, leading to the formation of faceted structure morphology [17]. Moreover, the transformation from spheroidal to faceted structure is influenced by the rate of deposition. A higher nucleation rate leads to a higher deposition rate, resulting in a variation in surface morphology [35]. Samples made with influences from

the north pole magnetic field have a low nucleation rate. Hence, having wider grain sizes than samples, caused by influencing the south pole magnetic field [14]. Moreover, an increase in the deposition rate from 12.83 to 13.67  $\mu\text{m}/\text{h}$  leads to a change in surface morphology near the spheroidal becoming faceted structure. The deposition rate between 13.67 and 14.51  $\mu\text{m}/\text{h}$  results in a faceted structure of surface morphology.

The south pole has an affecting magnetic field parallel to the current direction; therefore, Cu ions are more attracted to the Al alloy surface. On the contrary, the north pole has an affecting magnetic field that is anti-parallel to the current direction, reducing Cu ions' attraction onto the Al alloy surface. Moreover, Lorentz's forces rotate opposite each other on top of the surface specimen for different magnetic poles. This condition affected the sample film by influencing the South Pole to be smoother than the North Pole. Ji *et al.* stated that presenting a rotating magnetic field during electrodeposition makes surface morphology more uniform [24]. In this case, the paramagnetic force has a similar tendency for different magnetic poles. Therefore, influencing surface morphology could be neglected.



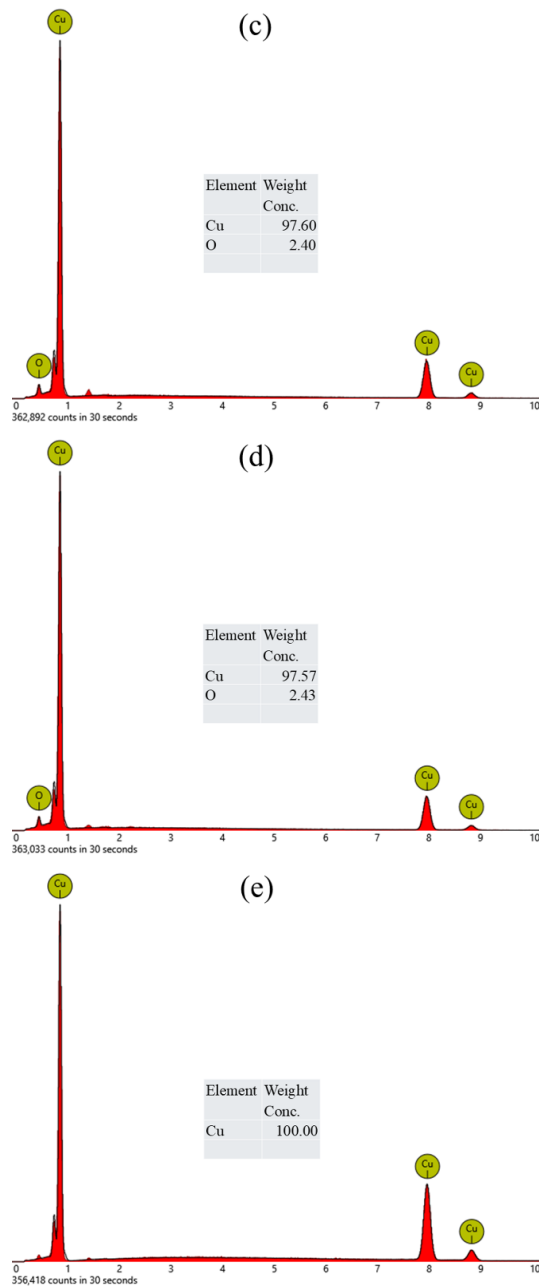


Fig. 6. EDS Cu layers: (a) CuR0; (b) CuRN50; (c) CuRN100; (d) CuRS50; and (e) CuRS100

According to Fig. 6, the spinning magnetic-assisted running at 50 rpm led to oxygen forming on the Cu surface. Moreover, enhanced magnetic rotation led to a decrease or disappearance of oxygen. Presenting oxygen on Cu film is one of the unique cases. Oxygen could form due to a secondary reaction on the anode. Moreover, oxygen could be formed due to sample storage and transport [5].

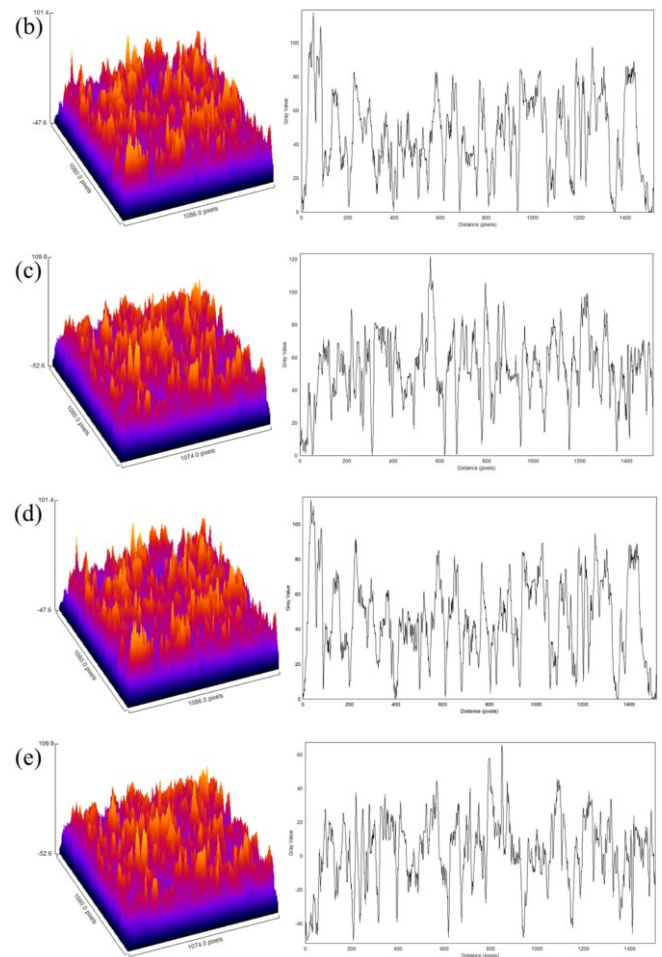
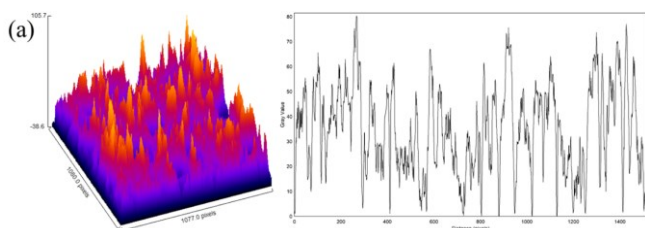


Fig. 7. Roughness Cu layers: (a) CuR0; (b) CuRN50; (c) CuRN100; (d) CuRS50; and (e) CuRS100

Fig. 7 presents the roughness analyzed result from the SEM image using ImageJ software. CuR0, CuRN50, CuRN100, CuRS50, and CuRS100 samples have a surface roughness of 34.62, 18.00, 17.38, 18.60, and 16.58  $\mu\text{m}$ , respectively. Presenting a magnetic field rotation during electrodeposition led to a decrease in the surface roughness of Cu film. More rotation could also decrease surface roughness, which perfectly agrees with the previous study [5]. Wang and Chen have found that presenting a magnetic field during electrodeposition with various rotating speeds could decrease surface roughness [23]. This behavior is probably due to additional MHD flow, which is in line with the deposition rate result and could enhance the Cu ions' movement. A higher deposition rate would result in a higher nucleation rate, consequently producing a smooth surface morphology. Moreover, the sample made by north pole magnet influence has more roughness than sample made by north pole magnet. This behavior probably due to MHD effect that could enhance the hydrogen evolution and resulting more roughness [18].

### 3.4. X-ray diffraction

The diffraction patterns of samples of Cu deposition on substrates composed of Al alloy plates are shown in Fig. 8. The five samples were identified to have Cu phase peaks at the indexed plane peaks (111), (200), (220), (311), and (222)

at angles  $2\theta = 43.31, 50.45, 74.13, 89.94, \text{ and } 95.15^\circ$ . The cubic crystal system is present in the Cu phase, and it has a space group of  $fm-3m$ . The cubic Cu phase peaks at these angles are consistent with findings from studies by Omar and Francisco Briones *et al.* [36,37]. This demonstrates that the procedure for depositing Cu on Al alloy plates has been successfully completed. At the indexed plane peaks (111), (200), (220), (311), and (400) of the five diffraction patterns, they were also found on the Al alloy plate substrate along with the copper phase. Xu *et al.* and Ayieko *et al.* presented a standard Al diffraction pattern that is identical to this peak of Al [38,39].

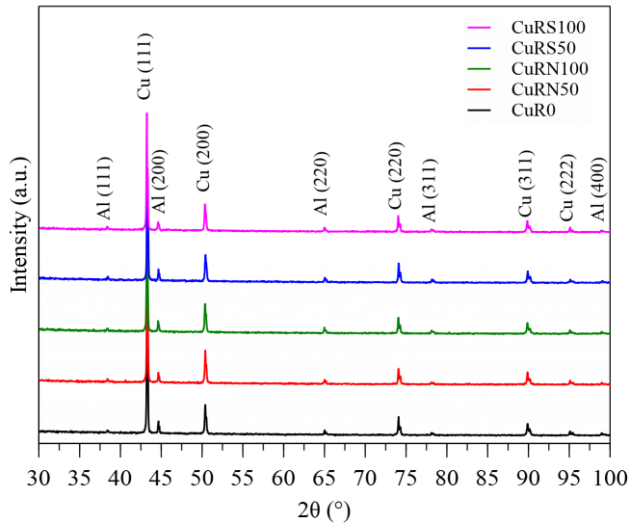


Fig. 8. X-ray diffraction pattern of various sample

Table 2. Crystallographic data calculated from various samples

Source	CuR0	CuRN50	CuRN100	CuRS50	CuRS100
Name: Copper (Cu)					
Phase	Space group: $Fm-3m$ (225)				
	Crystal system: cubic				
Lattice -a (nm)	0.3615	0.3615	0.3615	0.3615	0.3615
wRp (%)	10.10	10.37	10.24	9.86	10.30
GoF	1.067	1.106	1.087	1.045	1.056
Mean crystallite size (nm)	308	173	154	173	126
Micro-strain (%)	0.07	0.05	0.05	0.05	0.04

The mean crystallite size and lattice value of the five deposition samples are compared in order to further analyze the diffraction pattern. The Rietveld method was employed to determine the lattice of the five samples. The cubic Cu phase lattice of all five samples is measured at 0.3615 nm according to the calculation results. Changes in magnetic poles and rotating speed have no effect on the lattice value of the cubic Cu phase. The data from the crystallographic calculation can be found in Table 2. In order to determine the mean crystallite size, the Williamson-Hall plot method is utilized. In contrast

to the lattice value, the mean crystallite size is affected by the rotating speed and poles. The mean crystallite size becomes finer with the increase in magnet rotation speed which is perfectly matched with surface roughness analysis.

### 3.5. Antibacterial Activity

Antibacterial activity test after 24 hours of contact can be seen on Fig. 9. Material placement in the middle of Mueller Hinton agar inoculated with *S. aureus* ATCC 25923. Noticing the inhibition zones around the material; the calculation is presented in Table 3. The metal ions diffuse into the agar to inhibit the growth of *S. aureus*.

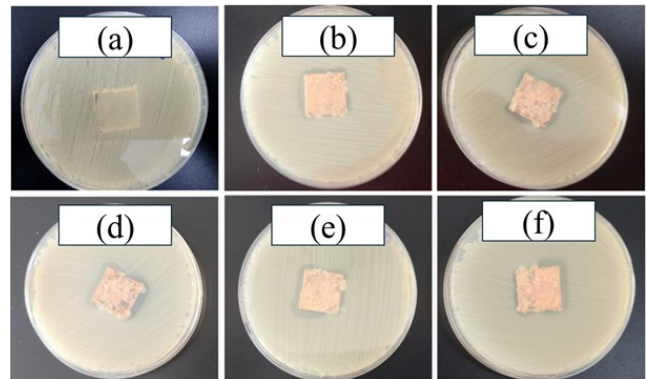


Fig. 9. Antibacterial activity test after 24 hours: (a) blank; (b) CuRN50; (c) CuRN100; (d) CuR0; (e) CuRS50; and (f) CuRS100

Cu, particularly in the form of metal-organic frameworks (MOFs) and nanoparticles, exhibits significant antibacterial activity against Gram-positive bacteria such as *S. aureus* [40]. The peptidoglycan layer in Gram-positive bacteria plays a significant role in their susceptibility to Cu, although its direct interaction with Cu is not as straightforward as with other antimicrobial agents. Cu can induce modifications in the peptidoglycan layer, such as increased cross-linkage, which can affect the overall structure and function of the cell wall. These modifications can either enhance or reduce the susceptibility of Gram-positive bacteria to Cu, depending on the specific bacterial strain and environmental conditions [41,42]. In this research, the Cu induces contact killing. The antimicrobial activity of Cu is believed to involve contact-mediated killing, initiating membrane degradation. The susceptibility of Gram-positive strains to Cu is attributed to the thick peptidoglycan layer, which reduces cell wall permeability to other metal ions, including Zinc [43].

According to Fig. 9, the inoculum was totally annihilated by electroplated materials. The log reduction is not calculated due to the total killing of the bacteria. However, the total reduction of  $> 105$  CFU/ml might suggest a percentage reduction of  $> 99.999\%$  (see Table 3). Moreover, there is a zone of inhibition between the sample and bacterial lawn that is also visible inside the zone's white crystals and some bluish color change inside the agar. This suggests the Cu material diffused and interacted with the agar, resulting in a zone of bacterial growth inhibition.

As seen in Table 3, the widest diffusion zone is observed in CuR0 with the zone of diffusion and inhibition areas of 6.99



cm<sup>2</sup> and 2.5 cm<sup>2</sup>. This is statistically significant with  $p < 0.001$  (ANOVA; CI 95%). There is also significance in independent T-Test analyses between CuR0 and CuR50 group ( $p < 0.001$ ; CI 95%), R0 and R100 group ( $p < 0.001$ ; CI 95%), also between CuR50 and CuR100 Group ( $p < 0.001$ ; CI 95%). To investigate whether there is significance between the polarities of the magnets, independent T-test analyses were performed. There is no significant difference in the outcome between the south pole group and the north pole group ( $p=0.063$ ; CI 95%). Moreover, there were no inhibitions in the blank group, and the bacteria grew underneath the metal. Comparing to the previous study, less inhibition is found in the present study [5]. This behavior is probably due to higher crystallite size form in the all samples [44]. Previous study found crystallite size between 95.66 – 100.50 nm [5]. While in the present study have crystallite size of Cu layer between 126 – 308 nm. Moreover, Ramyadevi *et al.* and Ahmed *et al.* in their studies found inhibition zone 2.2 cm and 2.4 cm when tested Cu nanoparticle for antibacterial activity using *S. aureus* [45,46].

Table 3. The reduction of colony, and diffusible metal observation

Sample	Microbial reduction assessment		Diffusible metal observation	
	Initial load 0 h (CFU/ml)	Final load 24 h (CFU/ml)	Zone of diffusion (cm <sup>2</sup> )	Inhibition area (cm <sup>2</sup> )
Blank		0	4.01 ±0.01	-0.48 ±0.01
CuR0		0	6.99 ±0.12	2.50 ±0.56
CuRN50	3.5 × 10 <sup>5</sup>	0	6.21 ±0.01	1.61 ±0.21
CuRN100		0	6.00 ±0.02	1.89 ±0.02
CuRS50		0	6.16 ±0.41	1.73 ±0.46
CuRS100		0	6.17 ±0.01	2.14 ±0.24

The use of magnetic rotation during material synthesis has a significant impact on the results. Materials synthesized without magnetic rotation (R0) show stronger antibacterial effects compared to those synthesized at 50 rpm or 100 rpm. However, increasing magnet rotation significantly enhances the size of the inhibition zone. As a result, the inhibition zone at 100 rpm is larger than that at 50 rpm. This condition is probably due to forming some oxygen on the Cu films surface as seen in EDS result which could disrupt transformation Cu to be Cu ions. Qu *et al.* has found that antibacterial behavior was influenced by Cu ions [26]. Release of Cu ions inside of the agar is lethal towards *S. aureus* [47].

As shown in Fig. 3, CuR0 surface morphology has formed near to spheroidal, while other samples have form faceted structure. Compared to Table 3, it can be seen that higher inhibition zone is seen in CuR0 sample. Therefore, it can be concluded that the spheroidal form results in the highest inhibition zone than the faceted structure, which is perfectly in agreement with previous study [5]. This condition probably occurs due to the spheroidal structure having a wider surface area than the faceted structure, where more Cu ions being released. Moreover, an increase in rotation leads to a decrease in roughness. Several researchers have found that roughness is independent of the inhibition zone which aligns with the

present study [5,48].

Moreover, the generation of reactive oxygen species (ROS) and damage to cell membranes are the main ways in which metals' broad antibacterial potential has been extensively studied [49–51]. Even so, metals can target particular cellular components and, when combined, are likely to improve pathogen clearance despite their non-specific activity. Conversely, Cu has the ability to change metabolic pathways in addition to causing damage to DNA and cell membranes through the generation of ROS [52]. The combined mode of action has not yet been investigated, to the authors' knowledge, despite the fact that the modes of action of various metal ions have been well explored. The variability in antimicrobial efficaciousness between various combinations can be explained by the diverse chemical reactivity of metal ions with bacterial cells and their specific biological targets [53].

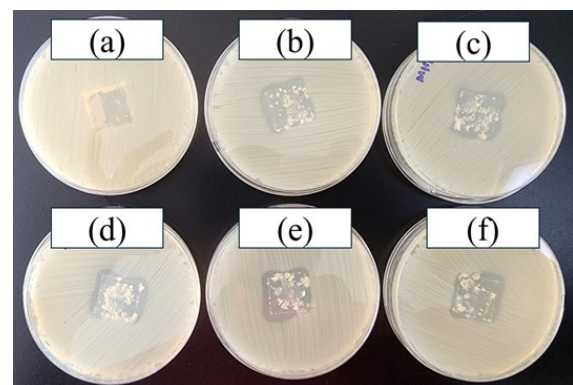


Fig. 10. After 24 hours of post contact test: (a) blank; (b) CuRN50; (c) CuRN100; (d) CuR0; (e) CuRS50; and (f) CuRS100

Fig. 10 shows the results after 24 hours of post-contact testing. The inhibitory zones appear after the removal of the material. There are some metal infiltrations inside of the agar on every plate that causes the agar to crack. This suggests that there is a gas-forming or exothermic reaction inside of the agar, increasing the antimicrobial ability of the material [54]. There are no anti-Staphylococcal effects on the blank material; therefore, there is a regrowth of microorganisms in the place where the metal was previously placed.

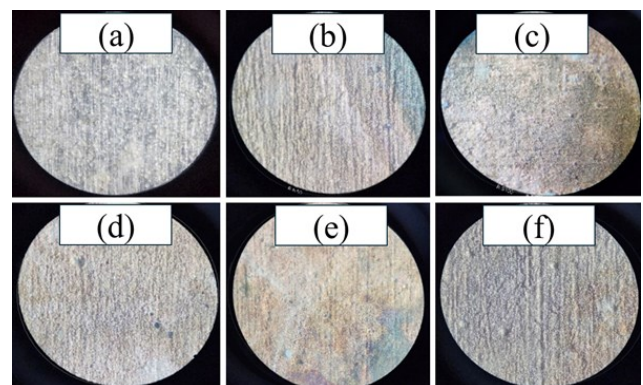


Fig. 11. Antibacterial activity pretest microscope observation: (a) blank; (b) CuRN50; (c) CuRN100; (d) CuR0; (e) CuRS50; and (f) CuRS100

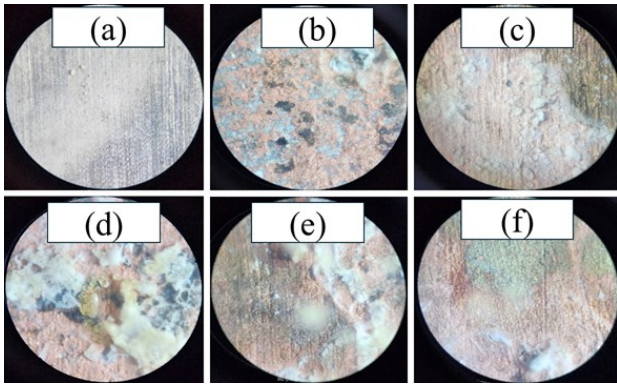


Fig. 12. Antibacterial activity post-test microscope observation: (a) blank; (b) CuRN50; (c) CuRN100; (d) CuR0; (e) CuRS50; and (f) CuRS100

Fig. 11 shows antibacterial activity pretest microscope observation, and Fig. 12 shows antibacterial activity post-test microscope observation. Microscopic observation of electroplated surfaces occurs under  $180 \times$  magnification optical microscope. There is a significant proportion in the formation of white crystals on the electroplated surface after tests. The crystals did not form on the surface of the blank. The Cu forms oxides, which change the color of the surface. According to Marković et al., change color in the Cu due to adsorption or reduction Cu ions [55].

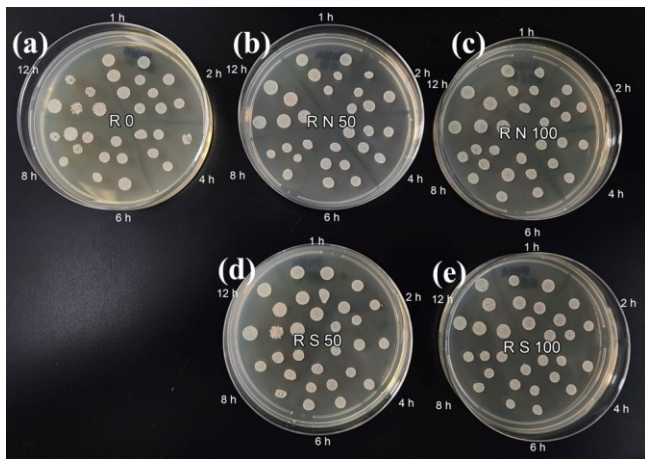


Fig. 13. Microbial reduction test observation: (a) CuR0; (b) CuRN50; (c) CuRN100; (d) CuRS50; and (e) CuRS100

To deep explore microbial reduction assessment, investigating at 1, 4, 6, 8, and 12 hours were conducted as seen in Fig. 13 and Table 4. At 6 hours of investigation, it can be seen that CuR0 sample has resulted in a reduction colony-forming units per milliliter around  $10^4$  which is in line with inhibition area value (higher inhibition area). While other samples are still showing similar results when initial exposure occurs (See Table 3).

Table 4. Microbial reduction assessment of Cu samples

Sample name	1 h	2 h	4 h	6 h	12 h
	(CFU/ml)				
CuR0	$>10^5$	$>10^5$	$>10^5$	$10^4$	$10^4$
CuRN50	$>10^5$	$>10^5$	$>10^5$	$>10^5$	$>10^5$
CuRN100	$>10^5$	$>10^5$	$>10^5$	$>10^5$	$>10^5$
CuRS50	$>10^5$	$>10^5$	$>10^5$	$>10^5$	$>10^5$
CuRS100	$>10^5$	$>10^5$	$>10^5$	$>10^5$	$>10^5$

### 3.6. Electrochemical Behavior

Fig. 14 shows OCP measurement result of various Cu samples. E<sub>OCP</sub> values of the CuR0, CuRN50, CuRN100, CuRS50, and CuRS100 are -0.643, -0.667, -0.658, -0.633, and -0.641 V vs Ag/AgCl, respectively. Previous study is found E<sub>OCP</sub> of Cu layer over Al alloy between -0.694 to -0.684 V vs Ag/AgCl [27]. All samples show shift to more negative value in order to reach steady state condition. According to Tasić et al. study, this condition implies the Cu oxide dissolution and CuCl layer formation [56]. The CuRN50 layer seems more stable than the other sample, which showing to reach steady state at around 600 s for OCP measurement.

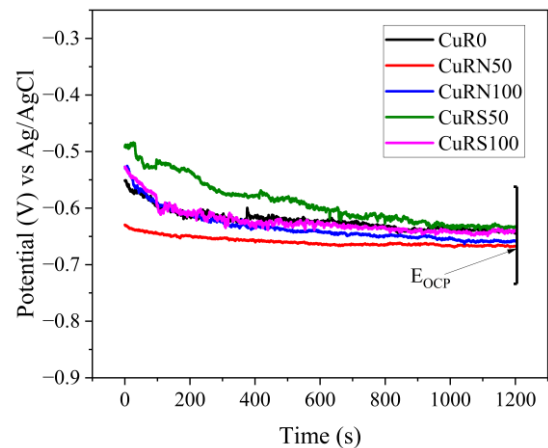


Fig. 14. OCP test curve

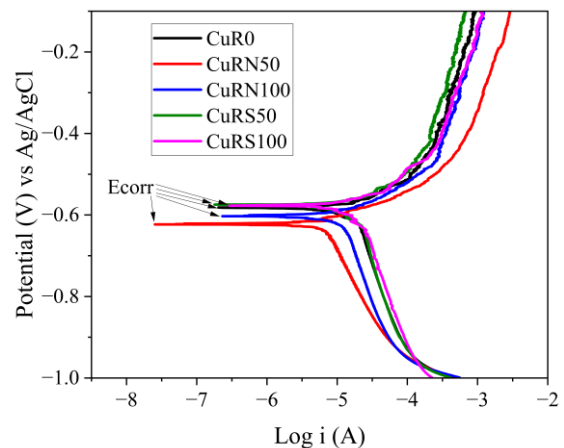


Fig. 15. Potentiodynamic polarization test curve

Fig. 15 represents potentiodynamic polarization test result in 0.9 % NaCl. Tafel extrapolation result could be seen in Table 4. Using Eq. (1) corrosion rate could be calculated and summarized in Table 5.

Table 5. Tafel extrapolation result and corrosion rate

Sample name	$E_{corr}$ (V) vs Ag/AgCl	$i_{corr}$ (A/cm <sup>2</sup> )	Corrosion rate (mmpy)
CuR0	-0.582	$1.27 \times 10^{-5}$	0.148
CuRN50	-0.623	$4.78 \times 10^{-6}$	0.055
CuRN100	-0.603	$8.77 \times 10^{-6}$	0.102
CuRS50	-0.574	$8.56 \times 10^{-6}$	0.099
CuRS100	-0.577	$1.14 \times 10^{-5}$	0.132

Based on Table 5, it can be seen that the sample with the lowest corrosion rate is the CuRN50 sample, probably due to highest oxygen on the Cu surface that could form an oxide [57]. According to Narayanan *et al.* oxygen content in the Cu film would be an obstacle for chloride ions to adsorb in the film [58]. Therefore, that oxide could result in better protection from aggressive species in the 0.9 % NaCl medium. Moreover, compared to Fig. 6, the oxygen content of the Cu layer is linear to the corrosion rate. Higher oxygen content led to decrease corrosion rate.

### 3.7. Hardness Test

Fig. 17 represents average hardness test result using 1 kg of load. The hardness test was conducting five repeatable measurements on top of Cu layer. The average hardness in the present study varies between 47.92 – 80.72 HV. Ghosh *et al.* has found that Cu layer hardness from 22.9 to 114.7 HV [59]. Previous study also found Cu layer hardness between 72.94 – 76.26 HV [5]. Moreover, Augustine *et al.* stated that hardness value is dependent on the crystallite size. The lowest crystallite size promoted to resulting higher hardness [4]. Comparing Fig. 16 to Table 2, there is linear correlation between hardness and crystallite size. Higher hardness value is seen at CURS sample, while smallest hardness is found at CuR0 sample.

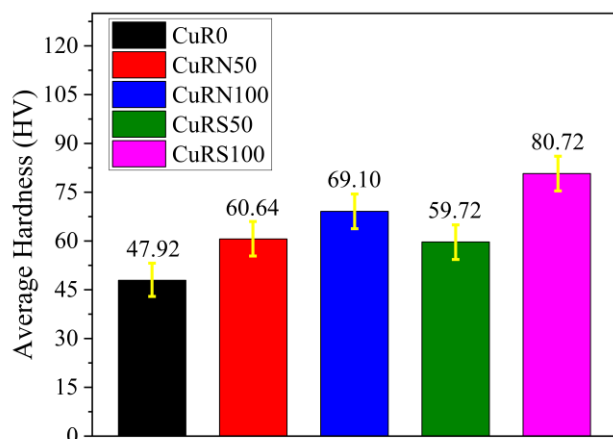


Fig. 16. Average of the hardness test result

## 4. Conclusion

The Cu films were fabricated under a spinning magnetic field with various rotation speeds and a magnetic pole was successfully conducted. Higher rotation speed is promoted to enhance deposition rate and current efficiency for both magnetic poles. The Cu sample was fabricated with an un-present spinning magnetic influence, which led to the forming morphology near the spheroidal. Cu samples were made with spinning magnetic influence, which led to the forming morphology near the faceted structure. Magnetic-assisted spinning at 50 rpm led to oxygen forming on the Cu surface for both magnetic poles and enhanced rotation, which led to the decrease or disappearance of oxygen. Presenting and more of a magnetic field rotation led to decreased surface roughness and crystallite size of Cu film for both magnetic poles. The Cu sample made without spinning magnetic fields influence has the highest inhibition zone size, probably due to the absence of oxygen on the Cu film surface and the morphology near the spheroidal. The oxygen content of the Cu layer is linear to the corrosion rate. Higher oxygen content led to decrease corrosion rate while the lowest crystallite size promoted to higher hardness. Generally, Cu films successfully covered Al alloy and could transform it into antibacterial material. Future recommendations for this study are conducting electrodeposition of Cu with influencing rotation magnetic higher than 100 rpm.

## Acknowledgements

This study has been supported by the Ministry of Education, Culture, Research, and Technology through grand funding Penelitian Fundamental-Reguler with contract number 087/LPPM-UNAS/VI/2024 and 815/LL3/AL.04/2024.

## References

1. D. A. Lytle and C. P. White, *The effect of phosphate on the properties of copper drinking water pipes experiencing localized corrosion*, J. Fail. Anal. Prev. 14 (2014) 203–219.
2. M. M. Lachowicz, *A metallographic case study of formicary corrosion in heat exchanger copper tubes*, Eng. Fail. Anal. 111 (2020) 104502.
3. N. Thokala, C. Kealey, J. Kennedy, D. B. Brady and J. B. Farrell, *Characterisation of polyamide 11/copper antimicrobial composites for medical device applications*, Mater. Sci. Eng. C 78 (2017) 1179–1186.
4. A. Augustin, P. Huilgol, K. R. Udupa and U. B. K., *Effect of current density during electrodeposition on microstructure and hardness of textured Cu coating in the application of antimicrobial Al touch surface*, J. Mech. Behav. Biomed. Mater. 63 (2016) 352–360.
5. Syamsuir, F. B. Susetyo, B. Soegijono, S. D. Yudanto, Basori, M. K. Ajiriyanto *et al.*, *Rotating-Magnetic-Field-Assisted Electrodeposition of Copper for Ambulance Medical Equipment*, Automot. Exp. 6 (2023) 290–302.
6. A. M. Alghamdi and F. Fadhillah, *Thin film composite polyelectrolyte multilayer nanofiltration membrane fabricated*

using spin assisted layer by layer assembly: Application of solution diffusion film model, Commun. Sci. Technol. 5 (2020) 10–15.

7. C. Santoso, Ratnawati and Slamet, *Utilization of glycerol solution for hydrogen production by a combination of photocatalysis and electrolysis processes with Fe-TiO<sub>2</sub> nanotubes*, Commun. Sci. Technol. 8 (2023) 208–215.
8. W. Trisunaryanti, K. Wijaya and A. M. Tazkia, *Preparation of Ni/ZSM-5 and Mo/ZSM-5 catalysts for hydrotreating palm oil into biojet fuel*, Commun. Sci. Technol. 9 (2024) 161–169.
9. A. Lelevic and F. C. Walsh, *Electrodeposition of Ni-P alloy coatings: A review*, Surf. Coatings Technol. 369 (2019) 198–220.
10. I. S. Brandt, M. A. Tumelero, S. Pelegrini, G. Zangari and A. A. Pasa, *Electrodeposition of Cu<sub>2</sub>O: growth, properties, and applications*, J. Solid State Electrochem. 21 (2017) 1999–2020.
11. A. Antenucci, S. Guarino, V. Tagliaferri and N. Ucciardello, *Improvement of the mechanical and thermal characteristics of open cell aluminum foams by the electrodeposition of Cu*, Mater. Des. 59 (2014) 124–129.
12. A. Kusior, J. Mazurkow, P. Jelen, M. Bik, S. Raza, M. Wdowiak et al., *Copper Oxide Electrochemical Deposition to Create Antiviral and Antibacterial Nanocoatings*, Langmuir 40 (2024) 14838–14846.
13. N. N. C. Isa, Y. Mohd, M. H. M. Zaki and S. A. S. Mohamad, *Electrodeposition of copper coating on 304 stainless steel substrate: Physicochemical properties and antibacterial activity*, in ADVANCED MATERIALS FOR SUSTAINABILITY AND GROWTH: Proceedings of the 3rd Advanced Materials Conference 2016 (3rd AMC 2016), 1901 (2017), pp. 020009.
14. H. A. Murdoch, D. Yin, E. Hernández-Rivera and A. K. Giri, *Effect of applied magnetic field on microstructure of electrodeposited copper*, Electrochem. commun. 97 (2018) 11–15.
15. Q. Long, Y. Zhong and J. Wu, *Research progress of magnetic field techniques for electrodeposition of coating*, Int. J. Electrochem. Sci. 15 (2020) 8026–8040.
16. K. Kołodziejczyk, E. Miękoś, M. Zieliński, M. Jaksender, D. Szczukocki, K. Czarny et al., *Influence of constant magnetic field on electrodeposition of metals, alloys, conductive polymers, and organic reactions*, J. Solid State Electrochem. 22 (2018) 1629–1674.
17. B. Soegijono, F. B. Susetyo, Yusmaniar and M. C. Fajrah, *Electrodeposition of paramagnetic copper film under magnetic field on paramagnetic aluminum alloy substrates*, e-Journal Surf. Sci. Nanotechnol. 18 (2020) 281–288.
18. D. Yin, H. A. Murdoch, B. Chad Hornbuckle, E. Hernández-Rivera and M. K. Dunstan, *Investigation of anomalous copper hydride phase during magnetic field-assisted electrodeposition of copper*, Electrochem. commun. 98 (2019) 96–100.
19. M. Miura, Y. Oshikiri, A. Sugiyama, R. Morimoto, I. Mogi, M. Miura et al., *Magneto-Dendrite Effect: Copper Electrodeposition under High Magnetic Field*, Sci. Rep. 7 (2017) 1–8.
20. S. V. Kovalyov, O. B. Girin, C. Debiemme-Chouvy and V. I. Mishchenko, *Copper electrodeposition under a weak magnetic field: effect on the texturing and properties of the deposits*, J. Appl. Electrochem. 51 (2021) 235–243.
21. Y. Liu, B. Zheng, T. Zhang, Y. Chen, J. Liu, Z. Wang et al., *Magnetic field intensified electrodeposition of low-concentration copper ions in aqueous solution*, Electrochim. Acta 432 (2022) 141201.
22. Sudibyo, M. B. How and N. Aziz, *Influences of magnetic field on the fractal morphology in copper electrodeposition*, in IOP Conference Series: Materials Science and Engineering, 285 (2018), pp. 012021.
23. T. Wang and W. Chen, *Effects of Rotating Magnetic Fields on Nickel Electro-Deposition*, ECS Electrochem. Lett. 4 (2015) D14–D17.
24. R. Ji, K. Han, H. Jin, X. Li, Y. Liu, S. Liu et al., *Preparation of Ni-SiC nano-composite coating by rotating magnetic field-assisted electrodeposition*, J. Manuf. Process. 57 (2020) 787–797.
25. S. Syamsuir, F. B. Susetyo, B. Soegijono, S. D. Yudanto, Basori and D. Nanto, *Nickel layers properties produced by electroplating were influenced by spinning permanent magnet*, in Journal of Physics: Conference Series, 2596 (2023), pp. 012008.
26. X. Qu, H. Yang, B. Jia, Z. Yu, Y. Zheng and K. Dai, *Biodegradable Zn–Cu alloys show antibacterial activity against MRSA bone infection by inhibiting pathogen adhesion and biofilm formation*, Acta Biomater. 117 (2020) 400–417.
27. Syamsuir, R. S. Kusumah, A. Premono, A. Lubi, B. Soegijono, S. D. Yudanto et al., *Spinning Effect of Barreling Plating on Physical Properties and Electrochemical Behavior of Copper Layers*, e-Journal Surf. Sci. Nanotechnol. 22 (2024) 120–128.
28. A. C. Larson and R. B. Von Dreele, *General Structure Analysis System (GSAS)*, Vol. 748, University of California, Los Alamos, 2004.
29. R. M. Yusron, R. M. Bisono and M. Pramudia, *Effect Electrolyte Temperature and Electrode Distance to Electroplating Hard-Chrome on Medium-Carbon Steel*, J. Phys. Conf. Ser. 1569 (2020) 042007.
30. X. Qiao, H. Li, W. Zhao and D. Li, *Effects of deposition temperature on electrodeposition of zinc-nickel alloy coatings*, Electrochim. Acta 89 (2013) 771–777.
31. M. A. Lopez-Heredia, P. Weiss and P. Layrolle, *An electrodeposition method of calcium phosphate coatings on titanium alloy*, J. Mater. Sci. Mater. Med. 18 (2007) 381–390.
32. G. Yang, D. Deng, Y. Zhang, Q. Zhu and J. Cai, *Numerical Optimization of Electrodeposition Thickness Uniformity with Respect to the Layout of Anode and Cathode*, Electrocatalysis 12 (2021) 478–488.
33. F. B. Susetyo, B. Soegijono and Yusmaniar, *Effect of a constant magnet position and intensity on a copper layer obtained by DC electrodeposition*, Int. J. Corros. Scale Inhib. 10 (2021) 766–782.
34. Y. Lin, J. Pan, H. F. Zhou, H. J. Gao and Y. Li, *Mechanical properties and optimal grain size distribution profile of gradient grained nickel*, Acta Mater. 153 (2018) 279–289.
35. D. Grujicic and B. Pesic, *Reaction and nucleation mechanisms of copper electrodeposition from ammoniacal solutions on vitreous carbon*, Electrochim. Acta 50 (2005) 4426–4443.
36. Halo Dalshad Omar, *Intensity Correction and Pole Figure Measurement of Copper Metallic by XRD*, J. Basic Appl. Sci. 12 (2016) 320–322.
37. F. Briones, V. Seriacopi, C. Martínez, J. L. Valin, D. Centeno and I. F. Machado, *The effects of pressure and pressure routes on the microstructural evolution and mechanical properties of sintered copper via SPS*, J. Mater. Res. Technol. 25 (2023) 2455–2470.
38. X. Xu, Z. Liu, B. Zhang, H. Chen, J. Zhang, T. Wang et al., *Effect of Mn content on microstructure and properties of 6000 series aluminum alloy*, Appl. Phys. A Mater. Sci. Process. 125 (2019) 1–9.
39. C. O. Ayieko, R. J. Musembi, A. A. Ogacho, B. O. Aduda, B. M. Muthoka and P. K. Jain, *Controlled Texturing of Aluminum Sheet for Solar Energy Applications*, Adv. Mater. Phys. Chem. 05 (2015) 458–466.



40. M. Hubab and M. A. Al-Ghouti, *Recent advances and potential applications for metal-organic framework (MOFs) and MOFs-derived materials: Characterizations and antimicrobial activities*, Biotechnol. Reports 42 (2024) e00837.
41. S. J. Kim, J. Chang and M. Singh, *Peptidoglycan architecture of Gram-positive bacteria by solid-state NMR*, Biochim. Biophys. Acta - Biomembr. 1848 (2015) 350–362.
42. X. Chen, Y. Li, K. Bai, M. Gu, X. Xu, N. Jiang et al., *Class A Penicillin-Binding Protein C Is Responsible for Stress Response by Regulation of Peptidoglycan Assembly in Clavibacter michiganensis*, Microbiol. Spectr. 10 (2022).
43. S. Xhafa, L. Olivieri, C. Di Nicola, R. Pettinari, C. Pettinari, A. Tombesi et al., *Copper and Zinc Metal–Organic Frameworks with Bipyrazole Linkers Display Strong Antibacterial Activity against Both Gram+ and Gram– Bacterial Strains*, Molecules 28 (2023) 6160.
44. A. Azam, A. S. Ahmed, M. Oves, M. S. Khan and A. Memic, *Size-dependent antimicrobial properties of CuO nanoparticles against Gram-positive and -negative bacterial strains*, Int. J. Nanomedicine 7 (2012) 3527–3535.
45. J. Ramyadevi, K. Jeyasubramanian, A. Marikani, G. Rajakumar and A. A. Rahuman, *Synthesis and antimicrobial activity of copper nanoparticles*, Mater. Lett. 71 (2012) 114–116.
46. M. Ahamed, H. A. Alhadlaq, M. A. M. Khan, P. Karuppiyah and N. A. Al-Dhabi, *Synthesis, characterization, and antimicrobial activity of copper oxide nanoparticles*, J. Nanomater. 2014 (2014).
47. L. Huang, E. M. Fozo, T. Zhang, P. K. Liaw and W. He, *Antimicrobial behavior of Cu-bearing Zr-based bulk metallic glasses*, Mater. Sci. Eng. C 39 (2014) 325–329.
48. M. A. Hajduga, S. Węgrzynkiewicz, J. Waś-Solipiwo, M. Hajduga and M. B. Hajduga, *Innovative solutions from the field of the material science and medicine in the interior of modern ambulances*, Mater. Sci. Forum 844 (2016) 50–54.
49. P. L. Lam, R. S. M. Wong, K. H. Lam, L. K. Hung, M. M. Wong, L. H. Yung et al., *The role of reactive oxygen species in the biological activity of antimicrobial agents: An updated mini review*, Chem. Biol. Interact. 320 (2020) 109023.
50. S. Alfai, G. C. Schito, A. M. Schito and G. Zuccari, *Reactive Oxygen Species (ROS)-Mediated Antibacterial Oxidative Therapies: Available Methods to Generate ROS and a Novel Option Proposal*, Int. J. Mol. Sci. 25 (2024).
51. A. A. Dayem, M. K. Hossain, S. Bin Lee, K. Kim, S. K. Saha, G. M. Yang et al., *The role of reactive oxygen species (ROS) in the biological activities of metallic nanoparticles*, Int. J. Mol. Sci. 18 (2017) 1–21.
52. A. R. Mir, J. Pichtel and S. Hayat, *Copper: uptake, toxicity and tolerance in plants and management of Cu-contaminated soil*, BioMetals 34 (2021) 737–759.
53. F. N. S. Raja, T. Worthington and R. A. Martin, *The antimicrobial efficacy of copper, cobalt, zinc and silver nanoparticles: alone and in combination*, Biomed. Mater. 18 (2023) 045003.
54. S. Y. Tsai, Y. M. Liu, Z. W. Lin and C. P. Lin, *Antimicrobial activity effects of electrolytically generated hypochlorous acid-treated pathogenic microorganisms by isothermal kinetic simulation*, J. Therm. Anal. Calorim. 148 (2023) 1613–1627.
55. D. Marković, C. Deeks, T. Nunney, Ž. Radovanović, M. Radoičić, Z. Šaponjić et al., *Antibacterial activity of Cu-based nanoparticles synthesized on the cotton fabrics modified with polycarboxylic acids*, Carbohydr. Polym. 200 (2018) 173–182.
56. Ž. Z. Tasić, M. B. Petrović Mihajlović, M. B. Radovanović and M. M. Antonijević, *Electrochemical investigations of copper corrosion inhibition by azithromycin in 0.9% NaCl*, J. Mol. Liq. 265 (2018) 687–692.
57. C. Zheng, J. Cao, Y. Zhang and H. Zhao, *Insight into the Oxidation Mechanism of a Cu-Based Oxygen Carrier (Cu → Cu<sub>2</sub>O → CuO) in Chemical Looping Combustion*, Energy and Fuels 34 (2020) 8718–8725.
58. B. Narayanan, S. A. Deshmukh, S. K. R. S. Sankaranarayanan and S. Ramanathan, *Strong correlations between structural order and passive state at water-copper oxide interfaces*, Electrochim. Acta 179 (2015) 386–393.
59. S. Ghosh, *Electroless copper deposition: A critical review*, Thin Solid Films 669 (2019) 641–658.

**Komentar  
Reviewer atau  
Editor 3**





Outlook

---

**[CST] Editor Decision**

---

**From** Meilana Dharma Putra (CST) <journal-noreply@kipmi.or.id>

**Date** Fri 2/21/2025 11:25 AM

**To** Basori Basori <basori@civitas.unas.ac.id>; Ruliyanta <ruliyanto@civitas.unas.ac.id>; Maman Kartaman Ajiriyanto <mama014@brin.go.id>; Rosika Kriswarini <rosi004@brin.go.id>; Heri Hardiyanti <heri016@brin.go.id>; Cahaya Rosyidan <cahayarosyidan@trisakti.ac.id>; Sigit Dwi Yudanto <sigi012@brin.go.id>; Evi Ulina Margaretha Situmorang <evi.situmorang@atmajaya.ac.id>; Daniel Edbert <daniel.edbert@atmajaya.ac.id>; Dwi Nanto <dwi.nanto@uinjkt.ac.id>; fbudhi@unj.ac.id <fbudhi@unj.ac.id>

Basori Basori, Ruliyanta, Maman Kartaman Ajiriyanto, Rosika Kriswarini, Heri Hardiyanti, Cahaya Rosyidan, Sigit Dwi Yudanto, Evi Ulina Margaretha Situmorang, Daniel Edbert, Dwi Nanto, Ferry Budhi Susetyo:

We have reached a decision regarding your submission to Communications in Science and Technology, "Rotating speed and magnetic pole dependency assisted on copper deposition onto aluminum alloy substrate for bacterial eradication application".

Our decision is to: Accept Submission

Please wait for the next instruction.

Meilana Dharma Putra  
Editor in Chief  
Communications in Science and Technology

The following message is being delivered on behalf of Communications in Science and Technology.

---

# **Paper Yang di Terbitkan**

# Rotating speed and magnetic pole dependency assisted on copper deposition onto aluminum alloy substrate for bacterial eradication application

Basori<sup>a,\*</sup>, Ruliyanta<sup>b</sup>, Maman Kartaman Ajiriyanto<sup>c</sup>, Rosika Kriswarini<sup>c</sup>, Heri Hardiyanti<sup>c</sup>, Cahaya Rosyidan<sup>d</sup>, Sigit Dwi Yudanto<sup>e</sup>, Evi Ulina Margareta Situmorang<sup>f</sup>, Daniel Edbert<sup>g</sup>, Dwi Nanto<sup>h</sup>, Ferry Budhi Susetyo<sup>i</sup>

<sup>a</sup>Department of Mechanical Engineering, Universitas Nasional, Jakarta 12520, Indonesia

<sup>b</sup>Department of Electrical Engineering, Universitas Nasional, Jakarta 12520, Indonesia

<sup>c</sup>Research Center for Nuclear Material and Radioactive Waste Technology, National Research and Innovation Agency, Banten 15314, Indonesia

<sup>d</sup>Department of Petroleum Engineering, Universitas Trisakti, Jakarta 11440, Indonesia

<sup>e</sup>Research Center for Metallurgy, National Research and Innovation Agency, Banten 15314, Indonesia

<sup>f</sup>Department of Physiology School of Medicine and Health Sciences, Atma Jaya Catholic University of Indonesia, Jakarta 14440, Indonesia

<sup>g</sup>Department of Microbiology, Atma Jaya Catholic University of Indonesia, Jakarta 14440, Indonesia

<sup>h</sup>Department of Physics Education, UIN Syarif Hidayatullah, Jakarta 15412, Indonesia

<sup>i</sup>Department of Mechanical Engineering, Universitas Negeri Jakarta, Jakarta 13220, Indonesia

## Article history:

Received: 26 September 2024 / Received in revised form: 27 January 2025 / Accepted: 21 February 2025

## Abstract

Copper (Cu) is widely used in many sectors, such as drinking water piping, heat exchangers, and medical equipment. The present research conducted an electrodeposition of Cu over an aluminum (Al) alloy substrate under the influence of various magnetic poles and rotating speeds. In the present study, a number of investigations, including deposition rate, current efficiency, coating thickness, surface morphology and phase, crystallographic orientation, antibacterial activity, electrochemical behavior, and hardness test were conducted. Increasing the rotation speed promoted to enhanced deposition rate and current efficiency for both magnetic poles influence. An increase in the deposition rate from 12.83 to 13.67  $\mu\text{m/h}$  led to the increasing thickness, a change in surface morphology near the spheroidal, becoming a faceted structure. Presenting and rising in the rotation of a magnetic field led to a reduced surface roughness and crystallite size of Cu film for both magnetic poles influence. The Cu film made without spinning magnetic had a characteristic of highest bacterial inhibition zone around  $2.50 \pm 0.56 \text{ cm}^2$ . The CuRN50 sample had the lowest corrosion rate at around 0.055 mmpy, while the CuRS100 sample had the highest hardness value at approximately 80.72 HV for having the lowest crystallite size. Cu coated onto Al alloy could enhance its properties, such as being antimicrobial, being resistant against corrosion and having the hardness value.

**Keywords:** North and South Pole; SEM-EDS; XRD; electrochemical behavior; hardness

## 1. Introduction

Copper (Cu) due to its promising properties is widely used in many sectors, such as drinking water piping, heat exchangers, and medical equipment [1–3]. As film, it has a higher performance to kill bacteria compared to bulk Cu [4]. Additionally, coated onto aluminum (Al) alloy, Cu could enhance its properties, such as being antimicrobial, being resistant against corrosion and having hardness value [4,5]. Coating synthesis can be conducted by means of

electrochemical, spin coating, or spray methods [6–8]. In view of its simplicity and affordability, the electrodeposition is seen as a more suitable method for coating Cu onto Al alloy [9].

Cu electrodepositions attract many researchers to investigate the formed Cu films. Brands *et al.* investigated the structure, surface morphology, electrical, optical, and magnetic properties of electrodeposited  $\text{Cu}_2\text{O}$  [10]. Antenucci *et al.* improved (the mechanical and thermal properties) of open-cell Al foams through Cu electrodeposition [11]. Augustin *et al.* investigated the effect of current density at Cu electrodeposition on the microstructure, hardness, and antibacterial activity of Cu for antimicrobial Al touch application [4]. Furthermore, Kuisor *et al.* fabricated CuO film using electrodeposition in which the film was tested for

\* Corresponding author.

Email: [basori@civitas.unas.ac.id](mailto:basori@civitas.unas.ac.id)

<https://doi.org/10.21924/cst.10.1.2025.1547>



antibacterial activity using *Staphylococcus aureus* (*S. aureus*) that successfully reduced the bacterial colony during the experiment [12]. Isa *et al.* performed electrodeposition Cu over 304 stainless steels in which a coated sample was tested for antibacterial properties. In a 10-minute exposure to the coated sample, it could successfully achieve a 100 % reduction of *S. aureus* [13].

Many factors, including magnetic field, determine the formed Cu films when electrodeposition is performed. The existing magnetic field at the electrodeposition process can appear to have several forces. The Lorentz force acts on a moving ion in the solution, resulting in convection flow [14]. The effects of the magnetic field may also relate to the electrokinetic-magnetohydrodynamic (MHD) effect resulting in the body force acting in the diffuse layer [15]. Another force caused by the magnetic field is paramagnetic gradient force [16] that causes the movement of magnetic ions in the diffusion layer. Another possible force is a magnetic gradient force. It acts on paramagnetic and diamagnetic ions [17]. In general, introducing a magnetic field during the electrodeposition process leads to the arrangement of moving ions towards the cathode.

In view of many forces exhibited by presenting a magnet, the investigations of several researchers have been focused on unrotated magnetic field-induced Cu electrodeposition [14,18–22]. Investigating the electrodeposition of Cu under 15 T of magnetic field, Miura *et al.* found extraordinary dendritic growth [19]. Murdoch *et al.* conducted an electrodeposition of Cu using the influence of 0.25 and 0.5 T placed on the working electrode's reverse, and this resulted in the lowest thickness when influencing 0.25 and 0.5 T with the south pole rather than the north pole [14]. Sudibyo *et al.* conducted the electrodeposition of Cu using the influence of 300 and 900 G (neodymium magnet), resulting in higher grain when electrodeposition Cu using the influence of 900 G [22]. Yin *et al.* investigated anomalous Cu hydride phase during the magnetic field-assisted electrodeposition of Cu. Presenting an anti-parallel magnetic field affecting the magnetohydrodynamic effect could enhance the hydrogen evolution and result in poor film quality [18]. Kovalyov *et al.* found that a weak magnetic field (0.5 and 0.7 mT) could affect the electrodeposition process, surface morphology, and texture [20]. Liu *et al.* stated that magnetic field-assisted electrodeposition could change hydrogen bond structure, reduce the charge transfer resistance, and increase the electrolyte viscosity [21].

Due to its ability to enhance the properties of films, electrodeposition assisted with a spinning magnetic field is considered to attract several researchers. Wang and Chen used 0.18 T of a magnetic field with various rotating speeds (1000–3000 rpm) when electrodeposition of nickel (Ni) and results presenting a magnetic field with various rotating speeds could decrease surface roughness [23]. Ji *et al.* fabricated Ni-SiC using an electrodeposition process and found that the exhibited rotating magnetic field made SiC particle distribution more uniform [24]. Syamsuir *et al.* stated that presenting a rotating magnetic field (500 and 800 rpm) at electrodeposition process could make surface morphology of the film more uniform [25]. They found that increasing the rotating speed of a magnetic field (one piece of neodymium

magnet arranged spread five parts in the upside Teflon) at electrodeposition process could transform surface morphology from spheroidal to faceted structure [5].

Oxygen content on the Cu film surface can disrupt the transformation of Cu to Cu ions, reducing antibacterial performance [26]. The formation of surface morphology can have an impact on the antibacterial performance. Surface morphology, such as spheroidal and faceted structures, also contributes to the inhibition zone. A Cu film with spheroidal coating tends to create a higher inhibition zone [5].

The use of a magnetic field during electrodeposition can determine the movement of ions towards the cathode surface. Adjusting magnetic field rotation during electrodeposition also determines the ion movement. Furthermore, the different poles of the selected magnet also influence ion movement at electrodeposition process. Generally, the speed of ion movement can affect the properties of formed film. Based upon the literature review above, higher rotation was used ( $\geq 500$  rpm) to influence the electrodeposition; for this, the present study used the speed rotation of 50 and 100 rpm. The speed rotation was chosen on the basis of previous study conducting Cu electrodeposition by means of barreling apparatus [27]. Syamsuir *et al.* used one piece of neodymium magnet arranged to spread five parts in the upside Teflon [5]. Therefore, the present research used more neodymium magnets to result in more influence of the magnetic field. Here, the influence of spinning using different magnetic poles was also not considered. Murdoch *et al.* found that different magnetic poles influenced the deposition process, resulting in different surface morphologies in Cu films [14]. Therefore, the present research comprehensively investigated the influence of the rotating speed and magnetic pole during Cu electrodeposition on the formation of the film for bacterial eradication applications. The electrodeposition of Cu was determined by various magnetic poles (north and south) and magnetic rotating speeds (0, 50, and 100 rpm). Several investigations were conducted using digital scales, scanning electron microscopy equipped with energy dispersive spectroscopy (SEM-EDS), X-ray diffraction, digital camera, optical microscope, potentiostat dan Vickers hardness.

## 2. Materials and Methods

### 2.1. Materials

Al alloy (0.106 wt.% Si, 0.365 wt.% Fe, 0.055 wt.% Cu, 0.043 wt.% Mn, 0.030 wt.% Mg, 0.003 wt.% Zn, 0.002 wt.% Ni, 0.018 wt.% Ti, 0.003 wt.% Pb, and Al balance) was used as cathode, while pure Cu was used as anode. Electrolyte solution was prepared by dissolving  $\text{CuSO}_4 \cdot 5\text{H}_2\text{O}$  (Merck) in deionized water. Electrolyte solution (250 ml of volume) was used for electrodeposition with the composition of 0.5 M  $\text{CuSO}_4 \cdot 5\text{H}_2\text{O}$  plus 20 ml of  $\text{H}_2\text{SO}_4$ .

### 2.2. Sample preparation

It began by cutting Al alloy into  $2 \times 2$  cm for electrodeposition substrate using a shearing machine. Cu film was then made using a DC power supply (MDB PS-305DM) with 40 mA, and at 25°C, and pH 5.5 for one h. Cu films were

prepared under the influence of a clockwise rotating magnetic field, as seen in Fig. 1. The plating bath was placed on top of the rotation magnetic field equipment. Two pieces of neodymium magnet were stacked and arranged (six parts) in the upside Teflon, as seen in Fig. 1. One piece of neodymium magnet had 0.08 T of intensity (measured using gauss meter TD-8620). Five variation samples were made; one sample was made without the influence of a rotating magnetic field as a baseline. The sample was made by influencing 50 rpm and 100 rpm. Different pole variations were also used. Table 1 depicts the complete sample names.

Table 1. Sample name and remark

Sample name	Remark
CuR0	without the influence of a rotating magnetic field
CuRN50	50 rpm, north pole near the substrate
CuRN100	100 rpm, north pole near the substrate
CuRS50	50 rpm, south pole near the substrate
CuRS100	100 rpm, south pole near the substrate

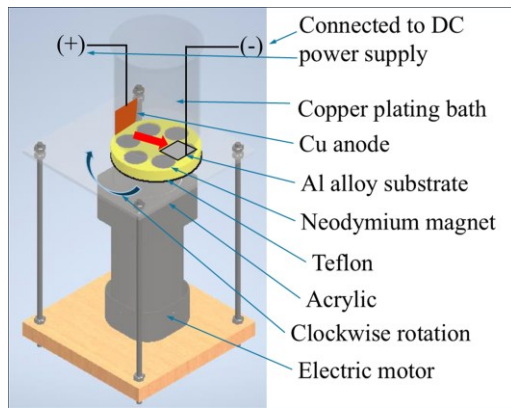


Fig. 1. Rotation magnetic field equipment

### 2.3. Characterizations

The deposition rate and current efficiency were measured similar to previous studies [17]. Thermo Scientific SEM-EDS was used to investigate surface morphology and elements. The cross section was also investigated using SEM apparatus to measure Cu layer thickness. According to SEM image, Image J software was used to measure grain distribution and the roughness of Cu film. Meanwhile, X-ray diffraction was conducted using PANalytical (Cu K radiation) with step size  $0.02^\circ$  and refined with the help of GSAS software [28].

Similarly, antibacterial activity was investigated according to previous studies [5]. The assessment of microbial reduction of various samples was adapted from ISO 22196 for non-porous material. *S. aureus* ATCC 25923 was used in this test. The inhibition zone was documented using a digital camera and assessed using an unaided eye and the area of inhibition was measured by Image J software. Each measurement was performed five times to ensure the data homogeneity. The diffusible area was calculated by subtracting the area of inhibition from the metal size. One-way ANOVA analysis was conducted to investigate whether there was significance between the polarities of the magnets. Moreover, the

specimen was removed from the plate using sterile forceps. The agar was re-incubated at  $35^\circ\text{C} \pm 2$  for 24 hours to observe the antimicrobial activity post-contact. The oxides of the metal formed before and after the test were observed by means of Olympus CX23 microscope under an  $180 \times$  magnification; any changes inside of the agar plate were documented. In addition, the observations of microbial reduction test were conducted (within 1, 2, 4, 6 and 12 h).

The electrochemical test was conducted using Ossila potentiostat in 0.9 % NaCl (room temperature). Prior to the electrochemical test, Cu films were mounted and left open area for  $1 \times 1 \text{ cm}^2$ . Here, Cu films were used as working electrode, Ag/AgCl and Pt wire were used as reference electrode and counter electrode, respectively. There are two kinds of test in electrochemical behavior measurement, those are open circuit potential (OCP) and potentiodynamic polarization. OCP is performed until 1200 seconds, while potentiodynamic polarization is performed from -1 to -0.1 V using 5 mV/s of scan rate. The potentiodynamic polarization data was analyzed through the Tafel extrapolation method to find  $I_{\text{corr}}$  and  $E_{\text{corr}}$ . Afterward, corrosion rate could be calculated using following equation [29].

$$\text{Corrosion rate (mmpy)} = K ((a I_{\text{corr}})/(n D)) \quad (1)$$

where K is constant (0.00327 mmpy), a is atomic weight,  $I_{\text{corr}}$  is corrosion current density ( $\mu\text{A}/\text{cm}^2$ ), n is the number electron involved, and D is Cu density ( $\text{g}/\text{cm}^3$ ).

The hardness test was performed using Future-Tech (FV-300e) Vickers hardness tester. Five repeatable measurements were conducted over Cu layer by using 1 kg of load.

## 3. Results and Discussion

### 3.1. Deposition rate and current efficiency

Fig. 2 shows the deposition rate and current efficiency of electrodeposition Cu over an Al alloy substrate. They had similar tendencies; an increase in magnet rotation speed led to a rise in deposition rate and current efficiency.

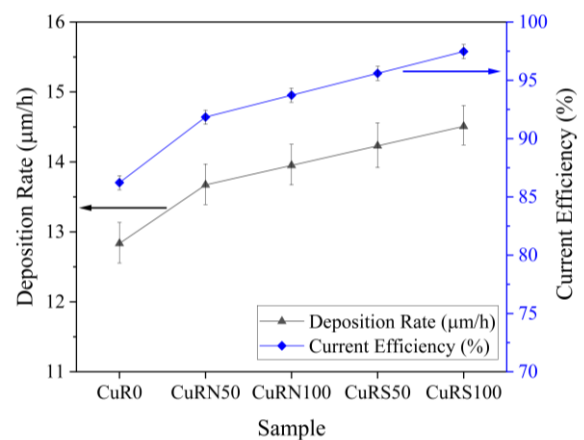


Fig. 2. Deposition rate and current efficiency of Cu electrodeposition

In the process of Cu electrodeposition, the oxidation process occurs at the anode and a reduction process occurs at the cathode. An Al alloy (substrates) to be plated is placed at

the cathode. When the current is applied, the Cu ions are depleted in the surroundings of the cathode, making a diffusion film upper around the cathode. Hydrogen evolution is known to occur at the cathode during Cu electrodeposition from aqueous solutions [17]. Less hydrogen evolution can increase the deposition rate and current efficiency because hydrogen evolution is able to disturb the movement of the ions to the cathode [30,31]. Presenting an anti-parallel magnetic field (north pole) affecting the MHD effect could enhance the hydrogen evolution, decrease current efficiency, and result in poor film quality [18]. As shown in Fig. 2, hydrogen evolution seemed to influence the electrodeposition process when being determined by the north pole. Therefore, the electrodeposition process had a lesser current efficiency than the electrodeposition process when being influenced by the south pole.

Cu films made and influenced by the rotating south pole magnet has a higher deposition rate due to the magnetic field, which was parallel to the current direction and attracts more Cu ions onto the Al alloy surface [14]. Rotating the magnet under the electrolyte solution during the electrodeposition process could induce an Eddy electric field [5] that can act as an additional MHD flow convection effect [23]. Moreover, increasing the rotation speed could attract more Cu ions onto the Al alloy surface, consequently increasing the deposition rate and current efficiency.

### 3.2. Average thickness

Fig. 3 and Fig. 4 show the thickness of various Cu layers and average thickness of Cu layers. Compared to the average thickness to the deposition rate (Fig. 2), there was a correlation between them. Increasing the deposition rate led to an increase in the average of Cu layers thickness, similar to the study by Syamsuir *et al.* [27]. Furthermore, it seemed that average coating thickness was higher than thickness found by calculating from deposition rate. For example, average coating thickness of CuR0 sample ideally is 12.83  $\mu\text{m}$  due to deposition sample for one hour. Unfortunately, average coating thickness of CuR0 sample was 27.17  $\mu\text{m}$ . This behavior was probably due to the SEM cross section being conducted on an area near the anode (red arrow Fig. 1). According to Yang *et al.*, the end area of the cathode results in higher thickness compared to the middle area [32]. Therefore, average thickness is higher than deposition rate value.

### 3.3. SEM-EDS and roughness

Fig. 5 shows the SEM result and the grain distribution of various Cu film surfaces. Samples were made by influencing the north pole magnetic field, which had a larger grain size than samples created by affecting the south pole of a magnetic field. Generally, presenting the south pole magnetic field influence can lead to a decrease in grain size. While presenting south pole magnetic field influence can lead to an increase in grain size as in line with previous study [33]. Murdoch *et al.* stated that different poles are used to influence deposition process that will result different grain size [14]. Moreover, Lin *et al.* stated that deposition time contributes to the formed grain size [34].

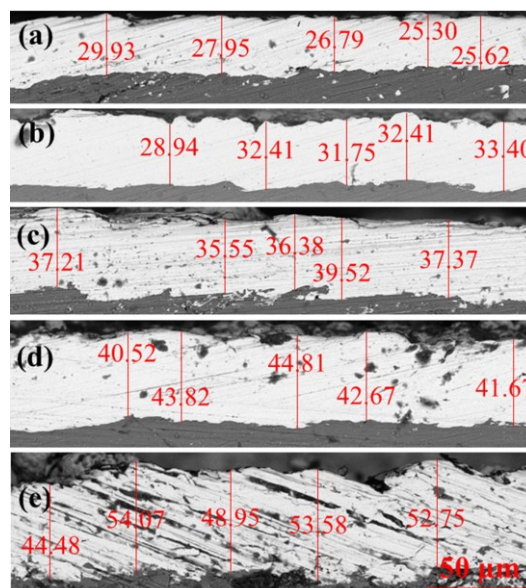


Fig. 3. Thickness of various Cu layers: (a) CuR0; (b) CuRN50; (c) CuRN100; (d) CuRS50; and (e) CuRS100

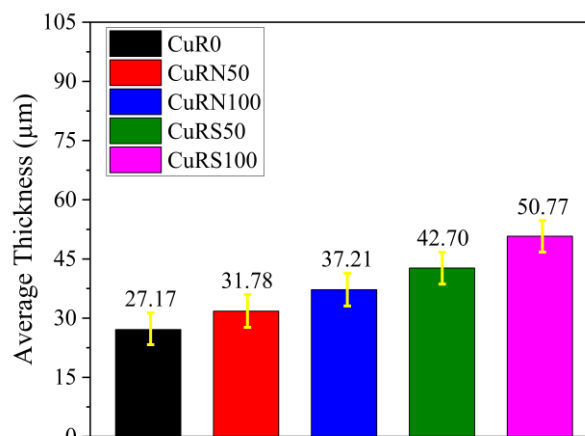


Fig. 4. Cu layers average thickness

As shown in Fig. 5, the Cu sample was made with no spinning magnetic influence, leading to the formation of morphology near the spheroidal. Cu samples made with spinning magnetic assistance led to the formation of faceted structure morphology [17]. Moreover, the transformation from spheroidal to faceted structure was determined by the deposition rate. A higher nucleation rate leads to a higher deposition rate, resulting in a variation in surface morphology [35]. Samples made with influences from the north pole magnetic field had a low nucleation rate. Hence, it had wider grain sizes than samples by influencing the south pole magnetic field [14]. Moreover, an increase in the deposition rate from 12.83 to 13.67  $\mu\text{m}/\text{h}$  led to a change in surface morphology near the spheroidal becoming faceted structure. The deposition rate between 13.67 and 14.51  $\mu\text{m}/\text{h}$  resulted in a faceted structure of surface morphology.

The south pole had an affecting magnetic field parallel to the current direction; therefore, Cu ions were more attracted to the Al alloy surface. In contrast, the north pole had an affecting magnetic field that was anti-parallel to the current direction, reducing Cu ions' attraction onto the Al alloy



surface. Moreover, Lorentz's forces rotated opposite each other on top of the surface specimen for different magnetic poles. This condition affected the sample film by influencing the South Pole to be smoother than the North Pole. Ji *et al.* stated that presenting a rotating magnetic field during electrodeposition can make surface morphology more uniform [24]. In this case, the paramagnetic force has a similar tendency for different magnetic poles. Therefore, influencing surface morphology could be neglected.

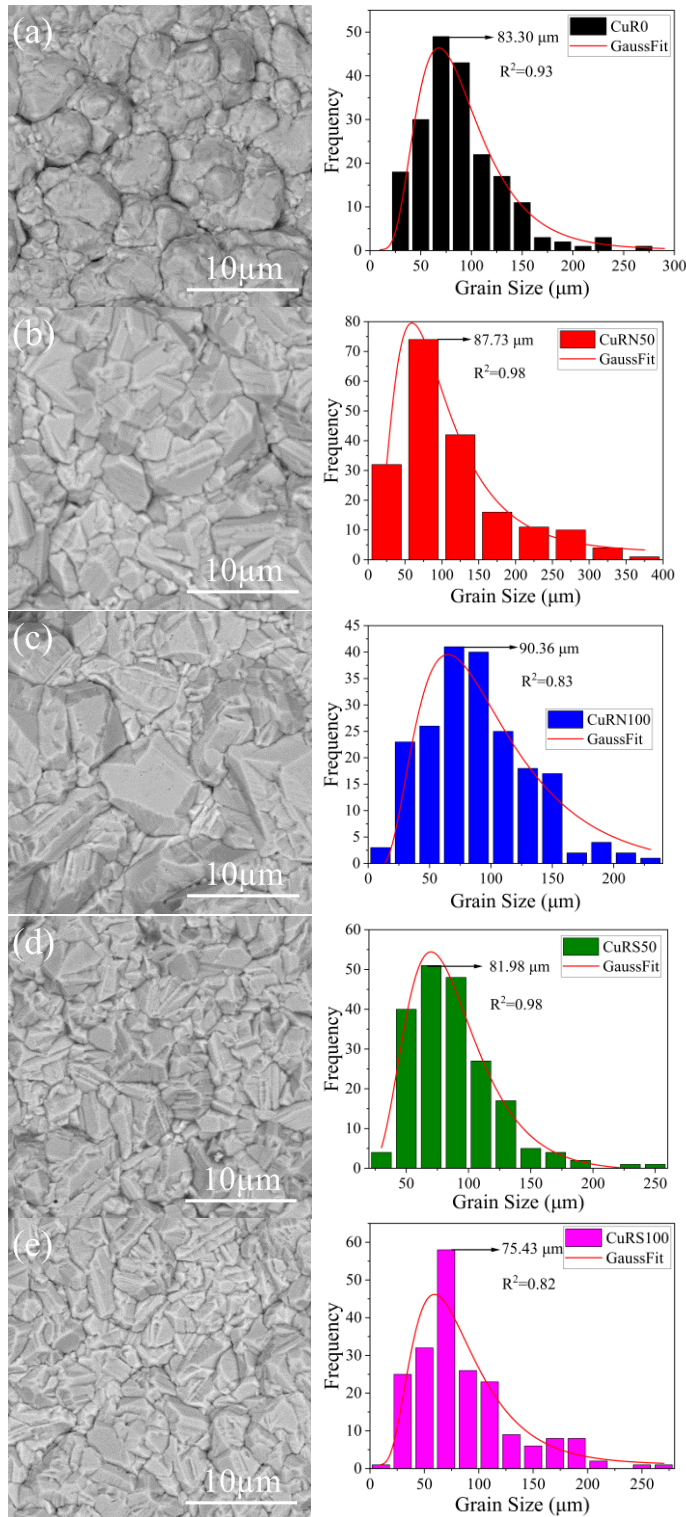


Fig. 5. SEM and grain distribution of Cu layers: (a) CuR0; (b) CuRN50; (c) CuRN100; (d) CuRS50; and (e) CuRS100

As shown in Fig. 6, the spinning magnetic-assisted running at 50 rpm led to oxygen formed on the Cu surface. Moreover, enhanced magnetic rotation led to a decrease or disappearance of oxygen. Presenting oxygen on Cu film is one of the unique cases in which oxygen can be formed due to both a secondary reaction on the anode and sample storage and transport [5].

Fig. 7 presents the roughness analyzed result from the SEM image using ImageJ software. CuR0, CuRN50, CuRN100, CuRS50, and CuRS100 samples had a surface roughness of 34.62, 18.00, 17.38, 18.60, and 16.58  $\mu\text{m}$ , respectively. Presenting a magnetic field rotation during electrodeposition led to a decrease in the surface roughness of Cu film. More rotation could also decrease surface roughness, which is perfectly in line with the previous study [5]. Wang and Chen found that presenting a magnetic field during electrodeposition with various rotating speeds could decrease surface roughness [23]. This behavior is probably due to additional MHD flow, which is in line with the deposition rate result and could enhance the Cu ions' movement. A higher deposition rate would result in a higher nucleation rate, consequently producing a smooth surface morphology. Moreover, the sample made by north pole magnet influence had more roughness than sample made by north pole magnet. This behavior probably due to MHD effect that could enhance the hydrogen evolution and result in more roughness [18].

### 3.4. X-ray diffraction

Fig. 8 shows the diffraction patterns of samples of Cu deposition on substrates consisting of Al alloy plates. The five samples were identified to have Cu phase peaks at the indexed plane peaks (111), (200), (220), (311), and (222) at angles  $2\theta = 43.31, 50.45, 74.13, 89.94, \text{ and } 95.15^\circ$ . The cubic crystal system was found in the Cu phase, and it had a space group of  $fm-3m$ . The cubic Cu phase peaks at these angles were found consistent with the findings from studies by Omar and Francisco Briones *et al.* [36,37]. This demonstrated that the procedure for depositing Cu on Al alloy plates has been successfully completed. At the indexed plane peaks (111), (200), (220), (311), and (400) of the five diffraction patterns, they were also found on the Al alloy plate substrate along with the copper phase. Xu *et al.* and Ayieko *et al.* presented a standard Al diffraction pattern identical to this peak of Al [38,39].

The mean crystallite size and lattice value of the five deposition samples were compared to further analyze the diffraction pattern. The Rietveld method was employed to determine the lattice of the five samples. The cubic Cu phase lattice of all five samples was measured at 0.3615 nm based upon the calculation results. Changes in magnetic poles and rotating speed showed no effect on the lattice value of the cubic Cu phase. Table 2 presents the data from the crystallographic calculation. To determine the mean crystallite size, the Williamson-Hall plot method was utilized. In contrast to the lattice value, the mean crystallite size was affected by the rotating speed and poles. The mean crystallite size became finer with the increase in magnet rotation speed perfectly matched with surface roughness analysis.

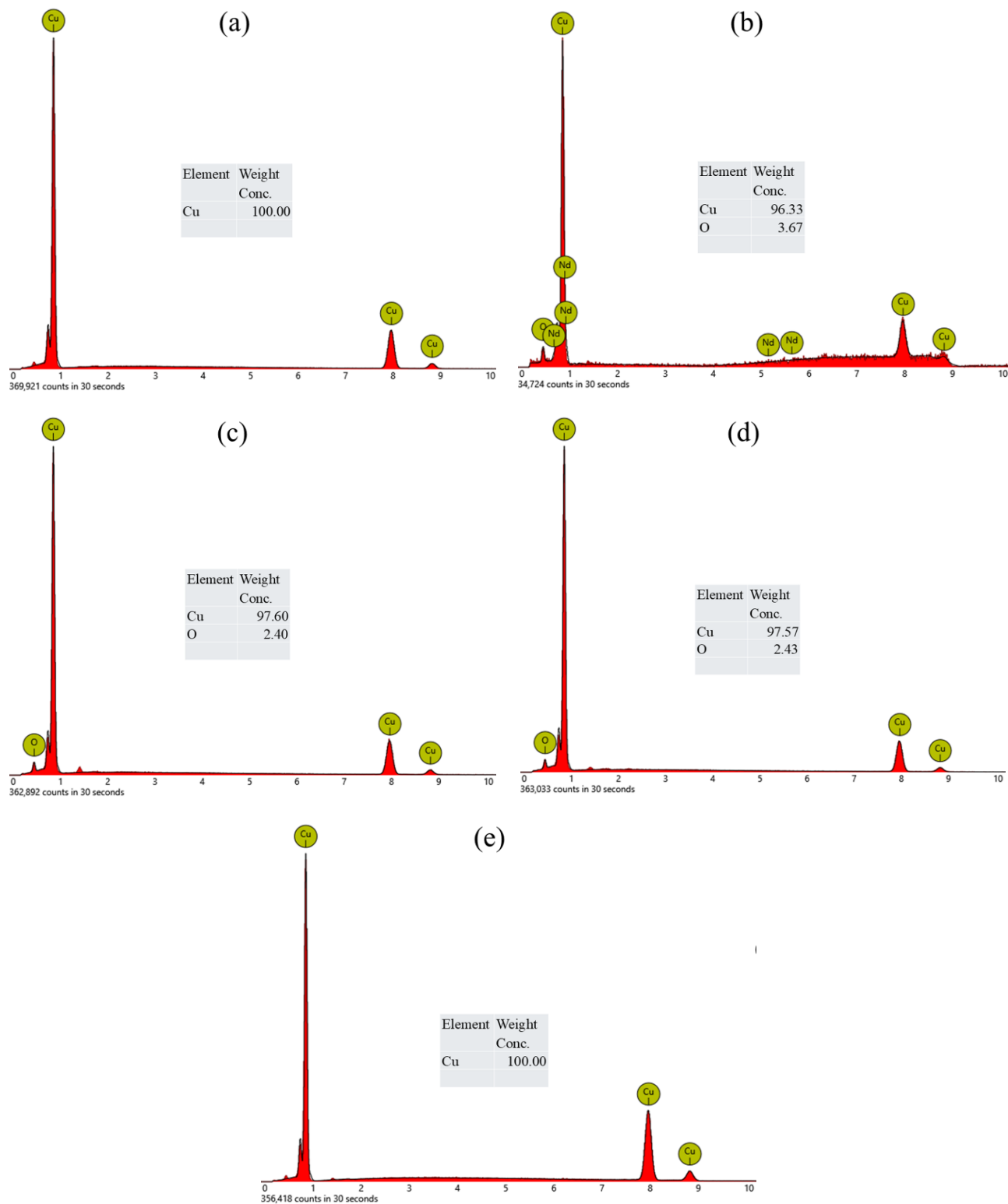


Fig. 6. EDS Cu layers: (a) CuR0; (b) CuRN50; (c) CuRN100; (d) CuRS50; and (e) CuRS100

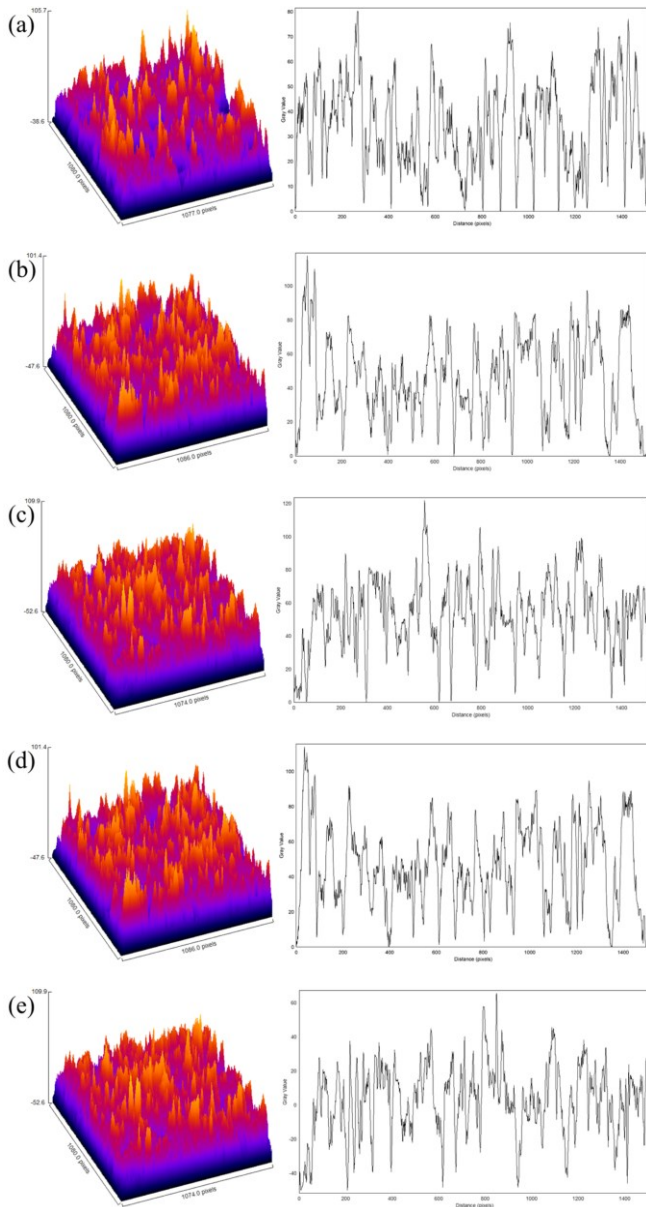


Fig. 7. Roughness Cu layers: (a) CuR0; (b) CuRN50; (c) CuRN100; (d) CuRS50; and (e) CuRS100

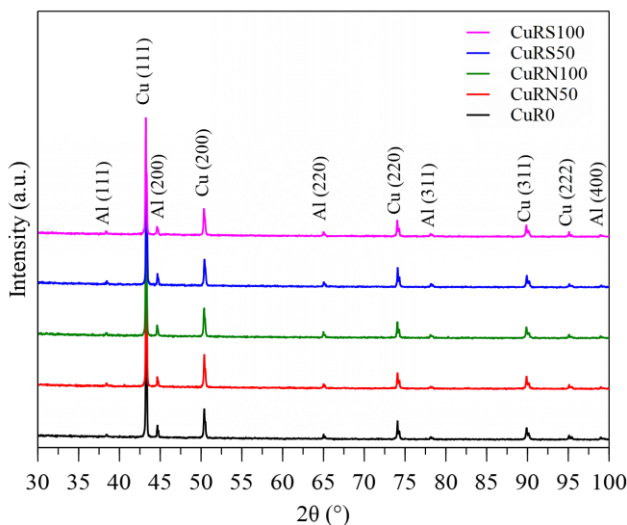


Fig. 8. X-ray diffraction pattern of various sample

Table 2. Crystallographic data calculated from various samples

Source	CuR0	CuRN50	CuRN100	CuRS50	CuRS100
Name: Copper (Cu)					
Space group: F m -3 m (225)					
Crystal system: cubic					
Lattice -a (nm)	0.3615	0.3615	0.3615	0.3615	0.3615
wRp (%)	10.10	10.37	10.24	9.86	10.30
GoF	1.067	1.106	1.087	1.045	1.056
Mean crystallite size (nm)	308	173	154	173	126
Micro-strain (%)	0.07	0.05	0.05	0.05	0.04

### 3.5. Antibacterial activity

Fig. 9 describes the antibacterial activity test after 24 hours of contact. Material placement in the middle of Mueller Hinton agar was inoculated with *S. aureus* ATCC 25923. Noticing the inhibition zones around the material; the calculation is presented in Table 3. The metal ions were diffused into the agar to inhibit the growth of *S. aureus*.

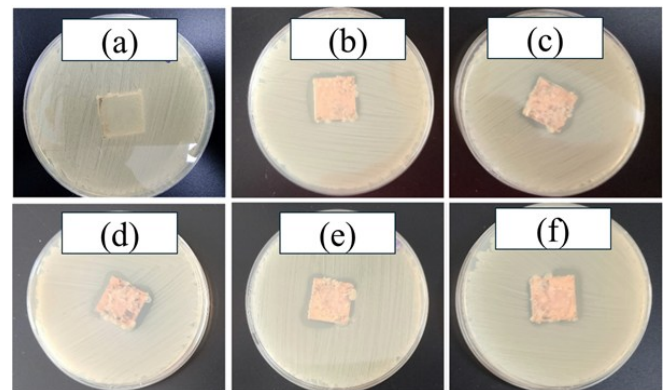


Fig. 9. Antibacterial activity test after 24 hours: (a) blank; (b) CuRN50; (c) CuRN100; (d) CuR0; (e) CuRS50; and (f) CuRS100

Cu, particularly in the form of metal-organic frameworks (MOFs) and nanoparticles, exhibited significant antibacterial activity against Gram-positive bacteria such as *S. aureus* [40]. The peptidoglycan layer in Gram-positive bacteria plays a significant role in their susceptibility to Cu although its direct interaction with Cu is not as straightforward as with other antimicrobial agents. Cu is able to induce modifications in the peptidoglycan layer, such as increased cross-linkage, which can affect the overall structure and function of the cell wall. These modifications can either enhance or reduce the susceptibility of Gram-positive bacteria to Cu, dependent on the specific bacterial strain and environmental conditions [41,42]. In this research, the Cu induced contact killing. The antimicrobial activity of Cu is believed to involve contact-mediated killing, initiating membrane degradation. The susceptibility of Gram-positive strains to Cu is attributed to the thick peptidoglycan layer, reducing cell wall permeability to other metal ions, including Zinc [43].



As shown in Fig. 9, the inoculum was totally annihilated by electroplated materials. The log reduction was not calculated due to the total killing of the bacteria. However, the total reduction of  $> 105$  CFU/ml might suggest a percentage reduction of  $> 99.999\%$  (see Table 3). Moreover, there was a zone of inhibition between the sample and bacterial lawn that was also visible inside the zone's white crystals and some bluish color change inside the agar. This suggests that the Cu material diffused and interacted with the agar can result in a zone of bacterial growth inhibition.

As seen in Table 3, the widest diffusion zone was observed in CuR0 with the zone of diffusion and inhibition areas of  $6.99 \text{ cm}^2$  and  $2.5 \text{ cm}^2$ . This was statistically significant with  $p < 0.001$  (ANOVA; CI 95%). Also, there was significance in independent T-Test analyses between CuR0 and CuR50 group ( $p < 0.001$ ; CI 95%), R0 and R100 group ( $p < 0.001$ ; CI 95%), and between CuR50 and CuR100 Group ( $p < 0.001$ ; CI 95%). To investigate whether there was significance between the polarities of the magnets, independent T-test analyses were performed. There was no significant difference in the outcome between the south pole group and the north one ( $p=0.063$ ; CI 95%). Moreover, there were no inhibitions in the blank group, and the bacteria grew underneath the metal. Comparing to the previous study, less inhibition was found in the present study [5]. This behavior was probably due to higher crystallite size form in the all samples [44]. Previous study found crystallite size between 95.66 and 100.50 nm [5]. While in the present study, the crystallite size of Cu layer was between 126 and 308 nm. Ramyadevi *et al.* and Ahmed *et al.* in their studies, when testing Cu nanoparticle for antibacterial activity using *S. aureus*, found the inhibition zone of 2.2 cm and 2.4 cm [45,46].

Table 3. The reduction of colony, and diffusible metal observation

Sample	Microbial reduction assessment		Diffusible metal observation	
	Initial load 0 h (CFU/ml)	Final load 24 h (CFU/ml)	Zone of diffusion ( $\text{cm}^2$ )	Inhibition area ( $\text{cm}^2$ )
Blank		0	$4.01 \pm 0.01$	$-0.48 \pm 0.01$
CuR0		0	$6.99 \pm 0.12$	$2.50 \pm 0.56$
CuRN50	$3.5 \times 10^5$	0	$6.21 \pm 0.01$	$1.61 \pm 0.21$
CuRN100		0	$6.00 \pm 0.02$	$1.89 \pm 0.02$
CuRS50		0	$6.16 \pm 0.41$	$1.73 \pm 0.46$
CuRS100		0	$6.17 \pm 0.01$	$2.14 \pm 0.24$

The use of magnetic rotation during material synthesis showed a significant impact on the results. Materials synthesized without magnetic rotation (R0) showed the stronger antibacterial effects compared to those synthesized at 50 rpm or 100 rpm. However, increasing magnet rotation significantly enhanced the size of the inhibition zone. As a result, the inhibition zone at 100 rpm was found larger than that of at 50 rpm. This condition was probably due to forming some oxygen on the Cu films surface as seen in EDS result, which could disrupt transformation Cu to be Cu ions. Qu *et al.* found that antibacterial behavior was determined by Cu ions

[26]. The release of Cu ions inside of the agar was lethal towards *S. aureus* [47].

As shown in Fig. 3, CuR0 surface morphology formed near to spheroidal, while other samples formed a faceted structure. In Table 3, it can be seen that higher inhibition zone was seen in CuR0 sample. Therefore, it can be concluded that the spheroidal form results in the higher inhibition zone compared to faceted structure, which is perfectly in agreement with previous study [5]. This condition probably occurred due to the spheroidal structure having a wider surface area than the faceted structure, where more Cu ions were released. Moreover, an increase in rotation leads to a decrease in roughness. Several researchers have found that roughness is independent of the inhibition zone, which aligns with the present study [5,48].

Moreover, the generation of reactive oxygen species (ROS) and damage to cell membranes are the main ways in which metals' broad antibacterial potential has been extensively studied [49–51]. Even so, metals can target particular cellular components and, when combined, are likely to improve pathogen clearance despite their non-specific activity. Conversely, Cu has an ability to change metabolic pathways in addition to cause damage to DNA and cell membranes through the generation of ROS [52]. The combined mode of action has not been investigated so far, despite the fact that the modes of action of various metal ions have been well explored. The variability in antimicrobial efficaciousness between various combinations can be explained by the diverse chemical reactivity of metal ions with bacterial cells and their specific biological targets [53].

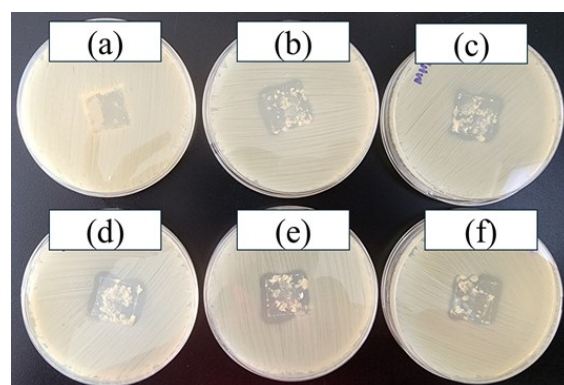


Fig. 10. After 24 hours of post contact test: (a) blank; (b) CuRN50; (c) CuRN100; (d) CuR0; (e) CuRS50; and (f) CuRS100

Fig. 10 shows the results after 24 hours of post-contact testing. The inhibitory zones appeared after the removal of the material. There were some metal infiltrations inside the agar on every plate making the agar cracked. This indicated gas-forming or exothermic reaction inside the agar, increasing the antimicrobial ability of the material [54]. There were no anti-Staphylococcal effects on the blank material; therefore, there was a regrowth of microorganisms in the place where the metal was previously placed.

Fig. 11 shows antibacterial activity pretest microscope observation, and Fig. 12 shows antibacterial activity post-test microscope observation. The microscopic observation of electroplated surfaces occurred under an  $180 \times$  magnification

optical microscope. There was a significant proportion in the formation of white crystals on the electroplated surface after tests. The crystals did not form on the surface of the blank. The Cu formed oxides, which changed the surface color. Marković et al. stated that color change in the Cu is in relation to adsorption or reduction Cu ions [55].

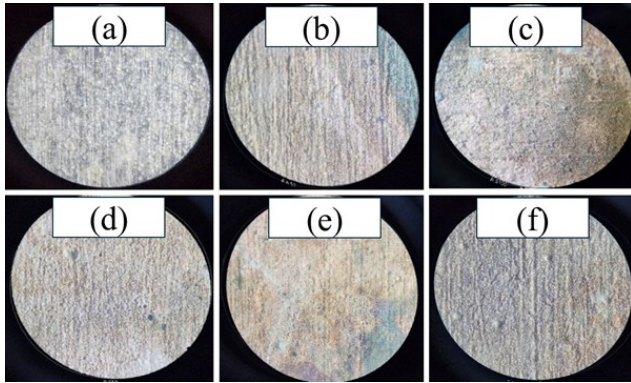


Fig. 11. Antibacterial activity pretest microscope observation: (a) blank; (b) CuRN50; (c) CuRN100; (d) CuR0; (e) CuRS50; and (f) CuRS100

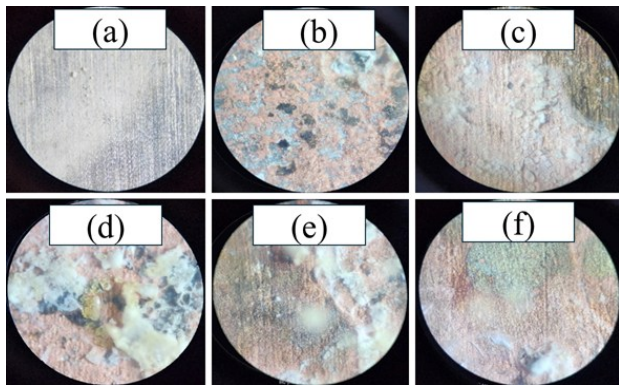


Fig. 12. Antibacterial activity post-test microscope observation: (a) blank; (b) CuRN50; (c) CuRN100; (d) CuR0; (e) CuRS50; and (f) CuRS100

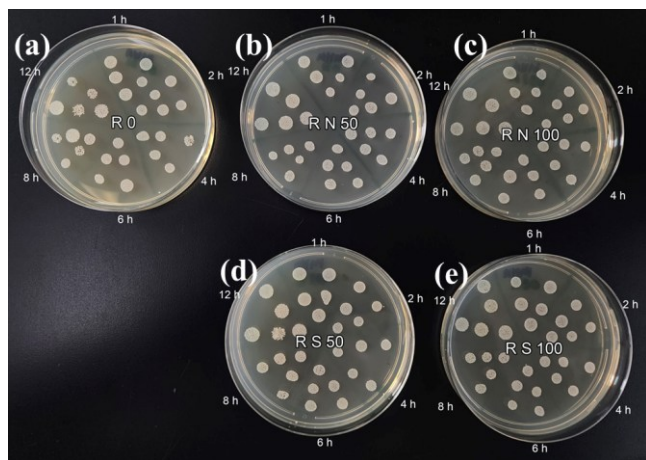


Fig. 13. Microbial reduction test observation: (a) CuR0; (b) CuRN50; (c) CuRN100; (d) CuRS50; and (e) CuRS100

As seen in Fig. 13 and Table 4, to deep explore microbial reduction assessment, investigating at 1, 4, 6, 8, and 12 hours

were conducted. At 6 hours of investigation, CuR0 sample resulted in a reduction colony-forming units per milliliter around  $10^4$ , which was in line with inhibition area value (higher inhibition area). While other samples still showed similar results when initial exposure occurred (See Table 3).

Table 4. Microbial reduction assessment of Cu samples

Sample name	1 h	2 h	4 h	6 h	12 h
	(CFU/ml)				
CuR0	$>10^5$	$>10^5$	$>10^5$	$10^4$	$10^4$
CuRN50	$>10^5$	$>10^5$	$>10^5$	$>10^5$	$>10^5$
CuRN100	$>10^5$	$>10^5$	$>10^5$	$>10^5$	$>10^5$
CuRS50	$>10^5$	$>10^5$	$>10^5$	$>10^5$	$>10^5$
CuRS100	$>10^5$	$>10^5$	$>10^5$	$>10^5$	$>10^5$

### 3.6. Electrochemical behavior

Fig. 14 shows the OCP measurement result of various Cu samples.  $E_{OCP}$  values of the CuR0, CuRN50, CuRN100, CuRS50, and CuRS100 were -0.643, -0.667, -0.658, -0.633, and -0.641 V vs Ag/AgCl, respectively. Previous study found  $E_{OCP}$  of Cu layer over Al alloy between -0.694 and -0.684 V vs Ag/AgCl [27]. All samples showed a shift to more negative value to reach a steady state. Tasić *et al.* stated that this condition implies the Cu oxide dissolution and CuCl layer formation [56]. The CuRN50 layer seemed more stable than other sample, showing to reach steady state at around 600 s for OCP measurement.

Fig. 15 represents potentiodynamic polarization test result in 0.9 % NaCl. Table 4 presents the tafel extrapolation result. Using Eq. (1), corrosion rate was calculated and summarized in Table 5.

As shown in Table 5, the CuRN50 sample was found as the sample with the lowest corrosion rate, probably due to the highest oxygen on the Cu surface that could form an oxide [57]. Narayanan *et al.* stated that oxygen content in the Cu film would be an obstacle for chloride ions to adsorb in the film [58]. Therefore, the oxide could result in better protection from aggressive species in the 0.9 % NaCl medium. Moreover, compared to Fig. 6, the oxygen content of the Cu layer was linear to the corrosion rate. Higher oxygen content led to decrease corrosion rate.

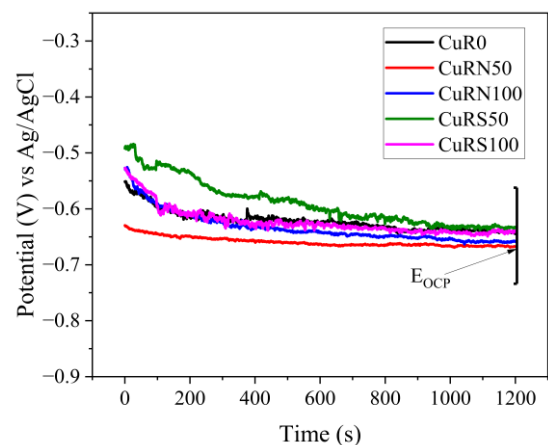


Fig. 14. OCP test curve

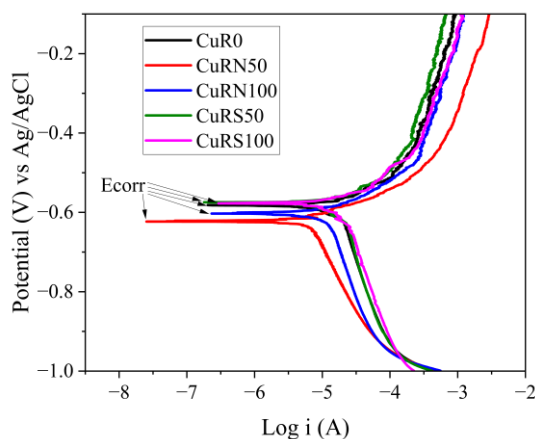


Fig. 15. Potentiodynamic polarization test curve

Table 5. Tafel extrapolation result and corrosion rate

Sample name	E <sub>corr</sub> (V) vs Ag/AgCl	I <sub>corr</sub> (A/cm <sup>2</sup> )	Corrosion rate (mmpy)
CuR0	-0.582	$1.27 \times 10^{-5}$	0.148
CuRN50	-0.623	$4.78 \times 10^{-6}$	0.055
CuRN100	-0.603	$8.77 \times 10^{-6}$	0.102
CuRS50	-0.574	$8.56 \times 10^{-6}$	0.099
CuRS100	-0.577	$1.14 \times 10^{-5}$	0.132

### 3.7. Hardness test

Fig. 16 represents average hardness test result using 1 kg of load. The hardness test was conducted with five repeatable measurements on top of Cu layer. The average hardness in the present study varied between 47.92 and 80.72 HV. Ghosh et al. found that Cu layer hardness from 22.9 to 114.7 HV [59]. Previous study also found Cu layer hardness between 72.94 and 76.26 HV [5]. Moreover, Augustine *et al.* stated that hardness value is dependent on the crystallite size. The lowest crystallite size promoted to resulting higher hardness [4]. Comparing Fig. 16 to Table 2, there was a linear correlation between hardness and crystallite size. Highest hardness value was seen at CuRS100 sample, while smallest one was found at CuR0 sample.

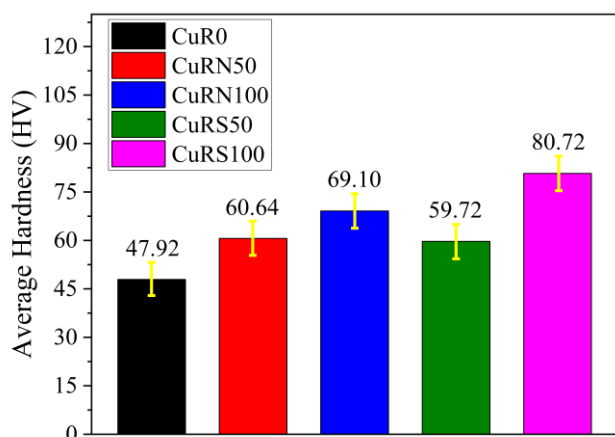


Fig. 16. Average of the hardness test result

## 4. Conclusion

This study has successfully conducted the Cu films fabricated under a spinning magnetic field with various rotation speeds and a magnetic pole. Higher rotation speed was promoted to enhance deposition rate and current efficiency for both magnetic poles. The Cu sample fabricated with no spinning magnetic influence led to the morphology formed near the spheroidal. Cu samples made with spinning magnetic influence led to the morphology formed near the faceted structure. Magnetic-assisted spinning at 50 rpm led to oxygen formed on the Cu surface for both magnetic poles and enhanced rotation. This then led to the decrease or disappearance of oxygen. Presenting and rising in magnetic field rotation led to decreased surface roughness and crystallite size of Cu film for both magnetic poles. The Cu sample made without spinning magnetic fields influence had the highest inhibition zone size, probably due to the absence of oxygen on the Cu film surface and the morphology near the spheroidal. The oxygen content of the Cu layer was found linear to the corrosion rate. Higher oxygen content led to decrease corrosion rate, while the lowest crystallite size promoted to higher hardness. Overall, Cu films successfully covered Al alloy and could transform it into antibacterial material. For future study, it is recommended to conduct the electrodeposition of Cu with spinning magnetic influence higher than 100 rpm.

## Acknowledgements

This study has been supported by the Ministry of Education, Culture, Research, and Technology through grand funding Penelitian Fundamental-Regular with contract number 087/LPPM-UNAS/VI/2024 and 815/LL3/AL.04/2024.

## References

1. D. A. Lytle and C. P. White, *The effect of phosphate on the properties of copper drinking water pipes experiencing localized corrosion*, J. Fail. Anal. Prev. 14 (2014) 203–219.
2. M. M. Lachowicz, *A metallographic case study of formicary corrosion in heat exchanger copper tubes*, Eng. Fail. Anal. 111 (2020) 104502.
3. N. Thokala, C. Kealey, J. Kennedy, D. B. Brady and J. B. Farrell, *Characterisation of polyamide 11/copper antimicrobial composites for medical device applications*, Mater. Sci. Eng. C 78 (2017) 1179–1186.
4. A. Augustin, P. Huilgol, K. R. Udupa and U. B. K., *Effect of current density during electrodeposition on microstructure and hardness of textured Cu coating in the application of antimicrobial Al touch surface*, J. Mech. Behav. Biomed. Mater. 63 (2016) 352–360.
5. Syamsuir, F. B. Susetyo, B. Soegijono, S. D. Yudanto, Basori, M. K. Ajiriyanto et al., *Rotating-Magnetic-Field-Assisted Electrodeposition of Copper for Ambulance Medical Equipment*, Automot. Exp. 6 (2023) 290–302.
6. A. M. Alghamdi and F. Fadhillah, *Thin film composite polyelectrolyte multilayer nanofiltration membrane fabricated using spin assisted layer by layer assembly: Application of solution diffusion film model*, Commun. Sci. Technol. 5 (2020) 10–15.



7. C. Santoso, Ratnawati and Slamet, *Utilization of glycerol solution for hydrogen production by a combination of photocatalysis and electrolysis processes with Fe-TiO<sub>2</sub> nanotubes*, Commun. Sci. Technol. 8 (2023) 208–215.
8. W. Trisunaryanti, K. Wijaya and A. M. Tazkia, *Preparation of Ni/ZSM-5 and Mo/ZSM-5 catalysts for hydrotreating palm oil into biojet fuel*, Commun. Sci. Technol. 9 (2024) 161–169.
9. A. Lelevic and F. C. Walsh, *Electrodeposition of Ni-P alloy coatings: A review*, Surf. Coatings Technol. 369 (2019) 198–220.
10. I. S. Brandt, M. A. Tumelero, S. Pelegrini, G. Zangari and A. A. Pasa, *Electrodeposition of Cu<sub>2</sub>O: growth, properties, and applications*, J. Solid State Electrochem. 21 (2017) 1999–2020.
11. A. Antenucci, S. Guarino, V. Tagliaferri and N. Ucciardello, *Improvement of the mechanical and thermal characteristics of open cell aluminum foams by the electrodeposition of Cu*, Mater. Des. 59 (2014) 124–129.
12. A. Kusior, J. Mazurkow, P. Jelen, M. Bik, S. Raza, M. Wdowiak et al., *Copper Oxide Electrochemical Deposition to Create Antiviral and Antibacterial Nanocoatings*, Langmuir 40 (2024) 14838–14846.
13. N. N. C. Isa, Y. Mohd, M. H. M. Zaki and S. A. S. Mohamad, *Antibacterial activity of copper coating electrodeposited on 304 stainless steel substrate*, in AIP Conference Proceedings, 1901 (2017), pp. 020009.
14. H. A. Murdoch, D. Yin, E. Hernández-Rivera and A. K. Giri, *Effect of applied magnetic field on microstructure of electrodeposited copper*, Electrochem. commun. 97 (2018) 11–15.
15. Q. Long, Y. Zhong and J. Wu, *Research progress of magnetic field techniques for electrodeposition of coating*, Int. J. Electrochem. Sci. 15 (2020) 8026–8040.
16. K. Kołodziejczyk, E. Miękoś, M. Zieliński, M. Jaksender, D. Szczukocki, K. Czarny et al., *Influence of constant magnetic field on electrodeposition of metals, alloys, conductive polymers, and organic reactions*, J. Solid State Electrochem. 22 (2018) 1629–1674.
17. B. Soegijono, F. B. Susetyo, Yusmaniar and M. C. Fajrah, *Electrodeposition of paramagnetic copper film under magnetic field on paramagnetic aluminum alloy substrates*, e-Journal Surf. Sci. Nanotechnol. 18 (2020) 281–288.
18. D. Yin, H. A. Murdoch, B. Chad Hornbuckle, E. Hernández-Rivera and M. K. Dunstan, *Investigation of anomalous copper hydride phase during magnetic field-assisted electrodeposition of copper*, Electrochem. commun. 98 (2019) 96–100.
19. M. Miura, Y. Oshikiri, A. Sugiyama, R. Morimoto, I. Mogi, M. Miura et al., *Magneto-Dendrite Effect: Copper Electrodeposition under High Magnetic Field*, Sci. Rep. 7 (2017) 1–8.
20. S. V. Kovalyov, O. B. Girin, C. Debiemme-Chouvy and V. I. Mishchenko, *Copper electrodeposition under a weak magnetic field: effect on the texturing and properties of the deposits*, J. Appl. Electrochem. 51 (2021) 235–243.
21. Y. Liu, B. Zheng, T. Zhang, Y. Chen, J. Liu, Z. Wang et al., *Magnetic field intensified electrodeposition of low-concentration copper ions in aqueous solution*, Electrochim. Acta 432 (2022) 141201.
22. Sudibyo, M. B. How and N. Aziz, *Influences of magnetic field on the fractal morphology in copper electrodeposition*, in IOP Conference Series: Materials Science and Engineering, 285 (2018), pp. 012021.
23. T. Wang and W. Chen, *Effects of Rotating Magnetic Fields on Nickel Electro-Deposition*, ECS Electrochem. Lett. 4 (2015) D14–D17.
24. R. Ji, K. Han, H. Jin, X. Li, Y. Liu, S. Liu et al., *Preparation of Ni-SiC nano-composite coating by rotating magnetic field-assisted electrodeposition*, J. Manuf. Process. 57 (2020) 787–797.
25. S. Syamsuir, F. B. Susetyo, B. Soegijono, S. D. Yudanto, Basori and D. Nanto, *Nickel layers properties produced by electroplating were influenced by spinning permanent magnet*, in Journal of Physics: Conference Series, 2596 (2023), pp. 012008.
26. X. Qu, H. Yang, B. Jia, Z. Yu, Y. Zheng and K. Dai, *Biodegradable Zn–Cu alloys show antibacterial activity against MRSA bone infection by inhibiting pathogen adhesion and biofilm formation*, Acta Biomater. 117 (2020) 400–417.
27. Syamsuir, R. S. Kusumah, A. Premono, A. Lubi, B. Soegijono, S. D. Yudanto et al., *Spinning Effect of Barreling Plating on Physical Properties and Electrochemical Behavior of Copper Layers*, e-Journal Surf. Sci. Nanotechnol. 22 (2024) 120–128.
28. A. C. Larson and R. B. Von Dreele, *General Structure Analysis System (GSAS)*, Vol. 748, University of California, Los Alamos, 2004.
29. R. M. Yusron, R. M. Bisono and M. Pramudia, *Effect Electrolyte Temperature and Electrode Distance to Electroplating Hard-Chrome on Medium-Carbon Steel*, J. Phys. Conf. Ser. 1569 (2020) 042007.
30. X. Qiao, H. Li, W. Zhao and D. Li, *Effects of deposition temperature on electrodeposition of zinc-nickel alloy coatings*, Electrochim. Acta 89 (2013) 771–777.
31. M. A. Lopez-Heredia, P. Weiss and P. Layrolle, *An electrodeposition method of calcium phosphate coatings on titanium alloy*, J. Mater. Sci. Mater. Med. 18 (2007) 381–390.
32. G. Yang, D. Deng, Y. Zhang, Q. Zhu and J. Cai, *Numerical Optimization of Electrodeposition Thickness Uniformity with Respect to the Layout of Anode and Cathode*, Electrocatalysis 12 (2021) 478–488.
33. F. B. Susetyo, B. Soegijono and Yusmaniar, *Effect of a constant magnet position and intensity on a copper layer obtained by DC electrodeposition*, Int. J. Corros. Scale Inhib. 10 (2021) 766–782.
34. Y. Lin, J. Pan, H. F. Zhou, H. J. Gao and Y. Li, *Mechanical properties and optimal grain size distribution profile of gradient grained nickel*, Acta Mater. 153 (2018) 279–289.
35. D. Grujicic and B. Pesic, *Reaction and nucleation mechanisms of copper electrodeposition from ammoniacal solutions on vitreous carbon*, Electrochim. Acta 50 (2005) 4426–4443.
36. Halo Dalshad Omar, *Intensity Correction and Pole Figure Measurement of Copper Metallic by XRD*, J. Basic Appl. Sci. 12 (2016) 320–322.
37. F. Briones, V. Seriacopi, C. Martínez, J. L. Valin, D. Centeno and I. F. Machado, *The effects of pressure and pressure routes on the microstructural evolution and mechanical properties of sintered copper via SPS*, J. Mater. Res. Technol. 25 (2023) 2455–2470.
38. X. Xu, Z. Liu, B. Zhang, H. Chen, J. Zhang, T. Wang et al., *Effect of Mn content on microstructure and properties of 6000 series aluminum alloy*, Appl. Phys. A Mater. Sci. Process. 125 (2019) 1–9.
39. C. O. Ayieko, R. J. Musembi, A. A. Ogacho, B. O. Aduda, B. M. Muthoka and P. K. Jain, *Controlled Texturing of Aluminum Sheet for Solar Energy Applications*, Adv. Mater. Phys. Chem. 05 (2015) 458–466.
40. M. Hubab and M. A. Al-Ghouti, *Recent advances and potential applications for metal-organic framework (MOFs) and MOFs-derived materials: Characterizations and antimicrobial activities*, Biotechnol. Reports 42 (2024) e00837.
41. S. J. Kim, J. Chang and M. Singh, *Peptidoglycan architecture of Gram-positive bacteria by solid-state NMR*, Biochim. Biophys. Acta - Biomembr. 1848 (2015) 350–362.
42. X. Chen, Y. Li, K. Bai, M. Gu, X. Xu, N. Jiang et al., *Class A Penicillin-Binding Protein C Is Responsible for Stress Response by Regulation of Peptidoglycan Assembly in *Clavibacter michiganensis**, Microbiol. Spectr. 10 (2022) .
43. S. Xhafa, L. Olivieri, C. Di Nicola, R. Pettinari, C. Pettinari, A. Tombesi et al., *Copper and Zinc Metal–Organic Frameworks with Bipyrzole Linkers Display Strong Antibacterial Activity against Both Gram+ and Gram– Bacterial Strains*, Molecules 28 (2023) 6160.

44. A. Azam, A. S. Ahmed, M. Oves, M. S. Khan and A. Memic, *Size-dependent antimicrobial properties of CuO nanoparticles against Gram-positive and -negative bacterial strains*, Int. J. Nanomedicine 7 (2012) 3527–3535.
45. J. Ramyadevi, K. Jeyasubramanian, A. Marikani, G. Rajakumar and A. A. Rahuman, *Synthesis and antimicrobial activity of copper nanoparticles*, Mater. Lett. 71 (2012) 114–116.
46. M. Ahamed, H. A. Alhadlaq, M. A. M. Khan, P. Karuppiyah and N. A. Al-Dhabi, *Synthesis, characterization, and antimicrobial activity of copper oxide nanoparticles*, J. Nanomater. 2014 (2014) .
47. L. Huang, E. M. Fozo, T. Zhang, P. K. Liaw and W. He, *Antimicrobial behavior of Cu-bearing Zr-based bulk metallic glasses*, Mater. Sci. Eng. C 39 (2014) 325–329.
48. M. A. Hajduga, S. Węgrzynkiewicz, J. Waś-Solipiwo, M. Hajduga and M. B. Hajduga, *Innovative solutions from the field of the material science and medicine in the interior of modern ambulances*, Mater. Sci. Forum 844 (2016) 50–54.
49. P. L. Lam, R. S. M. Wong, K. H. Lam, L. K. Hung, M. M. Wong, L. H. Yung et al., *The role of reactive oxygen species in the biological activity of antimicrobial agents: An updated mini review*, Chem. Biol. Interact. 320 (2020) 109023.
50. S. Alfei, G. C. Schito, A. M. Schito and G. Zuccari, *Reactive Oxygen Species (ROS)-Mediated Antibacterial Oxidative Therapies: Available Methods to Generate ROS and a Novel Option Proposal*, Int. J. Mol. Sci. 25 (2024) .
51. A. A. Dayem, M. K. Hossain, S. Bin Lee, K. Kim, S. K. Saha, G. M. Yang et al., *The role of reactive oxygen species (ROS) in the biological activities of metallic nanoparticles*, Int. J. Mol. Sci. 18 (2017) 1–21.
52. A. R. Mir, J. Pichtel and S. Hayat, *Copper: uptake, toxicity and tolerance in plants and management of Cu-contaminated soil*, BioMetals 34 (2021) 737–759.
53. F. N. S. Raja, T. Worthington and R. A. Martin, *The antimicrobial efficacy of copper, cobalt, zinc and silver nanoparticles: alone and in combination*, Biomed. Mater. 18 (2023) 045003.
54. S. Y. Tsai, Y. M. Liu, Z. W. Lin and C. P. Lin, *Antimicrobial activity effects of electrolytically generated hypochlorous acid-treated pathogenic microorganisms by isothermal kinetic simulation*, J. Therm. Anal. Calorim. 148 (2023) 1613–1627.
55. D. Marković, C. Deeks, T. Nunney, Ž. Radovanović, M. Radoičić, Z. Šaponjić et al., *Antibacterial activity of Cu-based nanoparticles synthesized on the cotton fabrics modified with polycarboxylic acids*, Carbohydr. Polym. 200 (2018) 173–182.
56. Ž. Z. Tasić, M. B. Petrović Mihajlović, M. B. Radovanović and M. M. Antonijević, *Electrochemical investigations of copper corrosion inhibition by azithromycin in 0.9% NaCl*, J. Mol. Liq. 265 (2018) 687–692.
57. C. Zheng, J. Cao, Y. Zhang and H. Zhao, *Insight into the Oxidation Mechanism of a Cu-Based Oxygen Carrier ( $\text{Cu} \rightarrow \text{Cu}_2\text{O} \rightarrow \text{CuO}$ ) in Chemical Looping Combustion*, Energy and Fuels 34 (2020) 8718–8725.
58. B. Narayanan, S. A. Deshmukh, S. K. R. S. Sankaranarayanan and S. Ramanathan, *Strong correlations between structural order and passive state at water-copper oxide interfaces*, Electrochim. Acta 179 (2015) 386–393.
59. S. Ghosh, *Electroless copper deposition: A critical review*, Thin Solid Films 669 (2019) 641–658.

# Rotating speed and magnetic pole dependency assisted on copper deposition onto aluminum alloy substrate for bacterial eradication application

*by* Cahaya Rosyidan FTKE

---

**Submission date:** 01-Aug-2025 02:38PM (UTC+0700)

**Submission ID:** 2562811315

**File name:** 1547-Article\_Text-5936-1-10-20250731.pdf (1.84M)

**Word count:** 8138

**Character count:** 42016

## Rotating speed and magnetic pole dependency assisted on copper deposition onto aluminum alloy substrate for bacterial eradication application

Basori<sup>a,\*</sup>, Ruliyanta<sup>b</sup>, Maman Kartaman Ajiriyanto<sup>c</sup>, Rosika Kriswarini<sup>c</sup>, Heri Hardiyanti<sup>c</sup>, Cahaya Rosyidan<sup>d</sup>, Sigit Dwi Yudanto<sup>e</sup>, Evi Ulina Margareta Situmorang<sup>f</sup>, Daniel Edbert<sup>g</sup>, Dwi Nanto<sup>h</sup>, Ferry Budhi Susetyo<sup>i</sup>

<sup>a</sup>Department of Mechanical Engineering, Universitas Nasional, Jakarta 12520, Indonesia

<sup>b</sup>Department of Electrical Engineering, Universitas Nasional, Jakarta 12520, Indonesia

<sup>c</sup>Research Center for Nuclear Material and Radioactive Waste Technology, National Research and Innovation Agency, Banten 15314, Indonesia

<sup>d</sup>Department of Petroleum Engineering, Universitas Trisakti, Jakarta 11440, Indonesia

<sup>e</sup>Research Center for Metallurgy, National Research and Innovation Agency, Banten 15314, Indonesia

<sup>f</sup>Department of Physiology School of Medicine and Health Sciences, Atma Jaya Catholic University of Indonesia, Jakarta 14440, Indonesia

<sup>g</sup>Department of Microbiology, Atma Jaya Catholic University of Indonesia, Jakarta 14440, Indonesia

<sup>h</sup>Department of Physics Education, UIN Syarif Hidayatullah, Jakarta 15412, Indonesia

<sup>i</sup>Department of Mechanical Engineering, Universitas Negeri Jakarta, Jakarta 13220, Indonesia

### Article history:

Received: 26 September 2024 / Received in revised form: 27 January 2025 / Accepted: 21 February 2025

### Abstract

Copper (Cu) is widely used in many sectors, such as drinking water piping, heat exchangers, and medical equipment. The present research conducted an electrodeposition of Cu over an aluminum (Al) alloy substrate under the influence of various magnetic poles and rotating speeds. In the present study, a number of investigations, including deposition rate, current efficiency, coating thickness, surface morphology and phase, crystallographic orientation, antibacterial activity, electrochemical behavior, and hardness test were conducted. Increasing the rotation speed promoted to enhanced deposition rate and current efficiency for both magnetic poles influence. An increase in the deposition rate from 12.83 to 13.67  $\mu\text{m/h}$  led to the increasing thickness, a change in surface morphology near the spheroidal, becoming a faceted structure. Presenting and rising in the rotation of a magnetic field led to a reduced surface roughness and crystallite size of Cu film for both magnetic poles influence. The Cu film made without spinning magnetic had a characteristic of highest bacterial inhibition zone around  $2.50 \pm 0.56 \text{ cm}^2$ . The CuRN50 sample had the lowest corrosion rate at around 0.055 mmpy, while the CuRS100 sample had the highest hardness value at approximately 80.72 HV for having the lowest crystallite size. Cu coated onto Al alloy could enhance its properties, such as being antimicrobial, being resistant against corrosion and having the hardness value.

**Keywords:** North and South Pole; SEM-EDS; XRD; electrochemical behavior; hardness

### 1. Introduction

Copper (Cu) due to its promising properties is widely used in many sectors, such as drinking water piping, heat exchangers, and medical equipment [1–3]. As film, it has a higher performance to kill bacteria compared to bulk Cu [4]. Additionally, coated onto aluminum (Al) alloy, Cu could enhance its properties, such as being antimicrobial, being resistant against corrosion and having hardness value [4,5]. Coating synthesis can be conducted by means of

electrochemical, spin coating, or spray methods [6–8]. In view of its simplicity and affordability, the electrodeposition is seen as a more suitable method for coating Cu onto Al alloy [9].

Cu electrodepositions attract many researchers to investigate the formed Cu films. Brands *et al.* investigated the structure, surface morphology, electrical, optical, and magnetic properties of electrodeposited  $\text{Cu}_2\text{O}$  [10]. Antenucci *et al.* improved (the mechanical and thermal properties) of open-cell Al foams through Cu electrodeposition [11]. Augustin *et al.* investigated the effect of current density at Cu electrodeposition on the microstructure, hardness, and antibacterial activity of Cu for antimicrobial Al touch application [4]. Furthermore, Kuisor *et al.* fabricated CuO film using electrodeposition in which the film was tested for

\* Corresponding author.

Email: basori@civitas.unas.ac.id

<https://doi.org/10.21924/cst.10.1.2025.1547>



This open access article is distributed under a Creative Commons Attribution (CC-BY) 4.0 license

antibacterial activity using *Staphylococcus aureus* (*S. aureus*) that successfully reduced the bacterial colony during the experiment [12]. Isa *et al.* performed electrodeposition Cu over 304 stainless steels in which a coated sample was tested for antibacterial properties. In a 10-minute exposure to the coated sample, it could successfully achieve a 100 % reduction of *S. aureus* [13].

Many factors, including magnetic field, determine the formed Cu films when electrodeposition is performed. The existing magnetic field at the electrodeposition process can appear to have several forces. The Lorentz force acts on a moving ion in the solution, resulting in convection flow [14]. The effects of the magnetic field may also relate to the electrokinetic-magnetohydrodynamic (MHD) effect resulting in the body force acting in the diffuse layer [15]. Another force caused by the magnetic field is paramagnetic gradient force [16] that causes the movement of magnetic ions in the diffusion layer. Another possible force is a magnetic gradient force. It acts on paramagnetic and diamagnetic ions [17]. In general, introducing a magnetic field during the electrodeposition process leads to the arrangement of moving ions towards the cathode.

In view of many forces exhibited by presenting a magnet, the investigations of several researchers have been focused on unrotated magnetic field-induced Cu electrodeposition [14,18–22]. Investigating the electrodeposition of Cu under 15 T of magnetic field, Miura *et al.* found extraordinary dendritic growth [19]. Murdoch *et al.* conducted an electrodeposition of Cu using the influence of 0.25 and 0.5 T placed on the working electrode's reverse, and this resulted in the lowest thickness when influencing 0.25 and 0.5 T with the south pole rather than the north pole [14]. Sudibyo *et al.* conducted the electrodeposition of Cu using the influence of 300 and 900 G (neodymium magnet), resulting in higher grain when electrodeposition Cu using the influence of 900 G [22]. Yin *et al.* investigated anomalous Cu hydride phase during the magnetic field-assisted electrodeposition of Cu. Presenting an anti-parallel magnetic field affecting the magnetohydrodynamic effect could enhance the hydrogen evolution and result in poor film quality [18]. Kovalyov *et al.* found that a weak magnetic field (0.5 and 0.7 mT) could affect the electrodeposition process, surface morphology, and texture [20]. Liu *et al.* stated that magnetic field-assisted electrodeposition could change hydrogen bond structure, reduce the charge transfer resistance, and increase the electrolyte viscosity [21].

Due to its ability to enhance the properties of films, electrodeposition assisted with a spinning magnetic field is considered to attract several researchers. Wang and Chen used 0.18 T of a magnetic field with various rotating speeds (1000–3000 rpm) when electrodeposition of nickel (Ni) and results presenting a magnetic field with various rotating speeds could decrease surface roughness [23]. Ji *et al.* fabricated Ni-SiC using an electrodeposition process and found that the exhibited rotating magnetic field made SiC particle distribution more uniform [24]. Syamsuir *et al.* stated that presenting a rotating magnetic field (500 and 800 rpm) at electrodeposition process could make surface morphology of the film more uniform [25]. They found that increasing the rotating speed of a magnetic field (one piece of neodymium

magnet arranged spread five parts in the upside Teflon) at electrodeposition process could transform surface morphology from spheroidal to faceted structure [5].

Oxygen content on the Cu film surface can disrupt the transformation of Cu to Cu ions, reducing antibacterial performance [26]. The formation of surface morphology can have an impact on the antibacterial performance. Surface morphology, such as spheroidal and faceted structures, also contributes to the inhibition zone. A Cu film with spheroidal coating tends to create a higher inhibition zone [5].

The use of a magnetic field during electrodeposition can determine the movement of ions towards the cathode surface. Adjusting magnetic field rotation during electrodeposition also determines the ion movement. Furthermore, the different poles of the selected magnet also influence ion movement at electrodeposition process. Generally, the speed of ion movement can affect the properties of formed film. Based upon the literature review above, higher rotation was used ( $\geq 500$  rpm) to influence the electrodeposition; for this, the present study used the speed rotation of 50 and 100 rpm. The speed rotation was chosen on the basis of previous study conducting Cu electrodeposition by means of barreling apparatus [27]. Syamsuir *et al.* used one piece of neodymium magnet arranged to spread five parts in the upside Teflon [5]. Therefore, the present research used more neodymium magnets to result in more influence of the magnetic field. Here, the influence of spinning using different magnetic poles was also not considered. Murdoch *et al.* found that different magnetic poles influenced the deposition process, resulting in different surface morphologies in Cu films [14]. Therefore, the present research comprehensively investigated the influence of the rotating speed and magnetic pole during Cu electrodeposition on the formation of the film for bacterial eradication applications. The electrodeposition of Cu was determined by various magnetic poles (north and south) and magnetic rotating speeds (0, 50, and 100 rpm). Several investigations were conducted using digital scales, scanning electron microscopy equipped with energy dispersive spectroscopy (SEM-EDS), X-ray diffraction, digital camera, optical microscope, potentiostat dan Vickers hardness.

## 2. Materials and Methods

### 2.1. Materials

Al alloy (0.106 wt.% Si, 0.365 wt.% Fe, 0.055 wt.% Cu, 0.043 wt.% Mn, 0.030 wt.% Mg, 0.003 wt.% Zn, 0.002 wt.% Ni, 0.018 wt.% Ti, 0.003 wt.% Pb, and Al balance) was used as cathode, while pure Cu was used as anode. Electrolyte solution was prepared by dissolving  $\text{CuSO}_4 \cdot 5\text{H}_2\text{O}$  (Merck) in deionized water. Electrolyte solution (250 ml of volume) was used for electrodeposition with the composition of 0.5 M  $\text{CuSO}_4 \cdot 5\text{H}_2\text{O}$  plus 20 ml of  $\text{H}_2\text{SO}_4$ .

### 2.2. Sample preparation

It began by cutting Al alloy into  $2 \times 2$  cm for electrodeposition substrate using a shearing machine. Cu film was then made using a DC power supply (MDB PS-305DM) with 40 mA, and at  $25^\circ\text{C}$ , and pH 5.5 for one h. Cu films were

prepared under the influence of a clockwise rotating magnetic field, as seen in Fig. 1. The plating bath was placed on top of the rotation magnetic field equipment. Two pieces of neodymium magnet were stacked and arranged (six parts) in the upside Teflon, as seen in Fig. 1. One piece of neodymium magnet had 0.08 T of intensity (measured using gauss meter TD-8620). Five variation samples were made; one sample was made without the influence of a rotating magnetic field as a baseline. The sample was made by influencing 50 rpm and 100 rpm. Different pole variations were also used. Table 1 depicts the complete sample names.

Table 1. Sample name and remark

Sample name	Remark
CuR0	without the influence of a rotating magnetic field
CuRN50	50 rpm, north pole near the substrate
CuRN100	100 rpm, north pole near the substrate
CuRS50	50 rpm, south pole near the substrate
CuRS100	100 rpm, south pole near the substrate

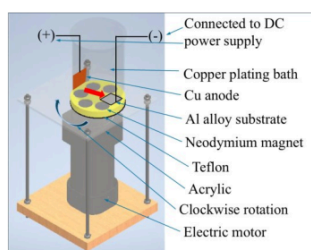


Fig. 1. Rotation magnetic field equipment

### 2.3. Characterizations

The deposition rate and current efficiency were measured similar to previous studies [17]. Thermo Scientific SEM-EDS was used to investigate surface morphology and elements. The cross section was also investigated using SEM apparatus to measure Cu layer thickness. According to SEM image, Image J software was used to measure grain distribution and the roughness of Cu film. Meanwhile, X-ray diffraction was conducted using PANalytical (Cu K radiation) with step size  $0.02^\circ$  and refined with the help of GSAS software [28].

Similarly, antibacterial activity was investigated according to previous studies [5]. The assessment of microbial reduction of various samples was adapted from ISO 22196 for non-porous material. *S. aureus* ATCC 25923 was used in this test. The inhibition zone was documented using a digital camera and assessed using an unaided eye and the area of inhibition was measured by Image J software. Each measurement was performed five times to ensure the data homogeneity. The diffusible area was calculated by subtracting the area of inhibition from the metal size. One-way ANOVA analysis was conducted to investigate whether there was significance between the polarities of the magnets. Moreover, the

specimen was removed from the plate using sterile forceps. The agar was re-incubated at  $35^\circ\text{C} \pm 2$  for 24 hours to observe the antimicrobial activity post-contact. The oxides of the metal formed before and after the test were observed by means of Olympus CX23 microscope under an  $180\times$  magnification; any changes inside of the agar plate were documented. In addition, the observations of microbial reduction test were conducted (within 1, 2, 4, 6 and 12 h).

The electrochemical test was conducted using Ossila potentiostat in 0.9 % NaCl (room temperature). Prior to the electrochemical test, Cu films were mounted and left open area for  $1 \times 1 \text{ cm}^2$ . Here, Cu films were used as working electrode, Ag/AgCl and Pt wire were used as reference electrode and counter electrode, respectively. There are two kinds of test in electrochemical behavior measurement, those are open circuit potential (OCP) and potentiodynamic polarization. OCP is performed until 1200 seconds, while potentiodynamic polarization is performed from -1 to -0.1 V using 5 mV/s of scan rate. The potentiodynamic polarization data was analyzed through the Tafel extrapolation method to find  $I_{\text{corr}}$  and  $E_{\text{corr}}$ . Afterward, corrosion rate could be calculated using following equation [29].

$$\text{Corrosion rate (mmpy)} = K \left( \frac{a I_{\text{corr}}}{n D} \right) \quad (1)$$

where  $K$  is constant (0.00327 mmpy),  $a$  is atomic weight,  $I_{\text{corr}}$  is corrosion current density ( $\mu\text{A}/\text{cm}^2$ ),  $n$  is the number electron involved, and  $D$  is Cu density ( $\text{g}/\text{cm}^3$ ).

The hardness test was performed using Future-Tech (FV-300e) Vickers hardness tester. Five repeatable measurements were conducted over Cu layer by using 1 kg of load.

## 3. Results and Discussion

### 3.1. Deposition rate and current efficiency

Fig. 2 shows the deposition rate and current efficiency of electrodeposition Cu over an Al alloy substrate. They had similar tendencies; an increase in magnet rotation speed led to a rise in deposition rate and current efficiency.

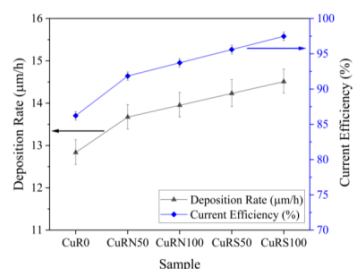


Fig. 2. Deposition rate and current efficiency of Cu electrodeposition

In the process of Cu electrodeposition, the oxidation process occurs at the anode and a reduction process occurs at the cathode. An Al alloy (substrates) to be plated is placed at



the cathode. When the current is applied, the Cu ions are depleted in the surroundings of the cathode, making a diffusion film upper around the cathode. Hydrogen evolution is known to occur at the cathode during Cu electrodeposition from aqueous solutions [17]. Less hydrogen evolution can increase the deposition rate and current efficiency because hydrogen evolution is able to disturb the movement of the ions to the cathode [30,31]. Presenting an anti-parallel magnetic field (north pole) affecting the MHD effect could enhance the hydrogen evolution, decrease current efficiency, and result in poor film quality [18]. As shown in Fig. 2, hydrogen evolution seemed to influence the electrodeposition process when being determined by the north pole. Therefore, the electrodeposition process had a lesser current efficiency than the electrodeposition process when being influenced by the south pole.

Cu films made and influenced by the rotating south pole magnet has a higher deposition rate due to the magnetic field, which was parallel to the current direction and attracts more Cu ions onto the Al alloy surface [14]. Rotating the magnet under the electrolyte solution during the electrodeposition process could induce an Eddy electric field [5] that can act as an additional MHD flow convection effect [23]. Moreover, increasing the rotation speed could attract more Cu ions onto the Al alloy surface, consequently increasing the deposition rate and current efficiency.

### 3.2. Average thickness

Fig. 3 and Fig. 4 show the thickness of various Cu layers and average thickness of Cu layers. Compared to the average thickness to the deposition rate (Fig. 2), there was a correlation between them. Increasing the deposition rate led to an increase in the average of Cu layers thickness, similar to the study by Syamsuir *et al.* [27]. Furthermore, it seemed that average coating thickness was higher than thickness found by calculating from deposition rate. For example, average coating thickness of CuR0 sample ideally is 12.83  $\mu\text{m}$  due to deposition sample for one hour. Unfortunately, average coating thickness of CuR0 sample was 27.17  $\mu\text{m}$ . This behavior was probably due to the SEM cross section being conducted on an area near the anode (red arrow Fig. 1). According to Yang *et al.*, the end area of the cathode results in higher thickness compared to the middle area [32]. Therefore, average thickness is higher than deposition rate value.

### 3.3. SEM-EDS and roughness

Fig. 5 shows the SEM result and the grain distribution of various Cu film surfaces. Samples were made by influencing the north pole magnetic field, which had a larger grain size than samples created by affecting the south pole of a magnetic field. Generally, presenting the south pole magnetic field influence can lead to a decrease in grain size. While presenting south pole magnetic field influence can lead to an increase in grain size as in line with previous study [33]. Murdoch *et al.* stated that different poles are used to influence deposition process that will result different grain size [14]. Moreover, Lin *et al.* stated that deposition time contributes to the formed grain size [34].

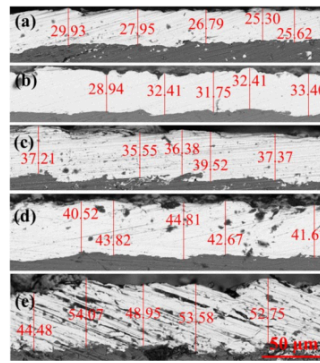


Fig. 3. Thickness of various Cu layers: (a) CuR0; (b) CuRN50; (c) CuRN100; (d) CuRS50; and (e) CuRS100

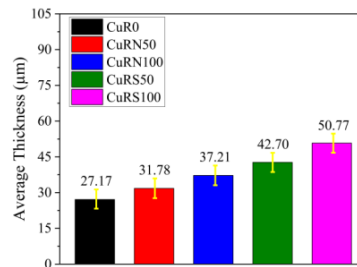


Fig. 4. Cu layers average thickness

As shown in Fig. 5, the Cu sample was made with no spinning magnetic influence, leading to the formation of morphology near the spheroidal. Cu samples made with spinning magnetic assistance led to the formation of faceted structure morphology [17]. Moreover, the transformation from spheroidal to faceted structure was determined by the deposition rate. A higher nucleation rate leads to a higher deposition rate, resulting in a variation in surface morphology [35]. Samples made with influences from the north pole magnetic field had a low nucleation rate. Hence, it had wider grain sizes than samples by influencing the south pole magnetic field [14]. Moreover, an increase in the deposition rate from 12.83 to 13.67  $\mu\text{m}/\text{h}$  led to a change in surface morphology near the spheroidal becoming faceted structure. The deposition rate between 13.67 and 14.51  $\mu\text{m}/\text{h}$  resulted in a faceted structure of surface morphology.

The south pole had an affecting magnetic field parallel to the current direction; therefore, Cu ions were more attracted to the Al alloy surface. In contrast, the north pole had an affecting magnetic field that was anti-parallel to the current direction, reducing Cu ions' attraction onto the Al alloy

surface. Moreover, Lorentz's forces rotated opposite each other on top of the surface specimen for different magnetic poles. This condition affected the sample film by influencing the South Pole to be smoother than the North Pole. Ji *et al.* stated that presenting a rotating magnetic field during electrodeposition can make surface morphology more uniform [24]. In this case, the paramagnetic force has a similar tendency for different magnetic poles. Therefore, influencing surface morphology could be neglected.

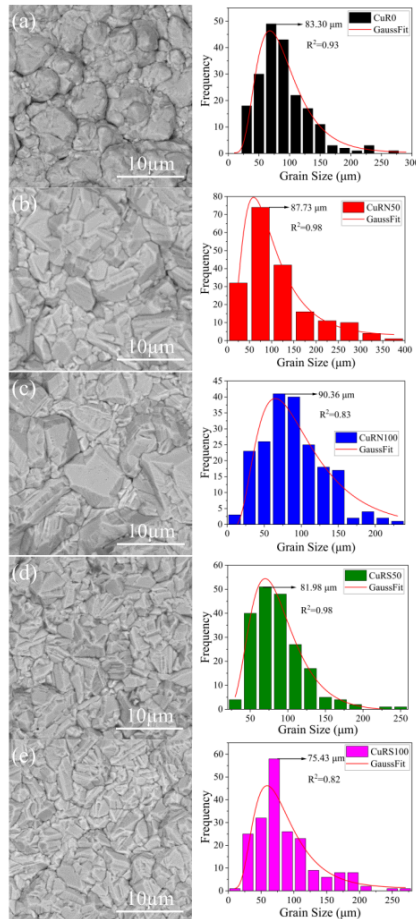


Fig. 5. SEM and grain distribution of Cu layers: (a) CuR0; (b) CuRN50; (c) CuRN100; (d) CuRS50; and (e) CuRS100

As shown in Fig. 6, the spinning magnetic-assisted running at 50 rpm led to oxygen formed on the Cu surface. Moreover, enhanced magnetic rotation led to a decrease or disappearance of oxygen. Presenting oxygen on Cu film is one of the unique cases in which oxygen can be formed due to both a secondary reaction on the anode and sample storage and transport [5].

Fig. 7 presents the roughness analyzed result from the SEM image using ImageJ software. CuR0, CuRN50, CuRN100, CuRS50, and CuRS100 samples had a surface roughness of 34.62, 18.00, 17.38, 18.60, and 16.58  $\mu\text{m}$ , respectively.

Presenting a magnetic field rotation during electrodeposition led to a decrease in the surface roughness of Cu film. More rotation could also decrease surface roughness, which is perfectly in line with the previous study [5]. Wang and Chen found that presenting a magnetic field during electrodeposition with various rotating speeds could decrease surface roughness [23]. This behavior is probably due to additional MHD flow, which is in line with the deposition rate result and could enhance the Cu ions' movement. A higher deposition rate would result in a higher nucleation rate, consequently producing a smooth surface morphology. Moreover, the sample made by north pole magnet influence had more roughness than sample made by north pole magnet. This behavior probably due to MHD effect that could enhance the hydrogen evolution and result in more roughness [18].

### 3.4. X-ray diffraction

Fig. 8 shows the diffraction patterns of samples of Cu deposition on substrates consisting of Al alloy plates. The five samples were identified to have Cu phase peaks at the indexed plane peaks (111), (200), (220), (311), and (222) at angles  $2\theta = 43.31, 50.45, 74.13, 89.94, \text{ and } 95.15^\circ$ . The cubic crystal system was found in the Cu phase, and it had a space group of  $\text{fm-3m}$ . The cubic Cu phase peaks at these angles were found consistent with the findings from studies by Omar and Francisco Briones *et al.* [36,37]. This demonstrated that the procedure for depositing Cu on Al alloy plates has been successfully completed. At the indexed plane peaks (111), (200), (220), (311), and (400) of the five diffraction patterns, they were also found on the Al alloy plate substrate along with the copper phase. Xu *et al.* and Ayieko *et al.* presented a standard Al diffraction pattern identical to this peak of Al [38,39].

The mean crystallite size and lattice value of the five deposition samples were compared to further analyze the diffraction pattern. The Rietveld method was employed to determine the lattice of the five samples. The cubic Cu phase lattice of all five samples was measured at 0.3615 nm based upon the calculation results. Changes in magnetic poles and rotating speed showed no effect on the lattice value of the cubic Cu phase. Table 2 presents the data from the crystallographic calculation. To determine the mean crystallite size, the Williamson-Hall plot method was utilized. In contrast to the lattice value, the mean crystallite size was affected by the rotating speed and poles. The mean crystallite size became finer with the increase in magnet rotation speed perfectly matched with surface roughness analysis.

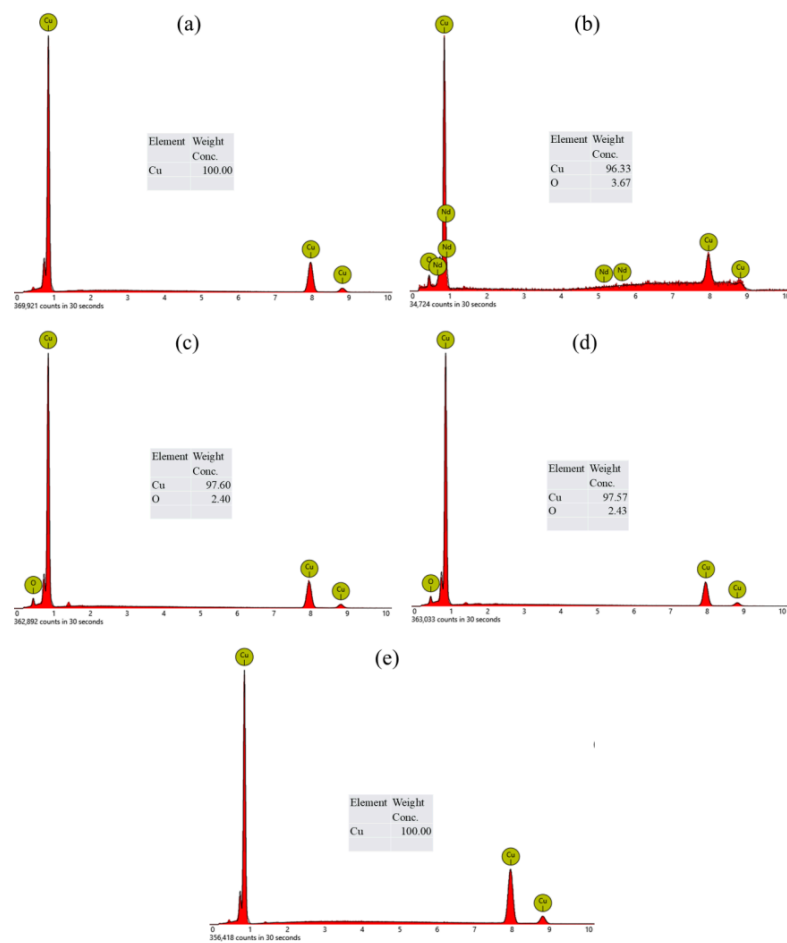


Fig. 6. EDS Cu layers: (a) CuR0; (b) CuRN50; (c) CuRN100; (d) CuRS50; and (e) CuRS100

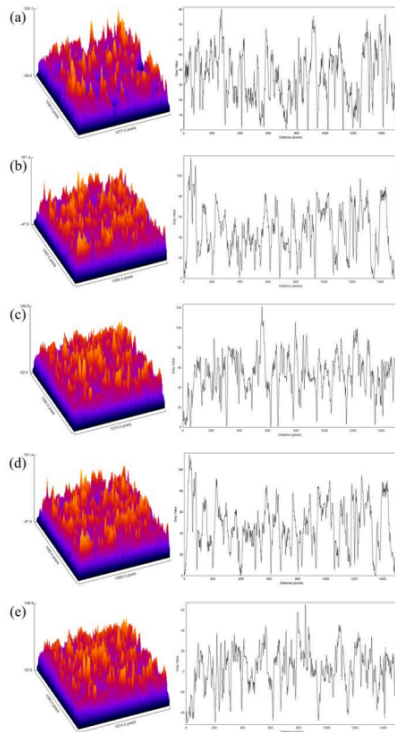


Fig. 7. Roughness Cu layers: (a) CuR0; (b) CuRN50; (c) CuRN100; (d) CuRS50; and (e) CuRS100

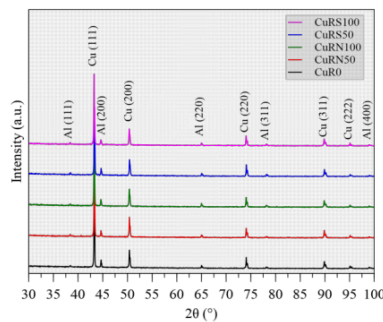


Fig. 8. X-ray diffraction pattern of various sample

Table 2. Crystallographic data calculated from various samples

Source	CuR0	CuRN50	CuRN100	CuRS50	CuRS100
Name: Copper (Cu)					
Space group: F m -3 m (225)					
Crystal system: cubic					
Lattice (nm)	0.3615	0.3615	0.3615	0.3615	0.3615
wRp (%)	10.10	10.37	10.24	9.86	10.30
GoF	1.067	1.106	1.087	1.045	1.056
Mean crystallite size (nm)	308	173	154	173	126
Micro-strain (%)	0.07	0.05	0.05	0.05	0.04

### 3.5. Antibacterial activity

Fig. 9 describes the antibacterial activity test after 24 hours of contact. Material placement in the middle of Mueller Hinton agar was inoculated with *S. aureus* ATCC 25923. Noticing the inhibition zones around the material; the calculation is presented in Table 3. The metal ions were diffused into the agar to inhibit the growth of *S. aureus*.

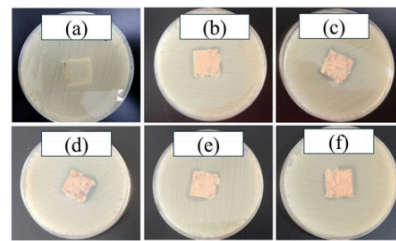


Fig. 9. Antibacterial activity test after 24 hours: (a) blank; (b) CuRN50; (c) CuRN100; (d) CuR0; (e) CuRS50; and (f) CuRS100

Cu, particularly in the form of metal-organic frameworks (MOFs) and nanoparticles, exhibited significant antibacterial activity against Gram-positive bacteria such as *S. aureus* [40]. The peptidoglycan layer in Gram-positive bacteria plays a significant role in their susceptibility to Cu although its direct interaction with Cu is not as straightforward as with other antimicrobial agents. Cu is able to induce modifications in the peptidoglycan layer, such as increased cross-linkage, which can affect the overall structure and function of the cell wall. These modifications can either enhance or reduce the susceptibility of Gram-positive bacteria to Cu, dependent on the specific bacterial strain and environmental conditions [41,42]. In this research, the Cu induced contact killing. The antimicrobial activity of Cu is believed to involve contact-mediated killing, initiating membrane degradation. The susceptibility of Gram-positive strains to Cu is attributed to the thick peptidoglycan layer, reducing cell wall permeability to other metal ions, including Zinc [43].

As shown in Fig. 9, the inoculum was totally annihilated by electroplated materials. The log reduction was not calculated due to the total killing of the bacteria. However, the total reduction of  $> 105$  CFU/ml might suggest a percentage reduction of  $> 99.999\%$  (see Table 3). Moreover, there was a zone of inhibition between the sample and bacterial lawn that was also visible inside the zone's white crystals and some bluish color change inside the agar. This suggests that the Cu material diffused and interacted with the agar can result in a zone of bacterial growth inhibition.

As seen in Table 3, the widest diffusion zone was observed in CuR0 with the zone of diffusion and inhibition areas of  $6.99 \text{ cm}^2$  and  $2.5 \text{ cm}^2$ . This was statistically significant with  $p < 0.001$  (ANOVA; CI 95%). Also, there was significance in independent T-Test analyses between CuR0 and CuR50 group ( $p < 0.001$ ; CI 95%), R0 and R100 group ( $p < 0.001$ ; CI 95%), and between CuR50 and CuR100 Group ( $p < 0.001$ ; CI 95%). To investigate whether there was significance between the polarities of the magnets, independent T-test analyses were performed. There was no significant difference in the outcome between the south pole group and the north one ( $p=0.063$ ; CI 95%). Moreover, there were no inhibitions in the blank group, and the bacteria grew underneath the metal. Comparing to the previous study, less inhibition was found in the present study [5]. This behavior was probably due to higher crystallite size form in the all samples [44]. Previous study found crystallite size between 95.66 and 100.50 nm [5]. While in the present study, the crystallite size of Cu layer was between 126 and 308 nm. Ramyadevi et al. and Ahmed et al. in their studies, when testing Cu nanoparticle for antibacterial activity using *S. aureus*, found the inhibition zone of 2.2 cm and 2.4 cm [45,46].

Table 3. The reduction of colony, and diffusible metal observation

Sample	Microbial reduction assessment		Diffusible metal observation	
	Initial load 0 h (CFU/ml)	Final load 24 h (CFU/ml)	Zone of diffusion ( $\text{cm}^2$ )	Inhibition area ( $\text{cm}^2$ )
Blank		0	$4.01 \pm 0.01$	$-0.48 \pm 0.01$
CuR0		0	$6.99 \pm 0.12$	$2.50 \pm 0.56$
CuRNS0	$3.5 \times 10^5$	0	$6.21 \pm 0.01$	$1.61 \pm 0.21$
CuRN100		0	$6.00 \pm 0.02$	$1.89 \pm 0.02$
CuRSS0		0	$6.16 \pm 0.41$	$1.73 \pm 0.46$
CuRS100		0	$6.17 \pm 0.01$	$2.14 \pm 0.24$

The use of magnetic rotation during material synthesis showed a significant impact on the results. Materials synthesized without magnetic rotation (R0) showed the stronger antibacterial effects compared to those synthesized at 50 rpm or 100 rpm. However, increasing magnet rotation significantly enhanced the size of the inhibition zone. As a result, the inhibition zone at 100 rpm was found larger than that of at 50 rpm. This condition was probably due to forming some oxygen on the Cu films surface as seen in EDS result, which could disrupt transformation Cu to be Cu ions. Qu et al. found that antibacterial behavior was determined by Cu ions

[26]. The release of Cu ions inside of the agar was lethal towards *S. aureus* [47].

As shown in Fig. 3, CuR0 surface morphology formed near to spheroidal, while other samples formed a faceted structure. In Table 3, it can be seen that higher inhibition zone was seen in CuR0 sample. Therefore, it can be concluded that the spheroidal form results in the higher inhibition zone compared to faceted structure, which is perfectly in agreement with previous study [5]. This condition probably occurred due to the spheroidal structure having a wider surface area than the faceted structure, where more Cu ions were released. Moreover, an increase in rotation leads to a decrease in roughness. Several researchers have found that roughness is independent of the inhibition zone, which aligns with the present study [5,48].

Moreover, the generation of reactive oxygen species (ROS) and damage to cell membranes are the main ways in which metals' broad antibacterial potential has been extensively studied [49–51]. Even so, metals can target particular cellular components and, when combined, are likely to improve pathogen clearance despite their non-specific activity. Conversely, Cu has an ability to change metabolic pathways in addition to cause damage to DNA and cell membranes through the generation of ROS [52]. The combined mode of action has not been investigated so far, despite the fact that the modes of action of various metal ions have been well explored. The variability in antimicrobial efficaciousness between various combinations can be explained by the diverse chemical reactivity of metal ions with bacterial cells and their specific biological targets [53].

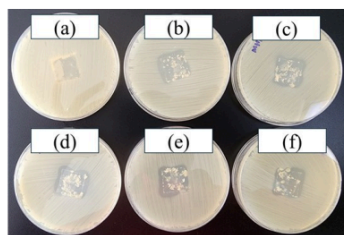


Fig. 10. After 24 hours of post contact test: (a) blank; (b) CuRNS0; (c) CuRN100; (d) CuR0; (e) CuRSS0; and (f) CuRS100

Fig. 10 shows the results after 24 hours of post-contact testing. The inhibitory zones appeared after the removal of the material. There were some metal infiltrations inside the agar on every plate making the agar cracked. This indicated gas-forming or exothermic reaction inside the agar, increasing the antimicrobial ability of the material [54]. There were no anti-Staphylococcal effects on the blank material; therefore, there was a regrowth of microorganisms in the place where the metal was previously placed.

Fig. 11 shows antibacterial activity pretest microscope observation, and Fig. 12 shows antibacterial activity post-test microscope observation. The microscopic observation of electroplated surfaces occurred under an  $180 \times$  magnification



optical microscope. There was a significant proportion in the formation of white crystals on the electroplated surface after tests. The crystals did not form on the surface of the blank. The Cu formed oxides, which changed the surface color. Marković et al. stated that color change in the Cu is in relation to adsorption or reduction Cu ions [55].

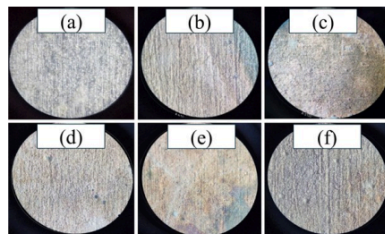


Fig. 11. Antibacterial activity pretest microscope observation: (a) blank; (b) CuRN50; (c) CuRN100; (d) CuR0; (e) CuRS50; and (f) CuRS100

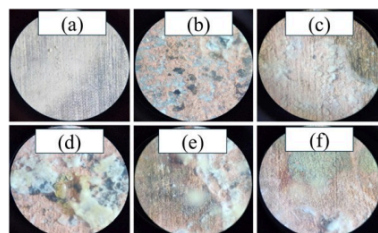


Fig. 12. Antibacterial activity post-test microscope observation: (a) blank; (b) CuRN50; (c) CuRN100; (d) CuR0; (e) CuRS50; and (f) CuRS100

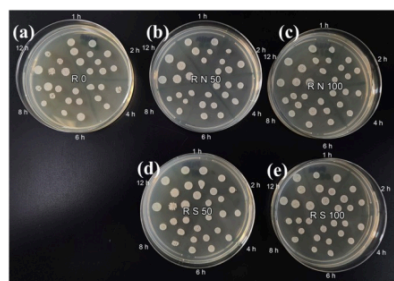


Fig. 13. Microbial reduction test observation: (a) CuR0; (b) CuRN50; (c) CuRN100; (d) CuRS50; and (e) CuRS100

As seen in Fig. 13 and Table 4, to deep explore microbial reduction assessment, investigating at 1, 4, 6, 8, and 12 hours

were conducted. At 6 hours of investigation, CuR0 sample resulted in a reduction colony-forming units per milliliter around  $10^4$ , which was in line with inhibition area value (higher inhibition area). While other samples still showed similar results when initial exposure occurred (See Table 3).

Table 4. Microbial reduction assessment of Cu samples

Sample name	1 h	2 h	4 h	6 h	12 h
	(CFU/ml)				
CuR0	$>10^5$	$>10^5$	$>10^5$	$10^4$	$10^4$
CuRN50	$>10^5$	$>10^5$	$>10^5$	$>10^5$	$>10^5$
CuRN100	$>10^5$	$>10^5$	$>10^5$	$>10^5$	$>10^5$
CuRS50	$>10^5$	$>10^5$	$>10^5$	$>10^5$	$>10^5$
CuRS100	$>10^5$	$>10^5$	$>10^5$	$>10^5$	$>10^5$

### 3.6. Electrochemical behavior

Fig. 14 shows the OCP measurement result of various Cu samples.  $E_{OCP}$  values of the CuR0, CuRN50, CuRN100, CuRS50, and CuRS100 were -0.643, -0.667, -0.658, -0.633, and -0.641 V vs Ag/AgCl, respectively. Previous study found  $E_{OCP}$  of Cu layer over Al alloy between -0.694 and -0.684 V vs Ag/AgCl [27]. All samples showed a shift to more negative value to reach a steady state. Tasić et al. stated that this condition implies the Cu oxide dissolution and CuCl layer formation [56]. The CuRN50 layer seemed more stable than other sample, showing to reach steady state at around 600 s for OCP measurement.

Fig. 15 represents potentiodynamic polarization test result in 0.9 % NaCl. Table 4 presents the tafel extrapolation result. Using Eq. (1), corrosion rate was calculated and summarized in Table 5.

As shown in Table 5, the CuRN50 sample was found as the sample with the lowest corrosion rate, probably due to the highest oxygen on the Cu surface that could form an oxide [57]. Narayanan et al. stated that oxygen content in the Cu film would be an obstacle for chloride ions to adsorb in the film [58]. Therefore, the oxide could result in better protection from aggressive species in the 0.9 % NaCl medium. Moreover, compared to Fig. 6, the oxygen content of the Cu layer was linear to the corrosion rate. Higher oxygen content led to decrease corrosion rate.

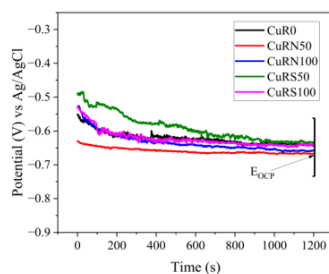


Fig. 14. OCP test curve



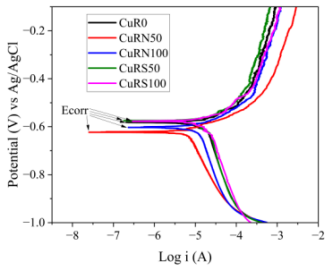


Fig. 15. Potentiodynamic polarization test curve

Table 5. Tafel extrapolation result and corrosion rate

Sample name	Ecorr (V) vs Ag/AgCl	Icorr (A/cm <sup>2</sup> )	Corrosion rate (mmpy)
CuR0	-0.582	$1.27 \times 10^{-5}$	0.148
CuRN50	-0.623	$4.78 \times 10^{-6}$	0.055
CuRN100	-0.603	$8.77 \times 10^{-6}$	0.102
CuRS50	-0.574	$8.56 \times 10^{-6}$	0.099
CuRS100	-0.577	$1.14 \times 10^{-5}$	0.132

3.7. Hardness test

Fig. 16 represents average hardness test result using 1 kg of load. The hardness test was conducted with five repeatable measurements on top of Cu layer. The average hardness in the present study varied between 47.92 and 80.72 HV. Ghosh et al. found that Cu layer hardness from 22.9 to 114.7 HV [59]. Previous study also found Cu layer hardness between 72.94 and 76.26 HV [5]. Moreover, Augustine *et al.* stated that hardness value is dependent on the crystallite size. The lowest crystallite size promoted to resulting higher hardness [4]. Comparing Fig. 16 to Table 2, there was a linear correlation between hardness and crystallite size. Highest hardness value was seen at CuRS100 sample, while smallest one was found at CuR0 sample.

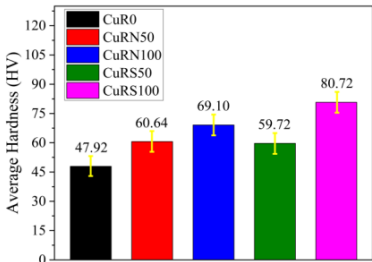


Fig. 16. Average of the hardness test result

4. Conclusion

This study has successfully conducted the Cu films fabricated under a spinning magnetic field with various rotation speeds and a magnetic pole. Higher rotation speed was promoted to enhance deposition rate and current efficiency for both magnetic poles. The Cu sample fabricated with no spinning magnetic influence led to the morphology formed near the spheroidal. Cu samples made with spinning magnetic influence led to the morphology formed near the faceted structure. Magnetic-assisted spinning at 50 rpm led to oxygen formed on the Cu surface for both magnetic poles and enhanced rotation. This then led to the decrease or disappearance of oxygen. Presenting and rising in magnetic field rotation led to decreased surface roughness and crystallite size of Cu film for both magnetic poles. The Cu sample made without spinning magnetic fields influence had the highest inhibition zone size, probably due to the absence of oxygen on the Cu film surface and the morphology near the spheroidal. The oxygen content of the Cu layer was found linear to the corrosion rate. Higher oxygen content led to decrease corrosion rate, while the lowest crystallite size promoted to higher hardness. Overall, Cu films successfully covered Al alloy and could transform it into antibacterial material. For future study, it is recommended to conduct the electrodeposition of Cu with spinning magnetic influence higher than 100 rpm.

Acknowledgements

This study has been supported by the Ministry of Education, Culture, Research, and Technology through grand funding Penelitian Fundamental-Regular with contract number 087/LPPM-UNAS/VI/2024 and 815/LL3/AL.04/2024.

References

1. D. A. Lytle and C. P. White, *The effect of phosphate on the properties of copper drinking water pipes experiencing localized corrosion*, J. Fail. Anal. Prev. 14 (2014) 203–219.
2. M. M. Lachowicz, *A metallographic case study of formicary corrosion in heat exchanger copper tubes*, Eng. Fail. Anal. 111 (2020) 104502.
3. N. Thokala, C. Kealey, J. Kennedy, D. B. Brady and J. B. Farrell, *Characterisation of polyamide 11/copper antimicrobial composites for medical device applications*, Mater. Sci. Eng. C 78 (2017) 1179–1186.
4. A. Augustin, P. Huilgol, K. R. Udapa and U. B. K. K, *Effect of current density during electrodeposition on microstructure and hardness of textured Cu coating in the application of antimicrobial Al touch surface*, J. Mech. Behav. Biomed. Mater. 63 (2016) 352–360.
5. Syamsuir, F. B. Susetyo, B. Soegijono, S. D. Yudanto, Basori, M. K. Ajriyanto et al., *Rotating-Magnetic-Field-Assisted Electrodeposition of Copper for Ambulance Medical Equipment*, Automot. Exp. 6 (2023) 290–302.
6. A. M. Alghamdi and F. Fadhillah, *Thin film composite polyelectrolyte multilayer nanofiltration membrane fabricated using spin assisted layer by layer assembly: Application of solution diffusion film model*, Commun. Sci. Technol. 5 (2020) 10–15.

7. C. Santoso, Ratnawati and Slamet, *Utilization of glycerol solution for hydrogen production by a combination of photocatalysis and electrolysis processes with Fe-TiO<sub>2</sub> nanotubes*, Commun. Sci. Technol. 8 (2023) 208–215.
8. W. Trisunaryanti, K. Wijaya and A. M. Tazkia, *Preparation of Ni/ZSM-5 and Mo/ZSM-5 catalysts for hydrotreating palm oil into biojet fuel*, Commun. Sci. Technol. 9 (2024) 161–169.
9. A. Lelevic and F. C. Walsh, *Electrodeposition of Ni-P alloy coatings: A review*, Surf. Coatings Technol. 369 (2019) 198–220.
10. I. S. Brandt, M. A. Tumelero, S. Pelegrini, G. Zangari and A. A. Pasa, *Electrodeposition of Cu<sub>2</sub>O: growth, properties, and applications*, J. Solid State Electrochem. 21 (2017) 1999–2020.
11. A. Antenucci, S. Guarino, V. Tagliaferri and N. Ucciardello, *Improvement of the mechanical and thermal characteristics of open cell aluminum foams by the electrodeposition of Cu*, Mater. Des. 59 (2014) 124–129.
12. A. Kusior, J. Mazurkow, P. Jelen, M. Bik, S. Raza, M. Wdowiak et al., *Copper Oxide Electrochemical Deposition to Create Antiviral and Antibacterial Nanocoatings*, Langmuir 40 (2024) 14838–14846.
13. N. N. C. Isa, Y. Mohd, M. H. M. Zaki and S. A. S. Mohamad, *Antibacterial activity of copper coating electrodeposited on 304 stainless steel substrate*, in AIP Conference Proceedings, 1901 (2017), pp. 020009.
14. H. A. Murdoch, D. Yin, E. Hernández-Rivera and A. K. Giri, *Effect of applied magnetic field on microstructure of electrodeposited copper*, Electrochem. commun. 97 (2018) 11–15.
15. Q. Long, Y. Zhong and J. Wu, *Research progress of magnetic field techniques for electrodeposition of coating*, Int. J. Electrochem. Sci. 15 (2020) 8026–8040.
16. K. Kołodziejczyk, E. Miłoś, M. Zieliński, M. Jaksender, D. Szczukocki, K. Czarny et al., *Influence of constant magnetic field on electrodeposition of metals, alloys, conductive polymers, and organic reactions*, J. Solid State Electrochem. 22 (2018) 1629–1674.
17. B. Soegijono, F. B. Susetyo, Yusmaniar and M. C. Fajrah, *Electrodeposition of paramagnetic copper film under magnetic field on paramagnetic aluminum alloy substrates*, e-Journal Surf. Sci. Nanotechnol. 18 (2020) 281–288.
18. D. Yin, H. A. Murdoch, B. Chad Hornbuckle, E. Hernández-Rivera and M. K. Dunstan, *Investigation of anomalous copper hydride phase during magnetic field-assisted electrodeposition of copper*, Electrochem. commun. 98 (2019) 96–100.
19. M. Miura, Y. Oshikiri, A. Sugiyama, R. Morimoto, I. Mogi, M. Miura et al., *Magneto-Dendrite Effect: Copper Electrodeposition under High Magnetic Field*, Sci. Rep. 7 (2017) 1–8.
20. S. V. Kovalyov, O. B. Girin, C. Debiemme-Chouvy and V. I. Mishchenko, *Copper electrodeposition under a weak magnetic field: effect on the texturing and properties of the deposits*, J. Appl. Electrochem. 51 (2021) 235–243.
21. Y. Liu, B. Zheng, T. Zhang, Y. Chen, J. Liu, Z. Wang et al., *Magnetic field intensified electrodeposition of low-concentration copper ions in aqueous solution*, Electrochim. Acta 432 (2022) 141201.
22. Sudibyo, M. B. How and N. Aziz, *Influences of magnetic field on the fractal morphology in copper electrodeposition*, in IOP Conference Series: Materials Science and Engineering, 285 (2018), pp. 012021.
23. T. Wang and W. Chen, *Effects of Rotating Magnetic Fields on Nickel Electro-Deposition*, ECS Electrochem. Lett. 4 (2015) D14–D17.
24. R. Ji, K. Han, H. Jin, X. Li, Y. Liu, S. Liu et al., *Preparation of Ni-SiC nano-composite coating by rotating magnetic field-assisted electrodeposition*, J. Manuf. Process. 57 (2020) 787–797.
25. S. Syamsuir, F. B. Susetyo, B. Soegijono, S. D. Yudianto, Basori and D. Nanto, *Nickel layers properties produced by electroplating were influenced by spinning permanent magnet*, in Journal of Physics: Conference Series, 2596 (2023), pp. 012008.
26. X. Qu, H. Yang, B. Jia, Z. Yu, Y. Zheng and K. Dai, *Biodegradable Zn–Cu alloys show antibacterial activity against MRSA bone infection by inhibiting pathogen adhesion and biofilm formation*, Acta Biomater. 117 (2020) 400–417.
27. Syamsuir, R. S. Kusumah, A. Premono, A. Lubi, B. Soegijono, S. D. Yudianto et al., *Spinning Effect of Barreling Plating on Physical Properties and Electrochemical Behavior of Copper Layers*, e-Journal Surf. Sci. Nanotechnol. 22 (2024) 120–128.
28. A. C. Larson and R. B. Von Dreele, *General Structure Analysis System (GSAS)*, Vol. 748, University of California, Los Alamos, 2004.
29. R. M. Yusron, R. M. Bisono and M. Pramudia, *Effect Electrolyte Temperature and Electrode Distance to Electroplating Hard-Chrome on Medium-Carbon Steel*, J. Phys. Conf. Ser. 1569 (2020) 042007.
30. X. Qiao, H. Li, W. Zhao and D. Li, *Effects of deposition temperature on electrodeposition of zinc-nickel alloy coatings*, Electrochim. Acta 89 (2013) 771–777.
31. M. A. Lopez-Heredia, P. Weiss and P. Layrolle, *An electrodeposition method of calcium phosphate coatings on titanium alloy*, J. Mater. Sci. Mater. Med. 18 (2007) 381–390.
32. G. Yang, D. Deng, Y. Zhang, Q. Zhu and J. Cai, *Numerical Optimization of Electrodeposition Thickness Uniformity with Respect to the Layout of Anode and Cathode*, Electrocatalysis 12 (2021) 478–488.
33. F. B. Susetyo, B. Soegijono and Yusmaniar, *Effect of a constant magnet position and intensity on a copper layer obtained by DC electrodeposition*, Int. J. Corros. Scale Inhib. 10 (2021) 766–782.
34. Y. Lin, J. Pan, H. F. Zhou, H. J. Gao and Y. Li, *Mechanical properties and optimal grain size distribution profile of gradient grained nickel*, Acta Mater. 153 (2018) 279–289.
35. D. Grujicic and B. Pesic, *Reaction and nucleation mechanisms of copper electrodeposition from ammoniacal solutions on vitreous carbon*, Electrochim. Acta 50 (2005) 4426–4443.
36. Halo Dalshad Omar, *Intensity Correction and Pole Figure Measurement of Copper Metallic by XRD*, J. Basic Appl. Sci. 12 (2016) 320–322.
37. F. Briones, V. Seriacopi, C. Martínez, J. L. Valin, D. Centeno and I. F. Machado, *The effects of pressure and pressure routes on the microstructural evolution and mechanical properties of sintered copper via SPS*, J. Mater. Res. Technol. 25 (2023) 2455–2470.
38. X. Xu, Z. Liu, B. Zhang, H. Chen, J. Zhang, T. Wang et al., *Effect of Mn content on microstructure and properties of 6000 series aluminum alloy*, Appl. Phys. A Mater. Sci. Process. 125 (2019) 1–9.
39. C. O. Ayieko, R. J. Musembi, A. A. Ogacho, B. O. Aduda, B. M. Muthoka and P. K. Jain, *Controlled Texturing of Aluminum Sheet for Solar Energy Applications*, Adv. Mater. Phys. Chem. 05 (2015) 458–466.
40. M. Hubab and M. A. Al-Ghouti, *Recent advances and potential applications for metal-organic framework (MOFs) and MOFs-derived materials: Characterizations and antimicrobial activities*, Biotechnol. Reports 42 (2024) e00837.
41. S. J. Kim, J. Chang and M. Singh, *Peptidoglycan architecture of Gram-positive bacteria by solid-state NMR*, Biochim. Biophys. Acta - Biomembr. 1848 (2015) 350–362.
42. X. Chen, Y. Li, K. Bai, M. Gu, X. Xu, N. Jiang et al., *Class A Penicillin-Binding Protein C Is Responsible for Stress Response by Regulation of Peptidoglycan Assembly in *Clavibacter michiganensis**, Microbiol. Spectr. 10 (2022).
43. S. Khafa, L. Olivieri, C. Di Nicola, R. Pettinari, C. Pettinari, A. Tombesi et al., *Copper and Zinc Metal–Organic Frameworks with Bipyrazole Linkers Display Strong Antibacterial Activity against Both Gram+ and Gram– Bacterial Strains*, Molecules 28 (2023) 6160.

44. A. Azam, A. S. Ahmed, M. Oves, M. S. Khan and A. Memic, *Size-dependent antimicrobial properties of CuO nanoparticles against Gram-positive and -negative bacterial strains*, Int. J. Nanomedicine 7 (2012) 3527–3535.
45. J. Ramyadevi, K. Jeyasubramanian, A. Marikani, G. Rajakumar and A. A. Rahuman, *Synthesis and antimicrobial activity of copper nanoparticles*, Mater. Lett. 71 (2012) 114–116.
46. M. Ahamed, H. A. Alhadlaq, M. A. M. Khan, P. Karupiah and N. A. Al-Dhabi, *Synthesis, characterization, and antimicrobial activity of copper oxide nanoparticles*, J. Nanomater. 2014 (2014).
47. L. Huang, E. M. Fozo, T. Zhang, P. K. Liaw and W. He, *Antimicrobial behavior of Cu-bearing Zr-based bulk metallic glasses*, Mater. Sci. Eng. C 39 (2014) 325–329.
48. M. A. Hajduga, S. Węgrzynkiewicz, J. Waś-Solipiwo, M. Hajduga and M. B. Hajduga, *Innovative solutions from the field of the material science and medicine in the interior of modern ambulances*, Mater. Sci. Forum 844 (2016) 50–54.
49. P. L. Lam, R. S. M. Wong, K. H. Lam, L. K. Hung, M. M. Wong, L. H. Yung et al., *The role of reactive oxygen species in the biological activity of antimicrobial agents: An updated mini review*, Chem. Biol. Interact. 320 (2020) 109023.
50. S. Alfei, G. C. Schito, A. M. Schito and G. Zuccari, *Reactive Oxygen Species (ROS)-Mediated Antibacterial Oxidative Therapies: Available Methods to Generate ROS and a Novel Option Proposal*, Int. J. Mol. Sci. 25 (2024).
51. A. A. Dayem, M. K. Hossain, S. Bin Lee, K. Kim, S. K. Saha, G. M. Yang et al., *The role of reactive oxygen species (ROS) in the biological activities of metallic nanoparticles*, Int. J. Mol. Sci. 18 (2017) 1–21.
52. A. R. Mir, J. Pichtel and S. Hayat, *Copper: uptake, toxicity and tolerance in plants and management of Cu-contaminated soil*, BioMetals 34 (2021) 737–759.
53. F. N. S. Raja, T. Worthington and R. A. Martin, *The antimicrobial efficacy of copper, cobalt, zinc and silver nanoparticles: alone and in combination*, Biomed. Mater. 18 (2023) 045003.
54. S. Y. Tsai, Y. M. Liu, Z. W. Lin and C. P. Lin, *Antimicrobial activity effects of electrolytically generated hypochlorous acid-treated pathogenic microorganisms by isothermal kinetic simulation*, J. Therm. Anal. Calorim. 148 (2023) 1613–1627.
55. D. Marković, C. Deeks, T. Nunney, Ž. Radovanović, M. Radoičić, Z. Šaponjić et al., *Antibacterial activity of Cu-based nanoparticles synthesized on the cotton fabrics modified with polycarboxylic acids*, Carbohydr. Polym. 200 (2018) 173–182.
56. Ž. Z. Tasić, M. B. Petrović Mihajlović, M. B. Radovanović and M. M. Antonijević, *Electrochemical investigations of copper corrosion inhibition by azithromycin in 0.9% NaCl*, J. Mol. Liq. 265 (2018) 687–692.
57. C. Zheng, J. Cao, Y. Zhang and H. Zhao, *Insight into the Oxidation Mechanism of a Cu-Based Oxygen Carrier ( $\text{Cu} \rightarrow \text{Cu}_2\text{O} \rightarrow \text{CuO}$ ) in Chemical Looping Combustion*, Energy and Fuels 34 (2020) 8718–8725.
58. B. Narayanan, S. A. Deshmukh, S. K. R. S. Sankaranarayanan and S. Ramanathan, *Strong correlations between structural order and passive state at water-copper oxide interfaces*, Electrochim. Acta 179 (2015) 386–393.
59. S. Ghosh, *Electroless copper deposition: A critical review*, Thin Solid Films 669 (2019) 641–658.

# Rotating speed and magnetic pole dependency assisted on copper deposition onto aluminum alloy substrate for bacterial eradication application

## ORIGINALITY REPORT

11%

SIMILARITY INDEX

7%

INTERNET SOURCES

7%

PUBLICATIONS

2%

STUDENT PAPERS

## PRIMARY SOURCES

1

[cst.kipmi.or.id](http://cst.kipmi.or.id)

Internet Source

2%

2

[www.ije.ir](http://www.ije.ir)

Internet Source

1%

3

B Basori, B Soegijono, S D Yudanto, D Nanto, F B Susetyo. "Effect of low magnetic field during nickel electroplating on morphology, structure, and hardness", Journal of Physics: Conference Series, 2023

Publication

1%

4

[www.jstage.jst.go.jp](http://www.jstage.jst.go.jp)

Internet Source

1%

5

Syamsuir, Rizky Septian Kusumah, Agung Premono, Ahmad Lubi et al. "Spinning Effect of Barreling Plating on Physical Properties and Electrochemical Behavior of Copper Layers", e-Journal of Surface Science and Nanotechnology, 2024

Publication

1%

6

Farah N S Raja, Tony Worthington, Richard A Martin. "The antimicrobial efficacy of copper, cobalt, zinc and silver nanoparticles: alone and in combination.", Biomedical Materials, 2023

Publication

1%

7

[journal.yrpiiku.com](http://journal.yrpiiku.com)

Internet Source

1%

8	Sarita Yadav, Yogesh Sharma. "Unravelling the potential of magnetic field in electrochemical energy storage: A review", Applied Energy, 2025 Publication	1 %
9	S Syamsuir, F B Susetyo, B Soegijono, S D Yudanto, Basori, D Nanto. "Nickel layers properties produced by electroplating were influenced by spinning permanent magnet", Journal of Physics: Conference Series, 2023 Publication	<1 %
10	Submitted to Universitas Indonesia Student Paper	<1 %
11	www.researchgate.net Internet Source	<1 %
12	link.springer.com Internet Source	<1 %
13	Alexander Poznyak, Gerhard Knörnschild, Alexander Hoha, Andrei Pligovka. "Porous and Ag-, Cu-, Zn-Doped Al <sub>2</sub> O <sub>3</sub> Fabricated via Barrier Anodizing of Pure Al and Alloys", Coatings, 2024 Publication	<1 %
14	research-repository.griffith.edu.au Internet Source	<1 %
15	www.science.gov Internet Source	<1 %
16	"Proceedings of the 9th International Conference and Exhibition on Sustainable Energy and Advanced Materials", Springer Science and Business Media LLC, 2024 Publication	<1 %

Exclude quotes      On  
Exclude bibliography      On

Exclude matches      < 15 words